UNIVERSITÀ DEGLI STUDI DI PADOVA

DIPARTIMENTO DI INGEGNERIA DELL'INFORMAZIONE

University of Padova

Department of Information Engineering

Master Degree in Bioengineering

Comparison of knee loading during walking via musculoskeletal modelling using marker-based and IMU-based approaches

SUPERVISOR

Prof Zimi Sawacha

CANDIDATE

Paola Zancanaro

CO-SUPERVISOR

Prof Ilse Jonkers

Dr Giacomo Di Raimondo, PhD

Dr Bryce A Killen, PhD

Academic Year 2021/2022

03 October 2022

Abstract

The current thesis is the result of the candidate's work over a six-month period with the assistance of the supervisor and co-supervisors, thanks to the collaboration between the Human Movement Bioengineering Laboratory Research group at the University of Padova (Italy) and the Human Movement Biomechanics Research group at KU Leuven (Belgium).

Gait analysis, at a clinical level, is a diagnostic test with multiple potentials, in particular in identifying functional limitations related to a pathological path. Three-dimensional motion capture is now consolidated as an approach for human movement research studies and consists of a set of very precise measurements, the latter are processed by biomechanical models, and curves relating to the kinematics and indirect dynamics, i.e., the joint angles and the relative forces and moments, can be obtained. These results are considered fully reliable and based on these curves it is decided how to intervene on the specific subject to make the path as less pathological as possible. However, the use of wearable sensors (IMUs) consisting of accelerometers, gyroscopes, and magnetic sensors for gait analysis, has increased in the last decade due to the low production costs, portability, and small size that have allowed for studies in everyday life conditions. Inertial capture (InCap) systems have become an appealing alternative to 3D Motion Capture (MoCap) systems due to the ability of inertial measurement units (IMUs) to estimate the orientation of 3D sensors and segments.

Musculoskeletal modelling and simulation provide the ideal framework to examine quantities *in silico* that cannot be measured *in vivo*, such as musculoskeletal loading, muscle forces and joint contact forces. The specific software used in this study is *Opensim*: an open-source software that allows modelling, analysis, and simulation of the musculoskeletal system.

The aim of this thesis is to compare a marker-based musculoskeletal modelling approach with an IMUs-based one, in terms of kinematics, dynamics, and muscle activations. In particular, the project will focus on knee loading, using an existing musculoskeletal model of the lower limb.

The current project was organized as follows: first, the results for the MoCap approach were obtained, following a specific workflow that used the COMAK IK tool and the COMAK algorithm [1] to get the secondary knee kinematics, muscle activations, and knee contact forces. Where COMAK is a modified static optimization algorithm that solves for muscle activations and secondary kinematics to obtain measured primary DOF accelerations while minimizing muscle activation [1].

Then these results were used to make a comparison with those obtained by the inertial-based

approach, with the attempt to use as little information as possible from markers while estimating kinematics from IMU data using an OpenSim toolbox called *OpenSense*. Afterward, in order to promote an approach more independent from the constraints of a laboratory, the Zero Moment Point (ZMP) method was used to estimate the center of pressure position of the measured ground reaction forces (GRFs), and a specific Matlab code was implemented to improve this estimation. Using the measured GRFs with the new CoPs, the results of Inverse Dynamics, muscle activations, and finally knee loading were calculated and compared to the MoCap results. The final step was to conduct a statistical analysis to compare the two approaches and emphasize the importance of using IMUs for gait analysis, particularly to study knee mechanics.

The thesis is divided into five chapters: the first provides a detailed description of gait analysis, including the procedure, guidelines, and instruments used to collect all the necessary data to study human locomotion. The second chapter discusses the characteristics of musculoskeletal modelling, with a focus on the steps required to obtain kinematics, dynamics, and muscle information. Attention is drawn to the procedures to obtain inverse kinematics driven by IMU data, by means of the *OpenSense* toolbox. The third chapter focuses on the knee joint, providing a brief overview of its anatomy and functions as well as the knee model used for the project [2]. The fourth chapter describes the experimental setup, including all procedures and methods used to achieve the objectives. Finally, in the latest chapter, the obtained results are reported and also the comparison results are reported in terms of RMSE (Root Mean Square Error), correlation coefficient, and maximum/median differences, as well as a general discussion of the project, including limitations and future developments.

Sommario

La presente tesi è il risultato del lavoro del candidato svolto per un periodo di sei mesi, con l'aiuto del relatore e dei supervisori, grazie alla collaborazione tra il gruppo di ricerca del Laboratorio di Bioingegneria del Movimento dell'Università di Padova (Italia) e il gruppo di ricerca Human Movement Biomechanics dell'Università di KU Leuven (Belgio).

L'analisi del cammino, a livello clinico, è un test diagnostico dalle molteplici potenzialità, in particolare nell'individuazione di limitazioni funzionali legate ad un percorso patologico. La Motion Capture tridimensionale (3D MoCap) è ormai un approccio negli studi di ricerca sul movimento umano e si basa su misure sperimentali di cinematica e cinetica, che supportate da modelli biomeccanici, permettono di ottenere una stima della cinematica e della cinetica articolare, assieme alle forze di reazione al suolo ed eventuale attivazione muscolare. Questi risultati sono ormai considerati attendibili e vengono utilizzati per pianificare eventuali interventi di riabilitazione e chirurgici. Oggigiorno, l'uso di sensori indossabili (IMUs) costituiti da accelerometri, giroscopi e sensori magnetici per l'analisi del cammino, è in continuo aumento, grazie ai bassi costi di produzione, le caratteristiche di portabilità e le ridotte dimensioni che hanno consentito lo svolgimento di studi nella vita di tutti i giorni. I sistemi Inertial Capture (InCap) sono diventati un'alternativa interessante ai sistemi 3D MoCap grazie alla capacità dei sensori inerziali (IMUs) di stimare l'orientamento tridimensionale di sensori e segmenti corporei.

La modellazione e simulazione muscoloscheletrica forniscono lo schema principale per esaminare le quantità *in silico* che non possono essere misurate *in vivo*, come le forze muscolari e le forze di contatto articolari. Il software specifico utilizzato in questo studio è *Opensim*: un software *open source* che consente la modellazione, l'analisi e la simulazione del sistema muscolo-scheletrico.

Questa tesi si propone di utilizzare due approcci: uno basato sull'utilizzo di marker (stereofotogrammetria) e uno sull'utilizzo di sensori inerziali (IMUs), per la stima di cinematica, dinamica e attivazioni muscolari. In particolare, si è focalizzata l'attenzione sui carichi del ginocchio, utilizzando un modello muscoloscheletrico esistente dell'arto inferiore.

Il progetto è organizzato come segue: innanzitutto sono stati ottenuti i risultati per l'approccio MoCap, seguendo uno schema di lavoro preciso che utilizza il tool specifico COMAK IK e l'algoritmo COMAK [1], per ottenere la cinematica secondaria del ginocchio, le attivazioni muscolari e le forze di contatto del ginocchio. COMAK è un algoritmo di ottimizzazione statica modificato che risolve le attivazioni muscolari e la cinematica secondarie per ottenere le

accelerazioni primarie misurate, riducendo al minimo l'attivazione muscolare [1].

Successivamente questi risultati sono stati utilizzati come confronto per quelli ottenuti con l'approccio basato su IMUs, con l'obiettivo di utilizzare il meno possibile le informazioni ricavate dai marker, stimando la cinematica dai dati IMUs utilizzando un toolbox di OpenSim chiamato *OpenSense*. Per rendere l'approccio più facilmente trasferibile al di fuori del laboratorio, è stato utilizzato il metodo Zero Moment Point (ZMP) per stimare la posizione del centro di pressione delle forze di reazione al suolo (GRFs), ed è stato implementato un codice *Matlab* specifico per migliorare la stima ottenuta. Utilizzando le GRFs stimate con i nuovi CoP, sono stati calcolati e confrontati i risultati MoCap in termini di dinamica inversa, attivazioni muscolari e infine carico al ginocchio. Il passaggio finale è stato quello di condurre un'analisi statistica per confrontare i due approcci e sottolineare l'importanza dell'utilizzo delle IMUs per l'analisi della camminata, in particolare per studiare la meccanica del ginocchio.

La tesi è suddivisa in cinque capitoli: il primo fornisce una descrizione dettagliata dell'analisi del cammino, comprese le procedure, le linee guida e gli strumenti utilizzati per raccogliere tutti i dati necessari allo studio della locomozione umana. Nel secondo capitolo vengono discusse le caratteristiche della modellazione muscolo-scheletrica, con particolare attenzione ai passaggi necessari per ottenere informazioni cinematiche, dinamiche e muscolari. Si richiama l'attenzione sulle procedure per ottenere la cinematica con i dati IMU, tramite il toolbox *OpenSense*. Il terzo capitolo si concentra sull'articolazione del ginocchio, fornendo una breve panoramica della sua anatomia e funzioni principali, e sul modello di ginocchio utilizzato per il progetto [2]. Il quarto capitolo descrive il setup sperimentale, comprese tutte le procedure e i metodi utilizzati per raggiungere gli obiettivi. Infine, nell'ultimo capitolo, i risultati del confronto tra i due metodi sono riportati in termini di RMSE (Root Mean Square Error), del coefficiente di correlazione e della mediana e massima differenza. Infine, viene riportata una discussione generale del progetto, compresi i limiti e gli sviluppi futuri.

Contents:

Chapter 1

1. Gait analysis

1.1 Introduction

Motion analysis is a technique that aims to collect quantitative information relating to the mechanics of the musculoskeletal system during the execution of a motor task that affect an overview of very different environments.
In fact, it can be a valid tool for many clinical applications because it enables the measurement and description of many different aspects of a locomotory activity, and it is aimed at improving motor performance, learning physiological knowledge, post-injury assessment, and technological improvement of the equipment present in the training environment. It also has applications in the sports field, computer games, physical rehabilitation, human recognition, modelling, and many other fields.
During the movements, kinematic quantities (displacement and therefore speed and acceleration in the space of the body segments), dynamics (analysis of the forces and couples involved between the internal structures, i.e., muscles, tendons, ligaments, and bones), and electromyography (muscles activated in movement) are recorded.

In the study of human locomotion, the most important branch is gait analysis**,** a study of walking. Gait analysis is becoming more and more important and interesting in different fields, such as clinical or sports, and the reason for this interest has changed over the years. Currently in the clinical setting, having accurate quantitative measures allows you to better define the etiology of a given pathology and to check the effectiveness of rehabilitation by studying the possible improvement of the patient [3]. It is also commonly used in sports biomechanics to help athletes run more efficiently, as well as to identify problems related to posture or movement related to injuries [4].

1.2 Gait analysis

The walk can be defined as a method of locomotion in which through the alternating and repeated use of lower limbs, the forward movement of the body is provided while allowing stable support [5]. Human movement is achieved through a highly coordinated complex

interaction between bones, muscles, ligaments, and joints of the musculoskeletal system, which is controlled by the nervous system. The central nervous system transmits commands through the peripheral nervous system to the musculoskeletal system [6]. The latter is capable of transmitting the forces necessary for the body to move and perform all the activities of daily life [7].

In recent centuries, the study of gait has improved with the advent of new and increasingly avant-garde technologies, but the first studies have already been made in antiquity. In fact, the ancient Greeks discovered that the harmony of mind and body required an athletic activity to complete the search for knowledge, and with the mechanical, mathematical, and anatomical paradigms developed at that time Aristotle wrote the first book about it entitled *De motu animanlum* in 344 BC. Subsequently other scholars became interested in the study of movement such as Leonardo da Vinci, representing in detail the movement and the human body, and Andreas Vescolius, publishing the first book of human anatomy. During the Renaissance, Galileo applied mechanical theory to the study of animal movement, treated in *De Animaliam Motibuse*, while one of his students, Borelli, estimated the center of mass of the entire body and wrote muscle dynamics during movement in the treatise *De Motu Animalum* [4].

Only with the birth of photography more detailed studies started to develop. Eitenne-Jules Marey (1830-1904) invented the "Cronophotography", using only a photographic machine to obtain multiple images, with different position of the subject moving (Fig. 1.1). In the same period Muybridge (1830-1904) improved photography by increasing the shutter speed to 1/100 per second thus obtaining a series of photographs very close in time, making it possible to observe the movement of the subject in detail. Christian Braune (1831-1892) took inspiration from Marey's work on photography who, together with the physiologist Otto Fischer (1861-1917), carried out experiments on a frozen corpse, determining the planes of the gravitational centers along the sagittal, frontal, and longitudinal plane. In addition, in 1890 they used stereophotogrammetry and ground reaction forces to study the gait using their first techniques of reconstruction of three-dimensional models, all with major limitations due to errors deriving from the manual identification of markers [4].

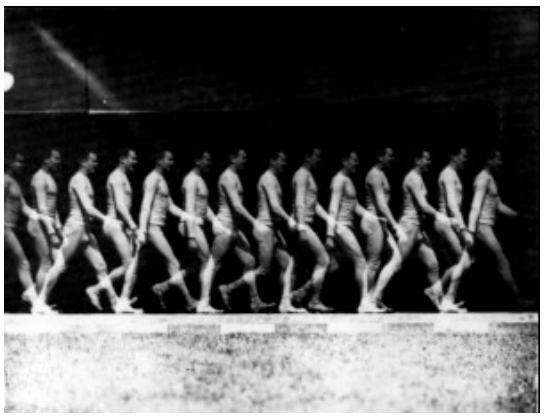

Fig. 1.1 Cronophotography of Etienne Jules Marey [8]

After the Second World War there was a strong interest in the three-dimensional study of walking in the clinical setting to provide better treatment for wounded or amputated soldiers. Verne Inman (1905-1980) applied mechanical engineering theory to clinical problems by designing prostheses for amputees and identified gait-determining characteristics of healthy subjects, assuming that a gait was more efficient when vertical and lateral excursions in the body's center of gravity (COG) are minimized [8]. Following his path, Jacqueline Perry (1918-2013) [5] divided the walk into five support phases and three swing phases, while David Sutherland (1923-2006) [9] perfected the walking cycle by defining three periods: double support initial, single support on one limb and double final support.

In the late 1970s, with the advancement of technology, the first optical motion analysis systems were developed, so the movement was recorded in the form of digital data and no longer analog. This allowed them to expand their studies and to complete them in a shorter time, these tools are still part of the study of movement.
In recent decades, interest has increased leading to the development not only of increasingly advanced instrumentation, but also of increasingly cheaper and more portable devices, thus opening research approaches outside the laboratory and studying movement in daily life, such as the use of inertial sensors in the clinical setting [10].

According to Perry's studies [5], the path can be analyzed under different aspects, as each of its phases involves the interaction between multiple body segments. The three main aspects foresee the subdivision of the path as follows:

- The division according to the **variations of mutual contact of the foot on the ground.** Therefore, an alternation of events in which the foot hits the ground (support phase) and subsequently is lifted (oscillation phase)

- The division that uses **space-time parameters** to describe the gait. For example, measuring how long a stride lasts or the distance traveled using the instants that divide the gait into the different phases
- The division according to the **basic functions** supported by the locomotor system (legs and lower limbs), that are generating an impulsive force, maintaining stability in posture changes, minimizing shocks during impact on the ground, conserving energy to reduce the demands of muscular effort

1.3 Gait cycle

The gait cycle can be defined as a period of time between two nominally identical events in the gait cycle. Generally, these two nominally identical events correspond to the instant in which a foot hits the ground and ends when the same foot hits the ground again (called *initial contact IC).*

During the gait cycle, the lower limb considers an alternating *stance phase* (foot in contact with the ground) and *swing phase* (foot not in contact with the ground). A gait cycle is therefore divided into a stance or stance period (about 60% of the cycle) and a swing period (about 40% of the cycle) of the right and left lower limbs (Fig 1.2). It is possible to make a subdivision based on the stance and swing phase of the two lower limbs: when both members are in the stance phase, this is a bipodal support and when one of the two members is in the swing phase it is a monopodalic support [5].

1.3.1 Division according to mutual contact of the foot on the ground

This first description of the gait cycle identifies the limbs as supporting elements of the body that move alternately in order to fulfill the assigned motor task. It has been said that the gait cycle is divided into two distinct phases: stance and swing. The stance begins with the initial contact while the swing begins with the removal of the foot from the ground (*toe off*).

The stance phase is divided as well into three phases: the *initial double support*, *single support* and *terminal double support*. The **double support phases** have the same duration (they are the same and only the role of the two feet is reversed) and they correspond to 20% of the gait cycle.

In these phases both feet rest on ground and body weight is distributed on both limbs, even though very much different.

The **single support** phase occurs when only one foot is in contact with the ground and the weight of the body rests entirely on the affected limb. It constitutes about 40% of the gait cycle, so the entire stance phase occupies about 60% of the total cycle. The single support of one limb corresponds to the oscillation phase of the other limb [5].

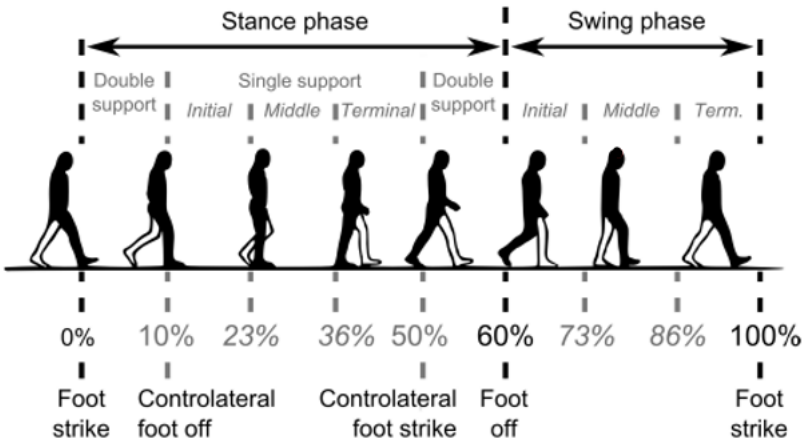

Fig. 1.2 Common temporal division of the gait cycle [5]

1.3.2 Functional division of the gait cycle

A more detailed description of the gait cycle can be adopted, based on the subdivision into sub-phases characterized by a precise function.

In particular, the stance phase can be divided into five functional sub-phases which occur in the following sequences: initial contact (IC), load response (LR), intermediate support (MSt), terminal support (TSt) and pre-oscillation (PSw). Similarly, the swing phase is divided into three functional sub-phases which occur in the following sequences: initial swing (ISw), intermediate swing (MSw) and terminal swing (TSw) [5] (Fig. 1.3).

These sub-sequence allow the lower limb to perform the three main functional tasks of walking: load acceptance, single support, and limb advancement.

- **Load acceptance** is the task with the most functional demands because all the weight is transferred to a limb that has just ended the swing and therefore in an unstable configuration. Initial contact is part of acceptance and includes the moment when the heel usually comes into contact with the ground, allowed by the ankle dorsiflexion. In

the load response phase (LR) there is an initial period of double support until the opposite foot comes off the ground with the knee flexion to absorb the impact, while the plantar flexion of the ankle allows the heel to roll by contacting the forefoot with the ground [11].

- **The single support** takes place in the intermediate support in which the body is aligned at the forefoot. The limb advances beyond the support foot by dorsal flexion of the ankle, while the knee and hip are in extension. The second half of the single stance phase (terminal stance) begins with the heel lift and ends when the contralateral limb touches the ground. The weight of the body is transferred beyond the forefoot and the body begins to fall forward. The hip joint continues to extend while the knee joint initially extends and then slightly flexes [11].

- The **advancement of the limb** is divided into 4 phases: pre swing, initial swing, intermediate swing and terminal swing. In pre-swing, the contralateral limb begins the double support phase and enters the load response phase, while the limb of interest positions itself for oscillation through an increase in plantar flexion of the ankle and knee flexion. During the initial swing, the foot is raised and the limb advances, with the hip and knee flexed while the ankle is partially dorsiflexed. The intermediate swing begins when the swinging limb is opposite to the one in support and ends when the tibia returns to a neutral vertical position. The hip flexes and the knee extends in response to gravity. Finally, the terminal swing begins with the vertical tibia and ends when the foot is in contact with the ground. The hip remains in initial flexion, the knee is extended while the ankle joint remains dorsiflexed up to the neutral position [11].

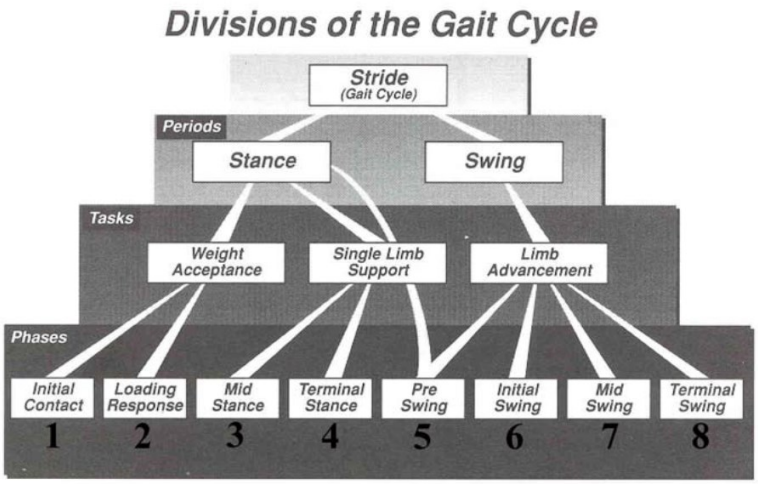

Fig. 1.3 Divisions of the Gait Cycle [5]

1.3.3 Muscle control during the gait cycle

Understanding how muscles behave during the gait is very important to assess normal and pathological gait (Fig. 1.4).

The first muscle to contract is the *hallucis extensor*, which is active throughout the pre-swing. Immediately after, during the intermedial swing there is an activation of the *anterior tibialis* and the *extensor digitorum longus*. The intensity of the contraction of the *tibialis anterior* increases rapidly during the initial swing, and in the terminal swing it increases again gradually, in order to position the foot for the support. The action of the *extensor digitorum longus* is the same as the *tibialis* but with a slightly smaller amplitude.

The action of the *soleus* muscle begins at the end of the load response phase, remaining constant throughout the intermediate stance and assuming a rapid and marked peak starting from 45% of the gait cycle. Subsequently the intensity of the action of the *soleus* decreases with a similar speed, until it stops at the beginning of the double support phase (pre-swing).

The medial head of the *gastrocnemius* is activated parallel to the *soleus*, while the initiation of the lateral head can be delayed until the intermediate support. The other perimalleolar muscles show a modest flexor plantar efficiency since their alignment gives them a different primary role during walking: the control of the foot joints.

The *posterior tibialis* becomes active at the initial contact and continues for the whole single support. The contact of the contralateral foot (50% of the gait cycle) is the signal for relaxation of the *posterior tibialis.* The action of the peroneal muscles begins early in the gait cycle and ends in the intermediate pre-swing (55-58% of the gait cycle) [5].

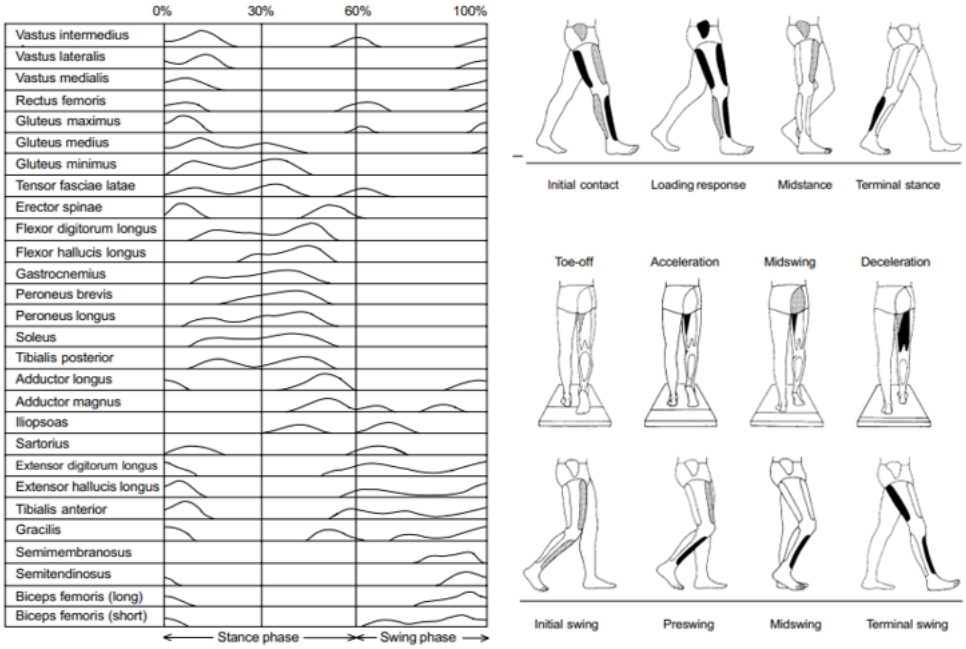

Fig. 1.4 The normal EMG pattern for 28 of the most important muscles in the lower extremities plotted as a function of the gait cycle [12]

1.3.4 Space-time parameters

During a gait cycle analysis some space-time parameters can be calculated to characterize quantitatively the gait of each subject. These can be obtained by recording the walk by means of different devices, through which you must be able to identify the events of the gait cycle, especially Heel-Strike (HS) and Toe-off (TO) [11]. The main temporal parameters are:

- *Stride duration* [s]: temporal interval between the two heel-contacts of the same foot
- *Stance duration* [s]: time interval between HS and TO of the same foot
- *Swing duration* [s]: time interval between TO and the next HS of the same foot
- *Step duration* [s]: time between ipsilateral and contralateral heel contact
- *Single support duration* [s]: defines the time in monopodalic support, it begins when the ipsilateral foot comes off the swing phase
- *Double support duration* [s]: defines the time in bipodalic support, and the support is on both feet
- *Cadence* [step/min]: defined as the number of steps at the minute

Similarly, it is possible to calculate spatial and space-time parameters such as:

- *Step length* [m]: the distance between a point of contact of one foot with the ground (usually the heel) and the same point of contact with the ground of the other foot
- *Speed of the step* [m/s]: linear velocity along walking direction measure on one or more steps

Using these parameters, it is possible to evaluate the differences between a healthy and a pathological subject, in fact a gait alteration can characterize the presence of a pathology or motor dysfunction.

To study the gait in detail, a quantitative analysis can therefore be used, using appropriate instrumentation, obtaining information regarding the kinematics and dynamics of the gait during the gait cycle. The first allows us to calculate the joint angles and the displacement of the individual moving body segments, while the second allows us to calculate the moments and forces applied.

1.4 Motion analysis

Human movement is the set of complex phenomena related to the execution of a motor task. The quantitative analysis of the motor function is carried out by sophisticated equipment and procedures that allow the detection of physical quantities relating to the mechanics of the musculoskeletal system during the execution of a specific motor task. The study of human movement finds application in various fields including the clinical, ergonomic and sports fields. The goal of this analysis is to provide descriptive information not only in situations of physiological posture and movement, but also in the case of pathological changes. This allows quantifying functional limitations, defining therapeutic pathways, monitoring the progress of rehabilitation therapy, and documenting the effectiveness of the use of aids or prostheses.

1.4.1 Basic movements

Movement of the human body is described by referring to the three axes and three planes as shown in figure 1.5. The main axes are:

- X: anteroposterior axis
- Y: vertical axis
- Z: medio-lateral or transverse axis

These axes identify the three main planes:

- Sagittal plane (X, Y): divides the human body into two symmetrical parts, respectively right and left
- Frontal or coronal plane (Y, Z): divides the body into two asymmetrical parts, respectively anterior and posterior
- Transversal plane (X, Z): divides the body into two asymmetrical parts, respectively upper and lower

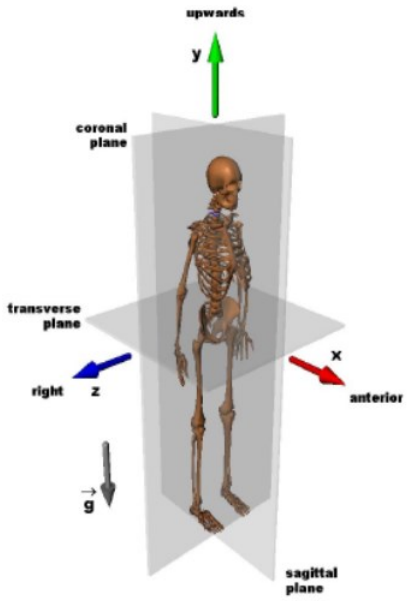

Fig. 1.5 Anatomical coordinates system and planes [11]

The elementary movements are performed around the principal axes and lie in these planes. They are classified into:

- flexion / extension: around the transverse axis, in the sagittal plane
- adduction / abduction: around the anteroposterior axis, in the frontal plane
- internal / external rotation: around the longitudinal axis, on the transverse plane.

The other possible movements are the combination of the latter. It should be noted that when the movements are not "elementary" the definition of the axes around which the rotations take place is no longer the one of the Cartesian axes fixed in space. The commonly adopted definition in biomechanics (Grood & Suntay, 1984) will be discussed in Section 1.4.5.

1.4.2 Rigid body kinematics

In the description of the movement of the human body, the information obtained refers to a model of the musculoskeletal system: the anatomical segment is kinematically defined by the movement of its bone component. By assumption, the various anatomical segments into which the human body is divided are considered rigid bodies, ignoring the possibility of deformation under load and the presence of surrounding soft tissues. Therefore, a system of reference defined using significant geometric points is always maintained in the same relationship with respect to the body itself. A rigid body can then be defined by knowing the position of its three points, two of which are necessary to identify the axis around which the body could rotate, while the third, as long as it is not aligned with the other two, prevents its rotation.
To know the position of any other point of the rigid body, it is sufficient to know the relative position of this point with respect to the three points chosen to identify the position of the rigid body. The relative position is expressed with respect to a reference system integral with the rigid body, called a **mobile reference system** (or local frame). It is a local cartesian axis system rigidly associated with a bone segment which can be defined as follows:

- The origin is in one of the three points
- The first axis corresponding to the line connecting the origin and one of the other two points
- The second axis directed perpendicular to the plane identified by the three points
- The third axis perpendicular to the two previous axes

The mobile reference system just defined has 12 parameters that locate it in space: the three coordinates of the origin of the cartesian axis system and the nine director cosines of the x, y, z axes (three per axis). The director cosines, or the angles that each axis of the first system forms with the three axes of the second, uniquely describe the orientation of the local system with respect to the global one; they are not independent from each other since the axes of the reference systems are orthogonal to each other.
By applying the fundamental equation of trigonometry, the rigid body has six free coordinates (therefore six degrees of freedom), three of which are the free coordinates necessary to define the translation and three for the orientation in space, i.e., the rotation with respect to the **fixed (global) reference system** (Fig 1.6). The latter is the axis frame with respect to which the stereophotogrammetric system provides the reconstructed coordinates of the markers, as discussed more in detail in Section 1.5.1.

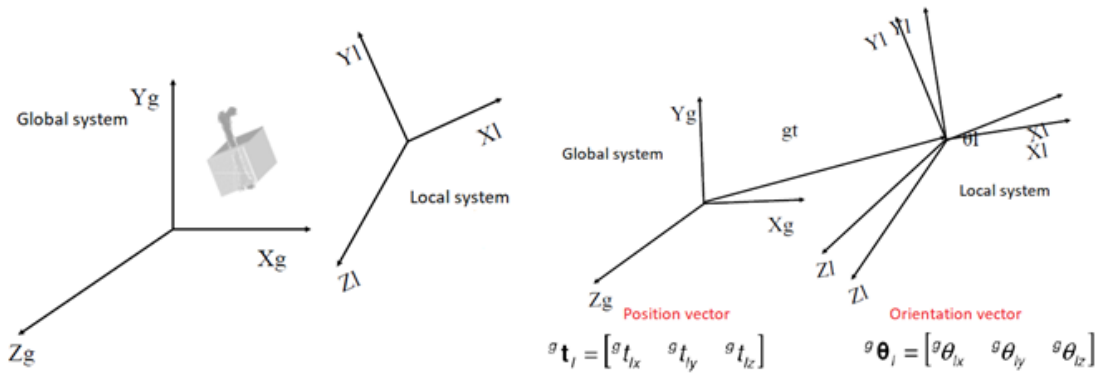

Fig. 1.6 Global and local system of a rigid body and its 6 degrees of freedom [11]

1.4.3 Joint kinematics

Joint kinematics is the study of the relative motion between two consecutive segments of the human body [13].

To describe the position of a bone segment in the global reference system, it is considered the local reference system rigidly associated with, rather than the segment.

After locating the reference system integral with the rigid body in space, the "relative" coordinates of any point belonging to it are known. To obtain these coordinates in the fixed reference system it is necessary to apply a roto-translation transformation, i.e., rigid transformations of points at each instant of time. The formula that expresses this transformation is as follows:

$$^{g}p = {}^{g}R_{l}\,{}^{l}p + {}^{g}O_{l}$$

Where ^{g}p and ^{l}p are the position vectors of the generic point p of the bone segment expressed respectively in the global and local system; the rigid translation is represented by the translation vector:

$$^{g}O_{l} = [{}^{g}O_{lx}, {}^{g}O_{ly}, {}^{g}O_{lz}]$$

The transformation of the coordinates of a point from a local and "rotated" reference system to the coordinates of the same point in a global and "fixed" reference system is given by the following rotation matrix:

$$ {}^{g}_{l}R = \begin{bmatrix} \cos\theta_{x_g x_l} & \cos\theta_{x_g y_l} & \cos\theta_{x_g z_l} \\ \cos\theta_{y_g x_l} & \cos\theta_{y_g y_l} & \cos\theta_{y_g z_l} \\ \cos\theta_{z_g x_l} & \cos\theta_{z_g y_l} & \cos\theta_{z_g z_l} \end{bmatrix} $$

A generic rotation matrix allows to obtain the position of the mobile reference system through three independent rotations of the fixed reference system; therefore, it can be obtained by composing three elementary rotations around predefined axes. This algebraically corresponds to multiplying three rotation matrices, each of which describes the elementary rotation performed. In order to have a physiological significance of the results, it would be advisable that the axes around which these rotations occur coincide with the functional articular rotation axes. This is also the reason why usually another reference system is used, called **anatomical reference frame.** This system is characterized by planes approximating the anatomical planes of human movement and whose axes are often used to represent the three translational and rotational degrees of freedom of a joint; it is determined using the relative anatomical landmarks identifiable by palpation and is therefore a system introduced to meet repeatability and intra/inter subjective requirements.

1.4.4 Anatomical components of the movement

The analysis of skeletal kinematics is based on the study of the relative position instant by instant of two rigid bodies, which represent two body segments. Supposing two adjacent body segments, one proximal and the other distal, connected by a rotational joint. Each segment is associated with a local reference system integral with it, which makes it possible to identify its position in space. In correspondence with the joint, a system of functional axes is defined around which the distal segment performs the following relative movements with respect to its proximal segment (Fig.1.7):

- *Flexion / Extension:* rotation of an angle α in the parasagittal plane belonging to the proximal segment
- *Adduction / Abduction*: rotation of a β angle that allows the segment to move towards / away from the medial plane of the body
- *Internal / external rotation:* rotation of an angle γ of the segment around its longitudinal axis

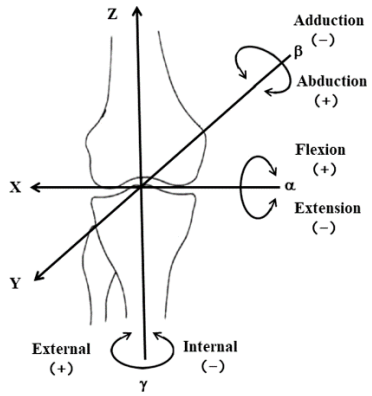

Fig. 1.7 Joint angles are defined by rotations occurring about the three joint coordinate axes [14]

The joint angles α, β and γ are used to quantify the extent of flexion/extension, adduction/abduction, and internal/external rotation movements. It is possible to identify, for each movement mentioned above, an axis around which it happens:

- The flexion/extension movement occurs around a mid-lateral axis of the proximal segment, therefore perpendicular to its sagittal plane
- The adduction/abduction movement occurs around an axis lying on the sagittal plane, oriented in a direction perpendicular to the longitudinal axis of the distal segment (anteroposterior if the flexion/extension is null)
- The internal/external rotation movement occurs around the longitudinal axis of the distal segment

1.4.5 Euler angles

An alternative method to uniquely identify the relative orientation between two cartesian axes is to use the Euler angles. By considering two triples, (O ', x, y, z) and (O, X, Y, Z), with the origin of the axes coincident, the intersection line of the X-Y and x-y planes is defined as the nodal axis N. It is possible to obtain the triad (O, X, Y, Z) by means of three successive rotations starting from the triad (O ', x, y, z).
Considering the two frames initially overlapping, a possible sequence of rotations is:

- the first rotation occurs around the z axis and has an amplitude α: the X axis overlaps the nodal axis N, the Y axis assumes a new position and the Z axis remains fixed
- the second rotation takes place around the N axis and has an amplitude β: the X axis remains fixed, the Y and Z axes assume a new position

- the third rotation takes place around the z axis and has amplitude γ: the X axis forms an angle γ with the N axis and, together with the Y and Z axes, assumes the final position

It is possible to observe the relative position between the two frames obtained following the three rotations in Figure 1.8.

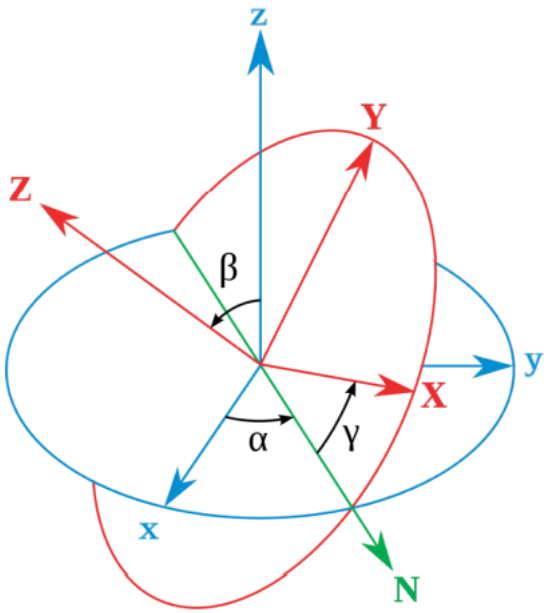

Fig. 1.8 Definition of Euler angles. Fixed system (O ', x, y, z), is represented in blue, the rotated system (O, X, Y, Z) is represented in red. The line of nodes N is represented in green. [15]

The three angles are called:

- *precession angle α*: angle between the N axis and the x axis, $0 \leq \alpha \leq 2\pi$
- *nutation angle* β: angle between the z axis and the Z axis, $0 \leq \beta \leq \pi$
- *intrinsic rotation angle γ:* angle between the x axis and the N axis, $0 \leq \gamma \leq 2\pi$

A rotation matrix is assigned to each rotation, which allows to obtain the coordinates of a point integral with the mobile frame with respect to the previous frame. It is possible to obtain these matrices by projecting the versors of the axes of the rotated system on the axes of the frame preceding the rotation. The total rotation matrix is the product of the three rotation matrices.

In addition to being an alternative to the use of director cosines, Euler angles are useful in determining the components of the angular velocity of the mobile system with respect to its axes and, adopting the Grood & Suntay convention, in uniquely defining the joint angles.

Considering the two triads integral to a proximal segment and a distal segment, the z axis is rotated by 90 ° until it assumes the orientation of the flexion/extension axis of the proximal segment, the Z axis assumes the function of axis of internal/external rotation as it is longitudinal to the distal segment, and the axis of the nodes N takes on the meaning of adduction/abduction axis (Fig. 1.9) [16].

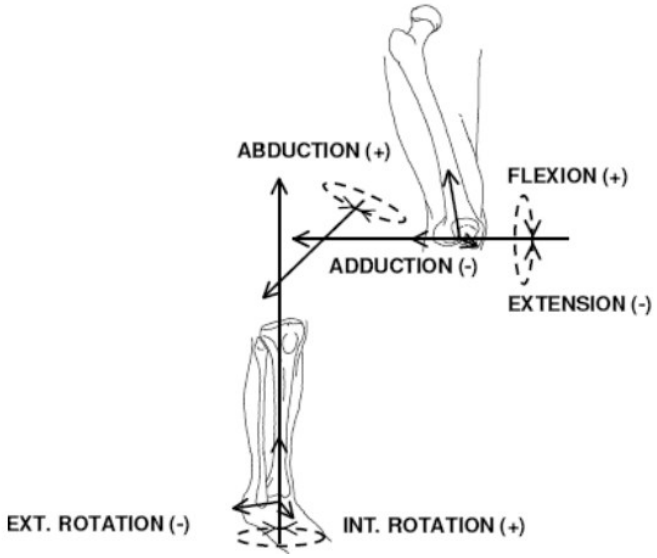

Fig. 1.9 Grood & Suntay convention [16]

1.5 Gait analysis instrumentation

In the last decade, the study of the gait has acquired considerable importance in various areas, in fact there are several tools available to quantitatively measure the path, which can be used both alone and in combination to get different information and a complete picture of the gait. In general they can be divided into [17]:

- **Non-wearable devices**: stereophotogrammetric systems, force platforms
- **Wearable devices**: electrogoniometers, foot switches, pressure and force sensors, electromyographic sensors, inertial sensors

1.5.1 Non-wearable devices

Non-wearable devices allow the simultaneous analysis of multiple parameters and measurements are controlled in real time by a specialist. Using this typology, it is possible to carry out tests and studies with high reproducibility, repeatability, and precision. Furthermore, they are not invasive systems and limited from an energy point of view since they do not need to work with a battery. However, they also have negative aspects, such as the cost of the tools and the inability to study the subject's daily activities outside the laboratory.

Stereophotogrammetric systems

The use of this system allows, through two or more cameras, to record the subject while walking or any other motor activity that you want to analyze. Gait analysis laboratory and specialized personnel are therefore required, which makes this method laborious and expensive in terms of time and practicality.

The system involves the use of markers, active or passive, positioned in anatomical points defined by appropriate protocols, which make the tests repeatable and comparable to each other as much as possible. By means of two or more cameras it is possible to reconstruct the position of each marker in three dimensions at any instant of time, in this way it is possible to calculate displacement, speed, acceleration and joint angles of each body segment in which there are at least three markers visible by the system (Fig. 1.10).

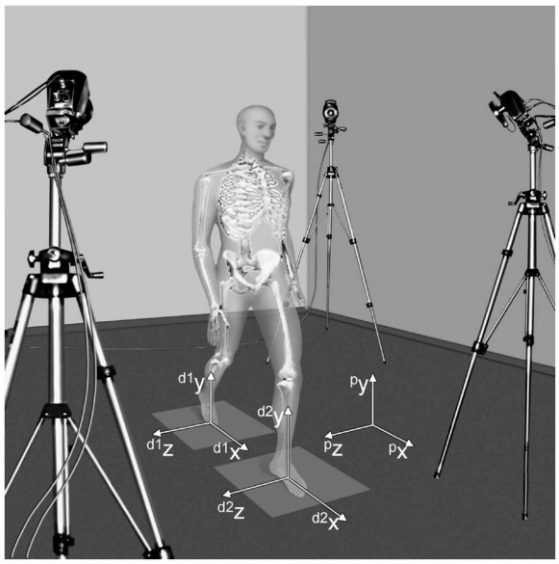

Fig. 1.10 Gait analysis by means of stereophotogrammetry [18]

Optoelectronic systems, which use cameras operating in the visible or near infrared range, represent, in fact, the most widespread technological solution for estimating human movement. Although they guarantee high accuracy, such systems provide an estimate and not a direct measure of the kinematic variables. They exploit geometric characteristics (points, lines, areas) located on the body surface of the subject, whose imaged acquired by several cameras are reconstructed in three dimensions [18].

The positive aspect therefore lies in the fact that the measurements are reliable, as they come from a video-recorded analysis processed with appropriate software, which makes this a **gold standard tool.** However, as previously mentioned, performing an examination of this type requires the use of a laboratory with expensive instrumentation and an accurate calibration is also required for the quality of the measured data. In fact, first, it is necessary to carry out a calibration procedure to define the calibration volume, the absolute reference system (origin and axes of the laboratory system), the internal and external parameters of the cameras. To obtain the three-dimensional reconstruction of the position of each marker, it must be framed, at any moment, by at least one pair of cameras. Following the acquisition, the markers are recognized and classified consistently with the protocol used. The various acquired signals are integrated and sent to the computer system for their elaboration and for the reconstruction of the kinematic trajectories. Through the latter, the joint angles of the movement considered at each moment are obtained.

Although these tools guarantee a high accuracy in the measurement of the coordinates of the markers, the kinematic variables relating to the joints obtained from them are affected by various types of errors. These errors can be classified into:

- **instrumental errors**: they can be systematic, due for example to an inaccurate calibration, or random, due to electronic noise or flickering of the markers
- **incorrect placement of the markers** on the anatomical landmarks: identifying the landmark can be complicated since it does not always correspond to specific points but sometimes to surfaces; furthermore, the process can be complicated by the presence of soft tissue
- **soft tissue artifacts (STA):** caused by sliding of the skin, deformations, inertial effects, movement of the underlying muscles and the presence of abundant adipose tissue

These errors represent a source of inaccuracy which compromises the determination of the coordinates of the anatomical points of reference, of the articular centers and of the axes of rotation in space and consequently the calculation of the kinematic variables [18].

1.5.2 Gait protocol

The different protocols for motion analysis have been developed with the aim of creating a standardized and repeatable over time methods of: carrying out the analyzes, positioning of the markers, calculating the variables of interest and the methods of presenting the results obtained. A protocol, in general, mainly has the following objectives:

- uniquely define the anatomical landmarks on which to apply the markers, to position them following a predisposed biomechanical model
- define the anatomical structures of reference, identifying the correspondence between the position of the markers and the underlying body segments
- define the procedures for data acquisition, processing, and analysis
- make kinematic and dynamic parameters clinically interpretable

Over the years, many protocols for motion analysis have been developed depending on the specifics of analysis and use. The most important are:

- Davis protocol (1991)
- CAST protocol of Cappozzo et al. (1995)
- IOR Gait protocol

I. DAVIS protocol:

The Davis et al. [19] was created in 1980 at Newington Children's Hospital (USA) with the aim of providing a quantitative assessment of human locomotor function.

The Davis protocol provides a succession of steps. The preliminary stages include:

- recording a series of videos of the subject's walk
- physical assessment of the subject to obtain information on strength, tone and possible muscle contractures, on the joint range of motion and on bone anomalies
- acquisition of anthropometric variables such as weight, height, length of the tibiae, distance between the femoral condyles (or the diameter of the knee), distance between the left and right anterior superior iliac spine (ASIS) and vertical distance between the ASIS and the greater trochanter, in the sagittal plane, of the supine subject. These measurements are subsequently used to estimate the position of the joint centers and the inertial parameters of the anatomical segments.

The next phase deals with the positioning of the passive reflective markers on the body surface using double-sided tape. In addition to the markers applied directly to the skin, the so-called "extended" markers are also used: these are spherical markers supported by a plastic wand fixed to a rectangular plastic support plate. The latter rests on the surface of the body segment of interest and is held in position by an elastic band. The marker-set is composed of a total of 22 markers, as shown in Figure 1.11, positioned according to the following specifications:

- **trunk:** three markers, two at the right (RS) and left (LS) sternoclavicular junctions and one at the level of the spinous process of C6 (N) placed on a wand so that the line passing through the sternum joint -clavicular and the C7 vertebra is parallel to the plane formed by the markers
- **pelvis:** three markers, two on the right (R) and left (B) anterior superior iliac spines ASIS and one at the level of the sacrum (H) placed on a wand. The three points are identified so that they lie in the plane containing the ASIS and the posterior superior iliac spines PSIS
- **thigh:** three markers at the greater trochanter (RH), the femoral epicondyle (RK) and one placed at 1/3 of the length of the thigh on a wand (RF). The three points are identified so that the plane on which they lie is parallel to the frontal plane
- **leg:** three markers, one on the lateral malleolus (RA), one on the fibula head (RP) and another at 1/3 the length of the leg on a wand (RB). The three points are positioned so that they lie on a plane containing both the epicondylar axis and the longitudinal axis of the leg
- **foot:** two markers, one on the metatarsal head of the fifth toe (RT) and another on the calcaneus (RQ) positioned so that the vector between the RT and RQ markers is aligned with the line of progression of the foot. The RQ marker is used only during static acquisition

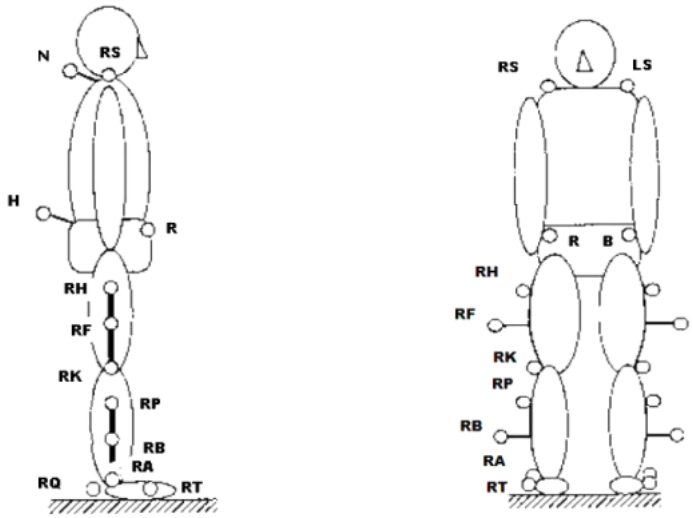

Fig. 1.11 Marker-set developed and used at Newington Children's Hospital [19]

The next phase involves a brief static acquisition of the subject in an upright position in order to obtain the initial position of the markers with respect to the body. This information, integrated with the anthropometric measurements taken in the preliminary phase, allows the estimation of the joint centers. Subsequently, at least three barefoot walking tests are acquired within the acquisition volume, from which the trajectories of the markers are obtained. They allow to obtain the kinematic variables such as the relative displacement of the body segments in the three dimensions, i.e., the joint angles. The knowledge of anthropometric measurements also allows calculating the masses of the segments, their center of mass and the calculation of the moments of inertia. Based on these variables, the reference system of each body segment is defined, which has its origin in its center of mass. For each lower limb, three reference systems are constructed (thigh, leg and foot) to which is added that of the pelvis. Figure 1.12 shows these reference systems and their orientation with respect to each segment.

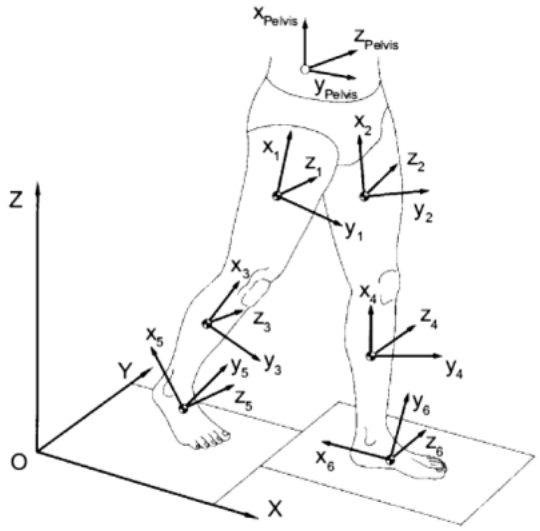

Fig. 1.12 Axis systems referring to the pelvis, thigh, leg, and foot segments according to the Davis et al Protocol [19]

The arrangement of these markers is optimal for acquisition as they are clearly visible. However, although it is chosen a layer of tissue that is as thin as possible for the application of the markers, one of the main sources of error in the reconstruction of the joint centers is due to the artifacts from soft tissue, which are related to the relative movement between the layer of skin on which the marker is applied and the reference point to which it refers. This artifact is more significant in the case of extended markers placed on the thigh and leg; in fact, the use of wands introduces errors because they are subject to vibrations and, in the case of rapid and large movements such as walking on a ladder, they are more subject to the activity of the underlying muscles. The error introduced in the reconstruction phase of the internal points, since the latter are used in the definition of the joint rotation axes, generates errors in the calculation of the kinematics.

II. CAST protocol:

The protocol developed by Cappozzo et al. in 1995 [20] is known with the name “Calibrated anatomical system technique” (CAST), that is an anatomical calibration technique. It was created in 1995 at the La Sapienza University of Rome, in partnership with the Rizzoli Orthopedic Institute of Bologna, to quantitatively describe the kinematics and joint dynamics in the clinical and research fields using stereophotogrammetric systems. Among the main objectives there is the reduction of soft tissue artifacts (STA), which represent the main source of error in the experimental determination of the orientation and three-dimensional position of

the bone segments. For the reconstruction of the joint kinematics, the CAST protocol uses the so-called "anatomical calibration" approach which allows to obtain the coordinates of the anatomical landmarks of interest (with respect to the technical reference system of the body segment considered) through additional acquisitions, without requiring anthropometric measurements.

To define the technical reference system, at least three misaligned markers (cluster of markers, Figure 1.13) are used, placed on the skin of the considered bone segment, in positions that do not correspond to anatomical points. In order to minimize STA, it is important the choice of the tissue area on which to apply these markers and sometimes it is chosen to place them on more or less rigid plates to limit relative movements. However, the use of plates could induce the patient to make incorrect and unnatural movements, altering the acquisitions and introducing other types of errors due to their weight.

After determining the technical reference systems, the position of the anatomical landmarks is obtained with respect to the systems. The number of such points is redundant compared to the one actually needed, but this allows a better estimate of the anatomical reference systems, of the joint axes and a more realistic graphic representation of the bone segments. Among the anatomical landmarks, the identifiable ones are directly used in the definition of the anatomical reference systems while the others are used to determine some of the aforementioned points, for example the center of the femoral head.

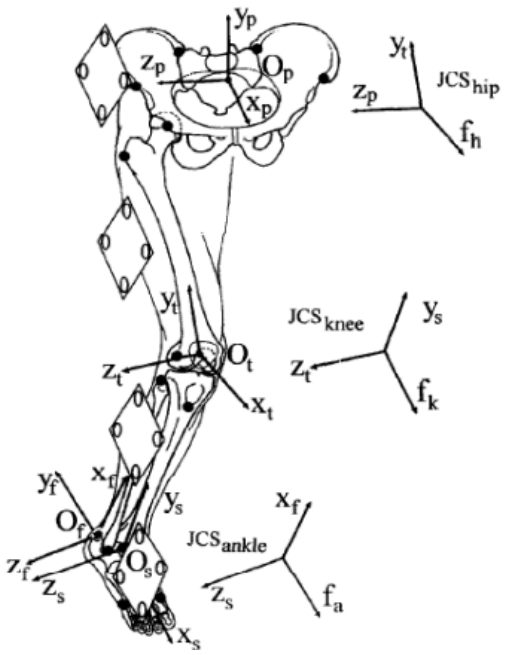

Fig. 1.13 Example of cluster on rigid plate; four markers (white dots) applied on the plate that is attached to the relative body segment. Representation of the technical reference systems and of the reconstructed anatomical landmarks (black dots) [20]

The marker-set of the CAST protocol provides for the identification of the following anatomical reference points:

- **pelvis:** anterior superior iliac spine (ASIS) and posterior (PSIS), center of the acetabulum (AC)
- **femur:** femoral head (FH), greater trochanter (GT), medial epicondyle (ME), lateral epicondyle (LE), anterolateral (LP) and anteromedial (MP) apex of the patellar surface, lateral (LC) and medial (MC) condyle
- **leg:** intercondylar eminence (IE), tibial tuberosity (TT), fibula head (HF), medial (MM) and lateral (LM) malleolus, medial (MMP) and lateral (MLP) points of the tibial surface
- **foot:** upper point of the calcaneus surface (CA), first (FM), second (SM) and fifth (VM) metatarsal head

The CAST protocol has the advantage of greater freedom in the positioning of markers and cameras and great efficiency in minimizing the variability introduced by the STA. However, it requires numerous calibrations (one for each anatomical landmark) which involve extensive patient preparation. Furthermore, if the plate slips with respect to the initial position during the movement, all the values obtained for the landmarks would inevitably be altered.

III. IOR Gait protocol:

The Leardini protocol, more commonly known as IOR-Gait, was developed in 2007 at the Rizzoli Orthopedic Institute, Bologna [21]. The aim was to satisfy two main, apparently conflicting, requirements:

- reduce the preparation and collection time of patient data, as well as the entire anatomical calibration procedure
- guarantee a certain accuracy and reliability of the results.

The first requirement, in addition to minimizing the disturbance caused to the patient, is necessary when he is unable to remain still for long periods, especially if numerous markers have been positioned. Furthermore, the calibration phase may require additional movements. This protocol takes into consideration both the need to minimize the marker-set and to apply them in easily accessible landmarks, and to limit the data acquisition procedures.

Leardini, with the proposed protocol, still wants to ensure a complete description of the 3D movement of the body segments and joints by means of an optoelectronic system, in accordance

with international directives. The proposed marker-set involves the use of passive markers with a diameter of about 10mm and reflective. They are located in the following positions (Figure 1.14):

- **pelvis:** four markers, two on the right anterior superior iliac spine (RASIS) and left (LASIS), two more on the right posterior superior iliac spine (RPSIS) and left (LPSIS)
- **femur:** two markers, one on the outermost protuberance of the greater trochanter (GT), the other on the lateral femoral epicondyle (LE)
- **leg:** three markers, one on the external apex of the fibula head (HF), one on the protuberance of the tibial tuberosity (TT) and the other on the external apex of the lateral malleolus (LM)
- **foot:** three markers, one on the heel (CA), two on the dorsal end of the fifth (VM) and first (FM) metatarsal head.

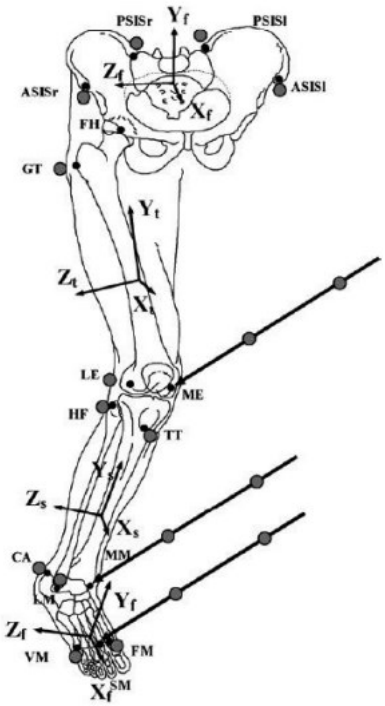

Fig. 1.14 Representation of anatomical landmarks (black dots), passive markers (gray dots) including those on the pointer for anatomical calibrations and anatomical reference systems for the pelvis (p), thigh (t), leg (s) and the foot (f) according to the IOR gait protocol [21]

The IOR Gait protocol offers a reliable definition of the anatomical planes. The good accuracy of the measurements is however limited by the use of markers on the skin, which are subject to the aforementioned STA.

1.6 Dynamics of the locomotor system

Human movement is a complex act resulting from the presence of internal (muscular and articular) and external (gravity, reaction to the ground) forces which presupposes the interaction of different systems in order to maintain postural control, balance and to allow the carrying out of motor acts. For this reason, it is necessary to complete the analysis of human movement with the calculation of dynamic variables such as moments and joint powers. This can be done through the solution of the *Dynamic Problem*, which allows in its *Direct* approach to obtain the resulting movement (displacements and rotations) from the application of a system of external forces and in its *Inverse* approach to calculate the forces associated with a certain movement. The most used approach in dynamic motion analysis is the *Inverse* one which starts from the knowledge of kinematic variables and, through algebraic nonlinear equations, calculates forces and moments.

Given the assumption of attributing the movement of an anatomical segment to its bone component and modelling it as a rigid body, also the inertial properties (mass and moments of inertia) of the entire anatomical part can be attributed to it. For the analysis of movement, the human body is schematized as a chain of rigid segments connected by ideal friction-free joints located at the joint centers. If we consider a part of the structure, which is ideally isolated from the rest of the body at point O, generating at its extreme forces and moments that the rest of the body exerted on it. Assuming that these segments are subject, in a certain instant, to a linear acceleration a of the center of gravity, an angular acceleration α and an external force F_e, the *dynamic equilibrium equations* referred to point O are the following:

$$d\Gamma/dt = \Sigma M$$
$$dQ/dt = \Sigma F$$

The dynamic problem can be traced back to a static problem by considering the forces and moments of inertia as external forces and moments applied to the system. The *equations of static equilibrium* will then be:

$$M_o + M_i + M_{Fi} + M_p + M_{Fe} = 0$$
$$F_o + F_i + F_p + F_e = 0$$

F_o and M_o are the net constraint reactions at the considered joint (point O), M_i and M_{Fi} are the rotational moment and the inertia force, F_p is the weight force and the resulting moment M_p and, finally, F_e and M_{Fe} are the force and the external moment. The resolution of these equations presupposes the knowledge of anthropometric, kinematic and inertial data. Part of the anthropometric data is collected during the preliminary stages of the acquisition; the rest are calculated with the use of data and tables. The kinematic variables, such as the position of the markers and the subsequent estimate of the joint centers, are calculated following the acquisition of evidence using stereo-photogrammetric systems (see *Paragraph 1.5.1*).

The inertial data, including dimensions, mass, position of the center of gravity and moments of inertia of each segment, can be obtained from specific anthropometric tables and are based on measurements made on anatomical samples from cadaver or estimates obtained on "in vivo" subjects. The data obtained, which refer to different populations, age ranges and sexes, are present in the literature in the form of statistical data. The use of such data inevitably involves an error due, for example, to the use of an anatomical measure (based on anatomical landmarks) rather than biomechanical (based on a subdivision of the segments corresponding to the joint centers), and it is necessary to take it into account when interpreting the results.

1.6.1 Force plates

Force platforms are rigid platforms coupled with force sensors and at least two are placed along the subject's path for a gait analysis examination.
The dynamometric platform (or force platform) is a tool based on the principle of action and reaction. For optimal use it needs to be anchored to the ground as any movements of the instrument generate errors in the measurements. In some cases, anchoring is not carried out with all possible precautions, because it may be necessary to move the platform easily and take measurements in multiple environments.
Force platforms measure and record the ground reaction forces (GRFs) and their point of application (centre of pressure, COP). A GRF is made up of three components acting at the centre of pressure. The three components can be categorized in an anatomical sense as vertical forces (the weight of the body and how it progresses over the supporting limb), anterior–posterior forces (the accelerating and braking forces) and medial–lateral forces (the force acting

from side to side) [22]. The analysis of these variables plays an important role in assessing the internal loads and the risk of injury to the lower limbs. Furthermore, the platforms can be perfectly integrated with a stereophotogrammetry system, thus knowing both the system of forces exchanged to the ground and the kinematics, it is possible to calculate the moments and powers at the various joints, and therefore carry out a complete analysis of the movement.

Force plates measure foot-ground reaction forces thanks to load cells consisting of resistive strain gauges or piezoelectric crystals.

Strain gauge force plates have 4 load cells. Strain gauges are able to vary their resistance according to the deformation to which they are subjected, according to the law:

$$R=\rho*(L/A)$$

Where: R is the resistance; ρ the resistivity of the material; L is the length of the strain gauge; A is the (constant) section of the strain gauge.

If fed with a current of intensity I it is able to produce a voltage V = R * I, that is an electrical signal that can be digitized and converted into the corresponding applied force value. As long as the deformation persists, the output signal also remains. Strain gauges therefore do not require dedicated electronics for measurements, but only a signal amplification and an electrical power supply.

Piezoelectric force plates on the other hand have three load cells containing a piezoelectric crystal, which behaves like a capacitor to which a potential difference has been applied. So, if the two faces are connected through an external circuit, an electric current is generated, called piezoelectric current that can be digitalized as well.

Each cell, whatever technology it uses, measures the force applied along the 3 axes of a predefined triad and returns a result in 3 dimensions. Using the statics equations, it is then possible to obtain the point of application and the modulus of the final resulting force in the three spatial directions. The coordinate system of the platform is determined by the alignment of the piezoelectric crystals on each pylon, which are aligned with the x, y and z axis of the platform (Figure 1.15)

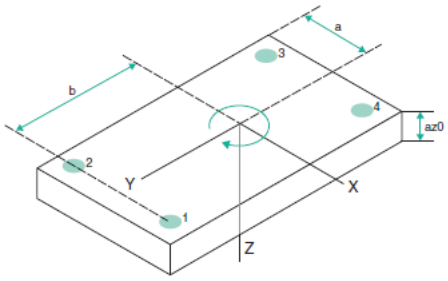

Fig. 1.15 The coordinate system of a force platform [22]

All platforms are subject to a disturbance called cross-talking, due to the fact that the channels are not only sensitive to a specific load component (x, y, or z, as it should be) but also to the other components. This problem can be solved via the calibration matrix. Multiplying the outputs of the force plate by the coefficients of the calibration matrix supplied by the manufacturer, it is possible to obtain values of the desired force components.
Data tables containing the following information are obtained from the processing software to which the platforms are connected:

- sample number (corresponds to the sampling time)
- measured force (FX, FY, FZ)
- position of the application point (PX, PY, PZ)

The acquisitions can take place synchronously for several platforms. Sampling takes place at the frequency set by the software.

1.6.2 Ground reaction forces during walking

A GRF is a force that acts on a body as a result of the body resting on the ground or hitting the ground. If we first consider a person standing on the floor without moving, the person will be exerting a force on the floor, but the floor will be exerting an equal and opposite reaction force on the person. This reaction force is known as the GRF [22].
The ground reaction (Ground Reaction Forces-GRF) is studied with respect to the different directions and the different events of the stance.
The body weight (BW) is used to normalize the support reactions of each subject. The maximum values of the reaction of support in the vertical direction are in the order of 110%

of the BW, in the order of 18% in the longitudinal direction and of the 5% in the transverse direction [15] (Fig. 1.16).

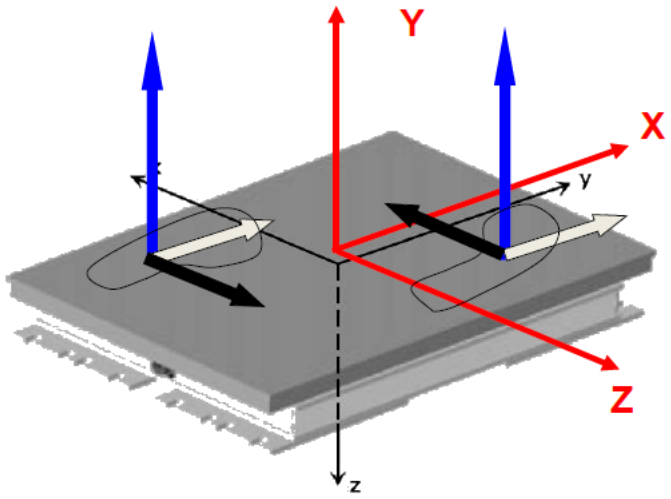

Fig. 1.16 Reference Frames force platform [15]

Where the reference frames of:
Platform (in black): x, y, in the ground, z vertical;
Global laboratory (in red): X gait direction, Y vertical upwards, Z lateral, Right Hand Rule; Ground reactions: FV vertical (+ upwards) in blue, FL longitudinal (+ forward) in grey, FT transversal (+ from Lateral to Medial) in black.

Vertical force measurements are by far the most quoted in the literature and a variety of useful measurements may be taken. Including the first peak or maximum vertical loading force; the dip trough, which can give useful information about the movement of the body over the stance limb; and the second peak or maximum vertical thrusting force. The timing at which these peaks and troughs occur can also be a very useful measure. So, corresponding timing measures are: the time to the first and second peaks (the time to maximum vertical loading and maximum vertical push-off force), the time to the trough (which is sometimes referred to as midstance), and the total contact time. (Fig 1.17) [22].

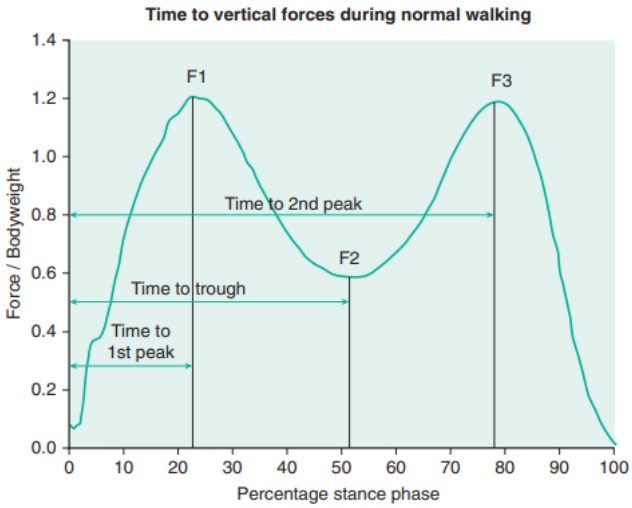

Fig. 1.17 Timing and force in vertical direction during normal walking [22]

The vertical component of the GRF can be split into four sections. Each section may be related to functional events during foot contact and can give us important information about the overall functioning of the lower limb:

- **Heel Strike to First Peak:** This is where the foot strikes the ground, and the body decelerates downwards and transfers the loading from the back foot to the front foot during initial double support. The first peak should be in the order of 1.2 times the person's body weight
- **First Peak (F1) to Trough (F2):** As the body starts to progress the knee extends, raising the center of mass. As the center of mass approaches its highest point it is slowing down or decelerating its upwards motion. This deceleration of the body upwards produces a dip or trough in the vertical force pattern, with the normal value being in the order of 0.7 times the person's body weight
- **Trough (F2) to Second Peak (F3):** The center of mass now falls as the heel lifts, and the foot is pushed down and back into the ground. Both the deceleration downward and propulsion from the foot and ankle complex cause the second peak. The second peak should be in the order of 1.2 times the person's body weight
- **Second Peak (F3) to Toe Off:** The foot is unloaded as the load is transferred to the opposite foot

1.7 Wearable devices

The wearable devices are easily miniaturized and cheap, some of these allow a real-time visualization of the acquisition data by an expert operator and the monitoring of the walk-in daily life and over long periods. However, some of these devices, such as inertial sensors, are limited in power consumption due to the short battery life. Furthermore, the measurable parameters are limited, and the sensors can be influenced by external uncontrollable factors.

1.7.1 Inertial sensor

Inertial Measurement Units or IMUs are miniaturized electronic devices that come with a full set of MEMS (micro electro-mechanical systems) sensor to determine the change in relative orientation of a body or body segment over time. IMUs usually include a combination of gyroscopes and accelerometers but may also include magnetometers or a global positioning system (GPS) to provide attitude, heading and global positioning. Triaxial sensors are used in IMUs, so that three-dimensional motion of segments relative to other segments can be calculated [22].

Inertial sensors can be used individually, but for biomechanical applications these have been incorporated into MoCap suits (e.g., the XSENS MVM suit) (Fig.1.19) and systems that can use two or more sensors to measure specific joints (e.g., Delsys). These systems use an inertial sensor to represent each body segment. They are an exciting development for clinicians, as they are able to measure three-dimensional movement outside of a laboratory setting. Their accuracy is, however, dependent upon the quality of the combined sensor system and the algorithms used to calculate the three-dimensional position and orientation of each segment. Inertial sensors have been used in sports, such as downhill skiing, speed skating, horse riding and baseball pitching, and in studies involving clinical gait assessment and clinical tasks, such as sit-to-stand [23].

Fig. 1.18 Xsens MVN consists of 17 inertial and magnetic motion trackers [24]

Accelerometers

Accelerometers are based on different technologies, but the operating principle is the same: it is based on the detection of the inertia of a mass subjected to acceleration. The mass is connected to an elastic element and its position over time is acquired by a sensor. In the presence of an acceleration, the mass (which has its own inertia) moves from its rest position in proportion to the acceleration. The sensor transforms this displacement into a digitizable electrical signal [11].

Accelerometers can be classified according to the operating principle of the position sensor:

- **Strain gauge accelerometer**: it uses the same principle of detection as the dynamometric platforms, i.e., the variation of resistance of a strain gauge. In these devices a mass is suspended on thin laminations. In the presence of an acceleration, the mass moves, flexing the laminations and deforming the strain gauges. The voltage produced is proportional to the acceleration
- **Piezoresistive accelerometer:** it is a variant of the strain gauge accelerometer, where piezoresistive sensors are used instead of strain gauges
- **LVDT accelerometer**: it uses a Linear Variable Differential Transformer (LVDT) sensor. In these devices, the mass is composed of a ferromagnetic material and flows (suspended on springs or other elastic elements) inside a coil generating an induced current in the coils. A special circuit detects the position of the core with respect to the coils and generates an electrical signal proportional to the displacement

- **Capacitive accelerometer:** it exploits the variation of the electrical capacity of a capacitor as the distance between its plates varies. The mass (made of conductive material) constitutes an armature, while the other is made on the fixed structure of the device. When the mass moves, the capacitance of the capacitor varies (which depends on the distance between the plates) and a special circuit detects the change according to the position
- **Piezoelectric accelerometer:** it uses the electrical signal generated by a piezoelectric crystal. The mass is suspended on the piezoelectric crystal, which, in this case, constitutes both the sensor and the elastic element. In the presence of an acceleration, the mass (which has a certain inertia) compresses the crystal

Accelerometers are generally monoaxial, to have a triaxial one you just have to arrange 3 monoaxial in order to form a cartesian triad.

Gyroscope

The gyroscope is a rotating physical device which, due to the conservation law of angular momentum, tends to keep its axis of rotation oriented in a fixed direction, providing direct measures of the angular velocity in the local coordinate system of the sensor in the three planes [22]. Essentially it consists of a toroid-shaped rotor that rotates around its axis, when the rotor is rotating its axis tends to remain parallel to itself and to oppose any attempt to change its orientation (Fig. 1.20). This mechanism was invented in 1852 by the physicist Jean Bernard Léon Foucault as part of his studies on the Earth's rotation. If a gyroscope is installed on a gimbal that allows the wheel to orient freely in the three directions of space, its axis will remain oriented in the same direction even if the support changes orientation, providing information on the relative orientation of the device that contains it.

There are mechanical, optical and microelectronic gyroscopes with vibrating mass. Conventional mechanical and optical gyroscopes are widely used in navigation field, but they are not suitable in human motion analysis as they are expensive and bulky. The MEMS vibrating mass gyroscopes, on the other hand, are small, economical and consume less. They are therefore ideal in the analysis of human movement.

In the biomechanical field, gyroscopes can be applied to any part of the body, and thanks to their portability they are often used for recording walking for long periods. In fact, from the measurement of the angular velocity, useful data can be obtained for clinical and sporting purposes such as: the length of the walking cycle, the length of the stride, the stance and swing

time, useful for both clinical and sporting purposes.

The main problem with gyroscopes is the presence of small offsets that cause signal drift and unacceptable errors during the integration process necessary to evaluate changes in orientation. As with accelerometers, a triaxial gyroscope can be obtained as a combination of three uniaxial gyros. The output of a calibrated 3D gyroscope is the angular velocity expressed in the sensor's reference system, i.e., the angular velocity measured with respect to the X, Y, and Z axes [25].

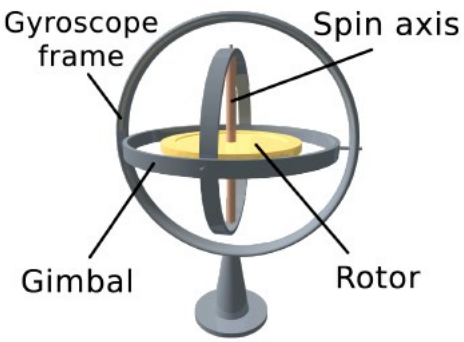

Fig. 1.19 Elements of a gyroscope

Magnetometer

The magnetometer is an instrument that measures the local magnetic field along three predetermined axes. The earth's magnetic field has a component parallel to the earth's surface that always points towards magnetic north, consequently its projection on the horizontal plane can be used to determine the orientation of a magnetometer in space.

The design of many magnetometers integrates three magnetic sensors, whose axes form a Cartesian triad. From the projections along the axes, it is possible to trace the horizontal component of the earth's magnetic field, as long as the inclination of the sensor's case is estimated using a gravity sensor.

In motion analysis, the measurement of the earth's magnetic field is necessary to allow monitoring in the three dimensions of the orientation of the sensors. Without it would not be possible to identify the local reference system of the sensors in the global reference system of the earth, in which the measurements are analyzed. In other words, the accelerations along the anatomical axes mentioned above could not be determined and the information from the sensors

would be almost unusable.
Magnetometers are affected by the magnetic fields created by electronic equipment and ferromagnetic material. For the measurement to be reliable it is therefore necessary to perform the measurements sufficiently far (at least 2 meters) from the acquisition equipment and from structural elements that can disturb the measurements (for example reinforced concrete walls or metal beams) [22].

1.7.2 IMU errors

IMUs are affected by error [11], in particular error in:

- **Repeatability:** the ability of a sensor to provide the same result, under the same circumstances, over time (Turn-on to Turn-on Bias).
- **Stability:** deals with the ability of the sensor to provide the same output, over time, if it receives the same constant input
- **Drift:** is an accumulation of an error in the signal over time, i.e., the variation of the signal output over time

Although IMUs are increasingly miniaturized and often combined with wireless data acquisition capabilities, which makes them extremely attractive for biomechanical analysis, they do suffer from inherent measurement issues. To measure the position and orientation of a segment, the IMU must integrate the raw data outputs from the accelerometer and the gyroscope. The position of the segment in space is calculated from the accelerometer, and then the orientation is calculated once the position is known, so the accuracy of the gyroscope depends on the accuracy of the accelerometer to determine the correct position. Therefore, a constant error in acceleration becomes a linear error in the estimate of the speed (integral) and a quadratic error in the estimate of the position (double integral).
Accelerometers tend to be sensitive to pressure, temperature and height changes and if these are not corrected, this can introduce a bias in the data which can cause drift.
Some IMUs compensate for temperature drift by using temperature sensors that correct the bias, and some eliminate pressure drift by creating a sealed environment at a fixed pressure [26]. Magnetometers can also be used to assist with the correction of drift bias, as they provide information on attitude and heading that can be included as part of a correction algorithm. Another issue with IMUs is that accelerometers suffer from noise. This results in overestimated, oscillatory acceleration measurements, which are usually corrected by filtering the raw signals

before the data is integrated.
Finally, the capture frequency of the IMU is important because the sensor can only estimate what happens in relation to position and orientation between each data point, which may mean that some of the real movement is lost if the sensor only captures at low frequency [22].

A fundamental issue with using IMUs to assess human motion is that each IMU sensor will have a global orientation which is not aligned with any physiologically meaningful axis [27].This orientation can be represented by a quaternion, a rotation matrix, or Euler angles. A number of algorithms have been proposed for sensor orientation estimation. Typically, these use the integration of the angular velocity to estimate angular orientation; however, the signal can ‘drift’. This can in part be reduced using acceleration and/or magnetometer measurements. although the presence of magnetic disturbances can affect the accuracy of the orientation estimates. Through a fusion and integration of these different measurements, the IMUs are able to estimate the orientation (roll, pitch and yaw), the position, and the direction of movement of the sensor in a global coordinate system. From this, the relative positioning of two or more sensors can be found. These can then be used to calculate the angle between sensors, which can be used to calculate joint angles in the different planes, providing an anatomical frame can be obtained

Therefore, the advantage of using this type is the high portability and low cost, thus allowing the study of the gait in everyday life having the smallest possible footprint for the subject. The disadvantages in using this sensor reside in the fact that, in addition to being susceptible to uncontrollable external interference, the measurements obtained from this sensor are indirect measurements and require complex algorithms for calculating the parameters of the gait cycle.

Chapter 2

2. Musculoskeletal modelling

Musculoskeletal models for biomechanical simulations have become increasingly popular for analyzing human movement. In addition to joint kinematics and kinetics, musculoskeletal models allow researchers and clinicians to evaluate other biomechanical variables that cannot be measured *in vivo*, such as muscle lengths and forces. Various software have been developed to model and analyze human movement (e.g., AnyBody, OpenSim, and Human Body Model) and there is always an increase in literature reporting motion analyzes based on these software systems [28].

This thesis will follow two basic approaches to get the results of joint kinematics, kinetics, muscle activations and joint contact forces. The first one using a musculoskeletal model of the lower limb together with marker trajectories and ground reaction forces, measured using 3D motion capture. While the second approach still uses the same knee model, but with only measurement data obtained from inertial measurement units (IMUs).
This second chapter will cover an overview of the functionality of the OpenSim software, focusing on the main steps necessary to create and analyze dynamic simulations of movement and underlining the main workflow of OpenSim when using Motion Capture and IMUs data.

2.1 OpenSim

OpenSim is an open-source software that allows modelling, analysis and simulation of the musculoskeletal system. The history of this program starts from the 90's, during which a development environment for the modelling of the musculoskeletal system called SIMM (Software for Interactive Musculoskeletal Modeling) was born, which allowed to evaluate and modify existing models or create new ones [29]. Many researchers began to approach this environment which nevertheless presented some limitations, in particular on the analysis of dynamic simulations. The biggest problem, however, was related to the source code of the program, which was not completely available, preventing the possibility of development, especially the commercial versions were limited to use only. To solve these limitations Opensim was born, whose main strength lies in being open source. The first version of the software was developed in 2007 by the American Society of Biomechanics Conference, to which an

Application Programming Interface (API) was added in the next version, in which users can access the program components by modifying them. The plug-in architecture encourages users to extend the functionality of the software through personal development of muscle models and data analysis obtained from simulations, thus providing a tool of rapid diffusion for the entire biomechanical community. Before the birth of these open-source systems, it was very difficult to carry out simulations outside the laboratory where they were developed, the results were therefore difficult to reproduce, and researchers were forced to spend a lot of time to implement new simulations and the related tools to analyze them.

With the development of these new software, various musculoskeletal systems were born, in particular for the lower limbs, through which various parameters can be estimated including the length of muscle fibers, speed, acceleration, in both physiological and pathological. The graphic interface has many features, for example you can view the 3D muscle model, add, or remove muscles to the model, view the simulation results directly on the model.

2.1.1 Musculoskeletal Models

To create a simulation of a movement, first of all a definition of a dynamic model of the musculoskeletal system must be done, and its interactions with the environment. The elements of the musculoskeletal system are modeled by differential equations describing the dynamics of muscle contraction, the geometry of the musculoskeletal system and the dynamics of body segments (Fig. 2.1). These equations characterize the time-dependent behavior of the musculoskeletal system in response to neuromuscular excitation.

The body segments (e.g., trunk, pelvis, and femur) require the definition of body segment parameters, i.e., the mass, inertia, and center of mass location. In the model, body segments are connected to each other by joints, which describe the degrees of freedom (DOF) or relative motion of the segments with respect to each other.
Therefore, in OpenSim, a musculoskeletal model consists of:

- Bodies: rigid segments representing bone components or other elements of the model like platforms
- Joints: connect the bodies to each other
- Forces: the muscles that extend between the bodies
- Constraints: lock degrees of freedom of the model

The OpenSim library provides musculoskeletal models already developed, which are mainly divided into models representing the lower limbs and upper limb models. These differ from each other in the presence of one limb or both, in the number of degrees of freedom available and in the muscles represented. In particular, a wide range of lower limb models is offered for applications such as gait analysis, landing from a jump, orthotic construction, while the upper limb models are found to be in smaller quantities and incomplete.

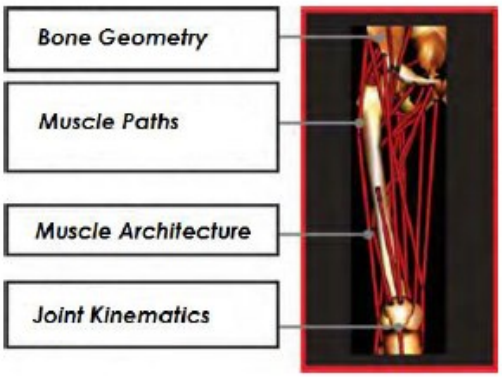

Fig. 2.1 OpenSim model, including body segments, joints, muscles [11]

2.1.2 Pipeline of Opensim

Once the dynamic model of the musculoskeletal system has been formulated, the next step is to find a model of muscular excitations that produce the particular motion of the study. Simulations are generally evaluated based on how well they really agree with the experimentally measured kinematics. Once a simulation has been created, it can be analyzed to assess how the muscle contributes to the movement of the various body segments and thus derive the muscle excitations [30]. The OpenSim software guides users to create a dynamic simulation through these main steps (Fig. 2.2):

1. First, a dynamic **model** of the musculoskeletal system and experimentally measured kinematics and reaction force data is required.
2. The generic model is first **scaled** to the subject dimensions, where the segments and segment parameters are scaled based on subject mass and length, and the muscles and muscle parameters are scaled based on the subject's length.

3. In the next phase, an **inverse kinematics** problem (Inverse Kinematics IK) is solved to determine the coordinate values (angles and positions of the virtual markers on space) of the model that best reproduce the movement recorded with motion capture.
4. Then Joint moments (**inverse dynamics**) are calculated.
5. Finally, muscle activations and forces (**muscle optimization techniques**), and resulting contact forces can be calculated.

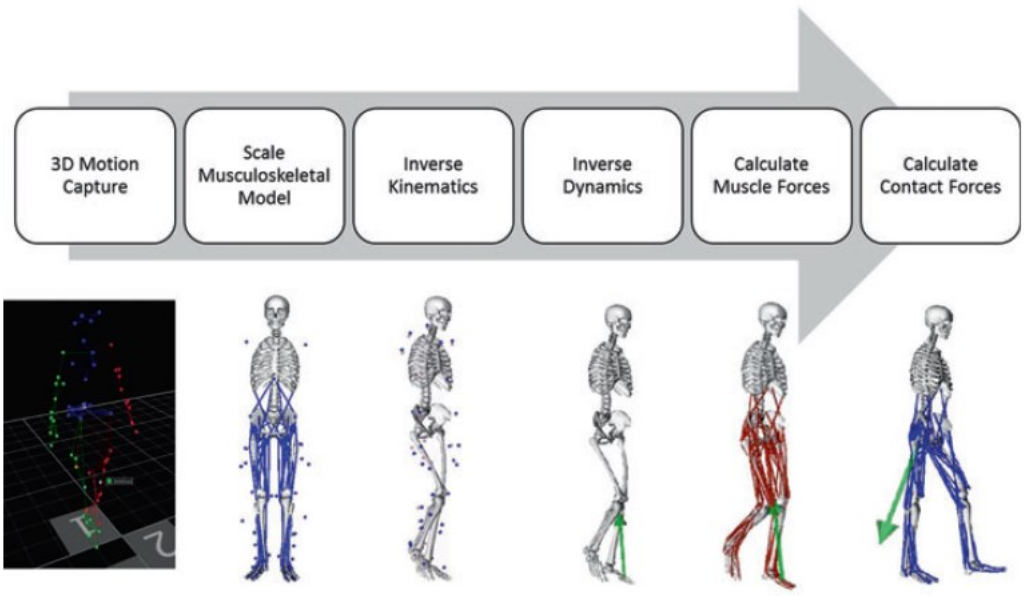

Fig. 2.2 Typical workflow used to calculate joint loading, in terms of contact forces, using musculoskeletal modelling and dynamic simulation [30]

2.1.3 Scaling of the model

Once the model has been imported into the OpenSim environment, the first step is to scale the generic model in order to attribute to the model the mass and anthropometric characteristics of a particular subject, from which the experimental data were collected.
The scaling process changes the dimensions of the bodies present in the model, the masses, the tensor of the moments of inertia and the lengths of the muscle fibers and tendons, while it does not modify the characteristic curves or the maximum isometric forces of the muscles. There are two processes for scaling the size of model bodies:

1. **Measurement-based Scaling:** the scale factor is determined by comparing the distance between the markers of the model with the positions of the experimental markers present on the subject under examination. For example, in the case in Figure 2.3, the scale factor is given by the ratio between e_1, calculated by averaging the distances between two markers considered in all the frames present in the experimental kinematics file and m_1

(distance between the virtual markers). This calculation is performed for each pair of markers in the three dimensions x, y and z.

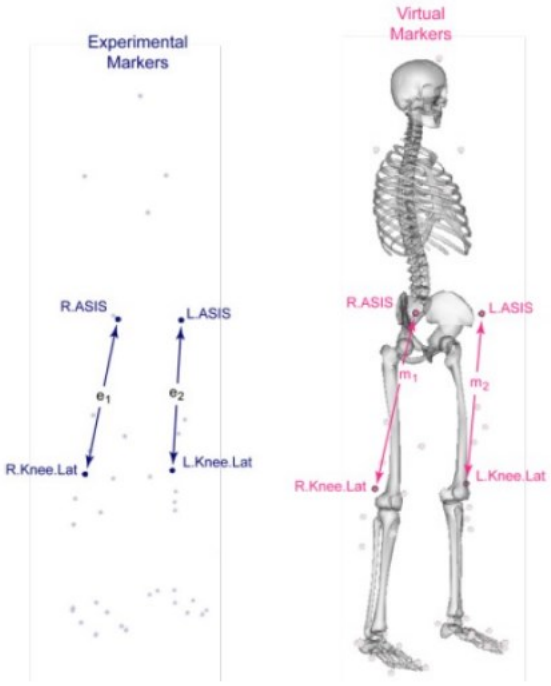

Fig. 2.3 Determination of scale factors through 'Measurement-based Scaling'

2. **Manual Scaling:** Predetermined scaling factors are used. This methodology is used if there is no static acquisition of the subject with the markers

It is also possible to use both methodologies, choosing one method for some markers, and the other for certain scale factors.

The masses of the bodies are scaled so that the total mass equals the specific mass of the subject. There are two methods for scaling the masses:

1. **Preserve the mass distribution:** it causes the masses of the subject's bodies to maintain the same proportion as those of the generic model
2. **Based on scale factors:** the total mass is equal to the one of the subject, but the scaled body mass reflects the scaling in size.

In any case, the inertia tensor is recalculated based on the new dimensions and masses. The scaling operation in OpenSim is carried out through the *Scale Tool*.

The required inputs and outputs are as follows:

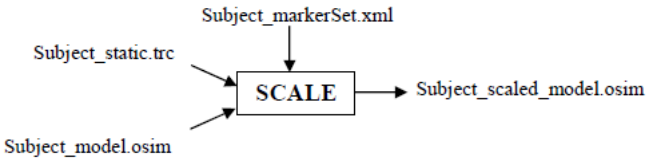

Settings:

Subject_markerSet contains a set of virtual marker position coordinates (x-y-z) to be applied on the model, representing exactly the markers that are applied on the subject during the experimental test

Input:

Subject_static.trc contains the trajectories of the experimental markers obtained following a static test, i.e., a test in which the subject is required to remain still for a few seconds in a known static position;
Subject_model.osim is the musculoskeletal model that will be used on the simulation and that can be loaded directly from OpenSim.

Output:

Subject_scaled_model is the model used as input but scaled in relation to the subject simulating that specific motor gesture.

2.1.4 Inverse kinematics

The term kinematics refers to the study of the movement of a subject or object without considering the forces and moments that are produced during the entire movement. Inverse kinematics is the process of determining the parameters of a subject, which satisfy the achievement of a desired pose. In the case of biomechanical simulations, this procedure is applied to make the musculoskeletal model perform a particular movement.

Fig. 2.4 With the Inverse Kinematics tool the virtual markers reproduce the trajectories of the experimental markers throughout the movement and while the joint angles vary [31]

The purpose of inverse kinematics, in the case study, is to find a set of generalized coordinates such as the joint angles and the positions of the body segments, for the musculoskeletal model that best reproduces the kinematics of a subject's movement.

OpenSim determines this "best match" by solving a weighted least squares optimization problem with the aim of minimizing the marker error. Each marker has an associated weight that specifies how strongly that marker error term should be minimized in the least squares problem.

The algorithm calculates the quadratic error:

$$err = \sum_{i=1}^{N} w_i (x_i^{exp} - x_i^{mod}(q))^2 + \sum_{j=1}^{M} w_j (q_j^{exp} - q_j^{mod}(q))^2$$

Where:

- N = numbers of markers
- M = numbers of degrees of freedom of the model (coordinates)
- w_i = weight of the i-th marker
- w_j = weight of the j-th coordinate
- x_i^{exp}= position of the i-th experimental marker
- x_i^{mod}= position of the i-th virtual marker which depends on the coordinate value q
- q_j^{exp}= value for the j-th experimental coordinate

- q_j^{mod}= value for the j-th virtual coordinate

Finally, this error is minimized for all possible coordinates q:

$$min_q(err)$$

Therefore, the result obtained from this minimization is a set of coordinates, which over time describe the position of the virtual markers and the joint angles of the model, in order to follow the real movement of the subject.

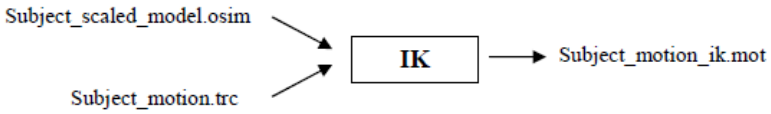

This tool is used in OpenSim through the *InverseKinematics Tool* command, entering the appropriately scaled model (*Subject_scaled_model.osim*.) and the file containing the trajectories of the experimental markers (*Subject_motion.trc)*. The Inverse Kinematics gives as output a file *(Subject_motion_ik.mot*) which contains the value of the angle at each instant in time for each degree of freedom of the system.

2.1.5 Inverse dynamics

Inverse dynamics uses the joint angles, angular velocities, and angular accelerations of the model, along with external forces and moments applied to the model, to resolve the reaction forces and moments in each of the joints.
To determine these forces and moments, the equations of motion for the system are solved iteratively to satisfy the condition of dynamic equilibrium.

The equations of motion can be written in the following form:

$$\tau = M(q)\ddot{q} - C(q,\dot{q}) - G(q) - F$$

Where:

- N= degrees of freedom of the system
- $q,\ \dot{q},\ \dot{q}$ = vectors containing the positions, velocities, and accelerations respectively

- $M(q)$ = matrix of the masses of the system
- $C(q, \dot{q})$ = vector of centrifugal and Coriolis forces
- $G(q)$ = vector of the gravitational forces
- F = vector of the ground reaction forces
- τ = vector of unknown generalized joint forces

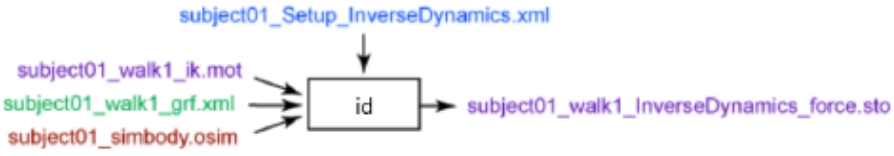

The Inverse Dynamics tool is accessible through the *InverseDynamics Tool* and requires the musculoskeletal model (*subject01_simbody.osim)*, the kinematics of movement (*subject01_walk1_ik.mot)* which can be filtered, if necessary, the initial and final instants of the simulation, and the external loads (*Subject01_walk1_grf.xml*) applied to the model, if any. The Inverse Dynamics returns a file (*subject01_walk1_InverseDynamics_force.sto*), containing for each degree of freedom the value of the moment associated with that articulation for each instant of time

2.1.6 Static optimization

Static optimization is an extension of the inverse dynamics, which resolves the joint net forces as muscle forces for each instant of time. It is a method of estimating the muscle activations and muscle forces that satisfy the positions, speeds, accelerations, and external forces (e.g., ground reaction forces) of a movement.

The technique is called "static" because the calculations are performed at each time interval, without integrating the equations of motion between the time passages. The static optimization tool uses the known motion of the model to solve the equations of motion for unknown generalized forces (e.g., joint pairs) subject to one of the following muscle activation-force conditions:

Ideal force generators:

$$\sum_{m=1}^{N}(a_m F_m^0) r_{m,j} = \tau_j \qquad (1.4)$$

Or, constrained by the strength-length-velocity properties of the muscle:

$$\sum_{m=1}^{N}(a_m F_m^0, l_m, v_m) r_{m,j} = \tau_j \quad (1.5)$$

While minimizing the objective function:

$$J = \sum_{m=1}^{N}(a_m)^p \quad (1.6)$$

Where:

- N = number of muscles in the model
- a_m = muscle activation level of the muscle m at the instant of time considered
- F_m^0 = maximum isometric force of the muscle
- l_m = length of the muscle
- v_m = speed of muscle contraction
- $f(F_m^0, l_m v_m)$ = surface force-length-velocity of the muscle
- $r_{m,j}$ = moment arm around the i-th joint
- τ_j = moment acting on the i-th joint
- p = constant defined by the user

To launch a static optimization, use the *StaticOptimization Tool* command and enter the current musculoskeletal model, the kinematics of movement, possibly low pass filtered, the value of the parameter p of the objective function, the method to be used to calculate the muscle force (equations 1.4 or 1.5), the initial and final instants of the simulation and any external loads present.

Through Static Optimization, two *.sto* files are obtained as output containing, respectively, for each muscle present in the model, the degree of activation of the muscle for each instant of time (from 0 to 1), and the force generated by the muscle; and an *.xml* file called *'_controls'* which contains the traces of muscle controls (neural excitation) for each muscle in the model and can be used as an input to Direct Dynamics.

2.1.7 Types of files in OpenSim

In OpenSim, to carry out the simulations, certain types of data must be imported:

- Trajectories of markers
- Ground reaction forces and moments and centers of pressure
- Joint angles

Depending on the input, the requested file extension changes. The main file extensions are .trc, .mot and .sto. The .trc (Track Row Column) file is used for the positions of the experimental markers acquired through a camera system; the .mot (Motion) file is used for kinematic data representing the variations of the model coordinates over time, but also the ground reaction forces. Finally, the .sto (Storage) file is generated by the OpenSim Static Optimization and Inverse Dynamics tools and always contains the time instants in the first column.

All three types are characterized by the presence of a header, which shows the characteristics of the file, for example the file name, the number of rows and columns, the data units of measurement, the sampling frequency. in the case of data coming from markers, and from a part containing numerical data.
The entries in the header, as well as the tabs in the data, are specific to each type of file and lead to the correct reading of the file by OpenSim (Fig. 2.5).

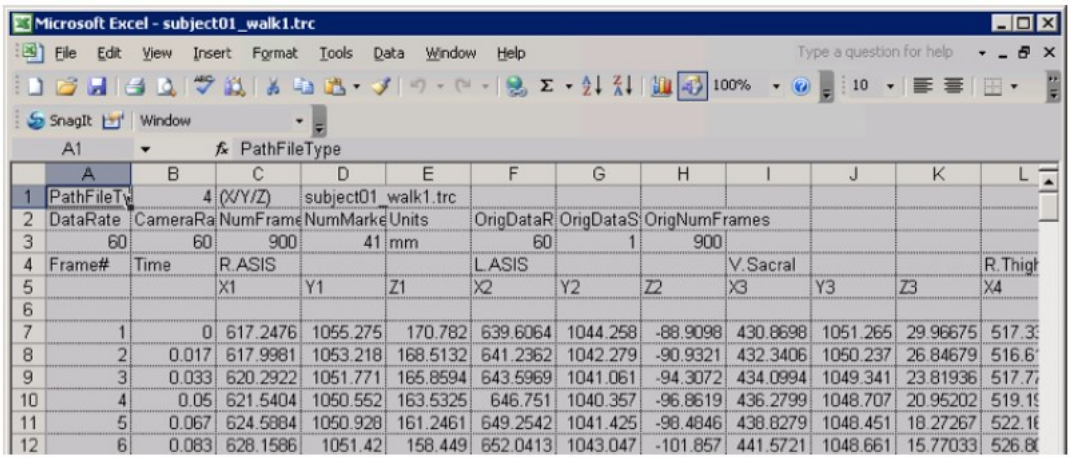

	A	B	C	D	E	F	G	H	I	J	K	L
1	PathFileTy	4	(X/Y/Z)	subject01_walk1.trc								
2	DataRate	CameraRa	NumFrame	NumMarke	Units	OrigDataR	OrigDataS	OrigNumFrames				
3	60	60	900	41	mm	60	1	900				
4	Frame#	Time	R.ASIS			L.ASIS			V.Sacral			R.Thigh
5			X1	Y1	Z1	X2	Y2	Z2	X3	Y3	Z3	X4
6												
7	1	0	617.2476	1055.275	170.782	639.6064	1044.258	-88.9098	430.8698	1051.265	29.96675	517.3
8	2	0.017	617.9981	1053.218	168.5132	641.2362	1042.279	-90.9321	432.3406	1050.237	26.84679	516.6
9	3	0.033	620.2922	1051.771	165.8594	643.5969	1041.061	-94.3072	434.0994	1049.341	23.81936	517.7
10	4	0.05	621.5404	1050.552	163.5325	646.751	1040.357	-96.8619	436.2799	1048.707	20.95202	519.1
11	5	0.067	624.5884	1050.928	161.2461	649.2542	1041.425	-98.4846	438.8279	1048.451	18.27267	522.1
12	6	0.083	628.1586	1051.42	158.449	652.0413	1043.047	-101.857	441.5721	1048.661	15.77033	526.8

Fig. 2.5 Example of .trc file containing the position of the experimental markers in space

2.2 OpenSim API

An Application Programming Interface (API) is the set of codes and rules that allow communication between different software. It serves as an interface between software to facilitate communication, in the way that a graphical interface facilitates communication between software and user.

The OpenSim API allows OpenSim communication with MATLAB, C ++ and Python. Through this communication, users are allowed to extend the functions of OpenSim, for example, it is possible to build new models, new analyzes or controls.

OpenSim is written using Object-Oriented Programming, which consists of a large set of classes divided in turn into subclasses: for example, the Model class contains all the components of a model, such as bodies, present in the Body class, the constraints, in the Joint class, the forces, in the Force class, and so on.

The various classes in the OpenSim hierarchical structure can be analyzed through the Doxygen, which is accessible through its own OpenSim installation directory following the procedure 'C:\OpenSim 3.3\ sdk \ doc\OpenSimAPI.html' or through the online documentation [32].

Using both paths you can access the hierarchical structure shown in Figure 2.6, in which each box represents a class accessible through the OpenSim API.

In this thesis it is used Matlab to compute kinematics, dynamics, muscle activations and knee contact forces.

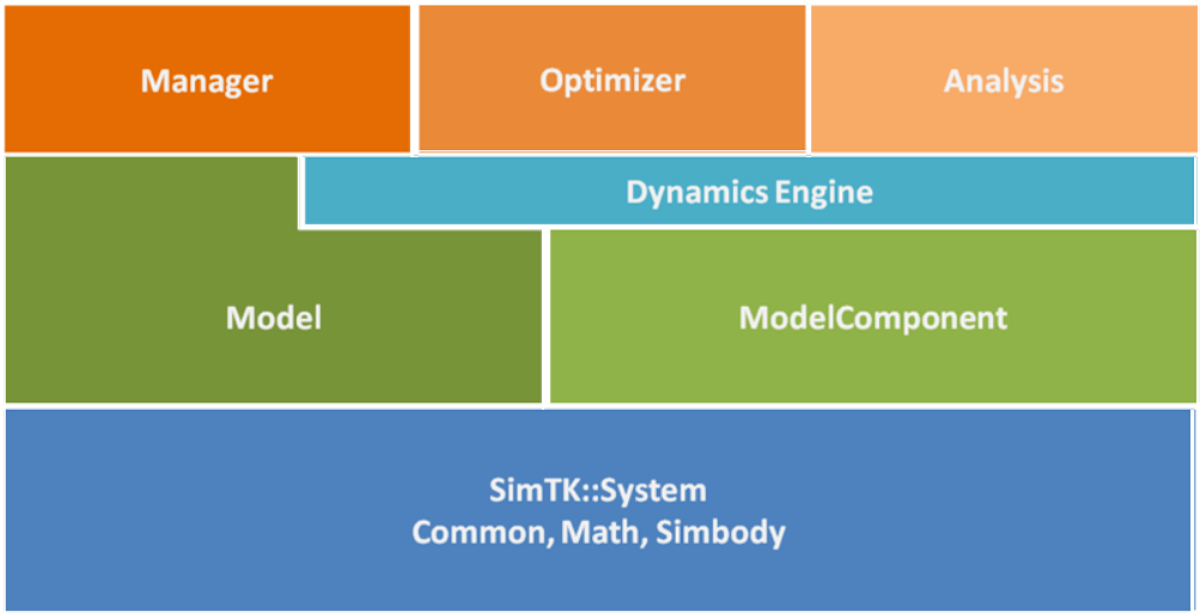

Fig. 2.6 OpenSim hierarchical structure.

2.3 Kinematics with IMU data

2.3.1 Introduction

In this project we focused on two different approaches to get a result of the knee contact forces. While obtaining gait data in free-living contexts (without researcher supervision) with standard, marker-based optical motion capture (MoCap) is difficult, it may be possible with wearable technology like inertial measurement units (IMUs). Therefore, it may be useful to study another approach, besides the traditional MoCap, that allows gait data collection in free-living environments, using wearable devices such as inertial measurement units (IMUs).

Participants can wear IMUs while performing real-world, everyday tasks, and many of them have battery and data storage capacities that enable days of continuous data gathering. These sensors have been used to estimate kinematics during movement for 30 years and in the recent times the accuracy of kinematics from IMU-based approaches have substantially improved. However, there are few studies that evaluate gait in free-living environments since it is difficult to employ IMUs for gait analysis outside of lab settings.

The difficulty of real-world IMU gait analysis is partially due to the fact that the data processing techniques required to convert IMU data (e.g., sensor-frame angular velocity, linear acceleration, and magnetic heading) into well-known kinematic outcomes, such as joint angles, are very different from those of MoCap gait analyses [33].

As a result, several research make use of commercially available automated software programs

that calculate joint kinematics and spatiotemporal results from IMU data. Even though these systems are quite simple to use, the algorithms are proprietary, making it impossible to duplicate or contrast studies conducted using other systems. Many proprietary technologies cannot be used outside of structured, researcher monitored data collection due to the requirements for precise sensor positioning and calibration.

OpenSense, an open-source software package that can be downloaded for free and used to estimate kinematics from IMU data, was recently released by OpenSim developers. To solve for traditional kinematic data like joint and segment angles, OpenSense combines sensor orientation estimations from IMU data with global optimization techniques (such as inverse kinematics [34]) and musculoskeletal models with anatomical constraints.
In this project, inverse kinematics will be computed from IMU measurement data using Opensense toolbox in OpenSim. The description of OpenSense's workflow will be the main topic of the next sections.

2.3.2 Opensense workflow

The OpenSense wokflow (Fig. 2.7) uses data from inertial measurement units (IMUs) to analyze movement.

Inputs

First of all, an OpenSim model including joints and degrees of freedom is needed. Additionally, you have to provide any orientation data from an IMU sensor or sensors.
Right now, only Xsens and APDM file formats are supported. Any other IMU system can be supported by a file converter, and it is assumed that a vendor's or third-party algorithm has been used to achieve sensor fusion and synchronizing. Many open-source sensor fusion techniques may be found on *GitHub* [35].

Registration and Calibration

Each IMU sensor can be connected to and registered with a body segment of an OpenSim model (as an IMU Frame) using the interface provided by OpenSense. The calibration procedure registers the first-time step of IMU data to the model's default pose. Modifying the model's default coordinate values will alter the registration pose. To optimize the model's initial pose for calibration using other data sources (markers, goniometer, etc), other calibration algorithms can be created using programs like Matlab, Python, etc. [35]

Computing Inverse Kinematics

The set of joint angles at each time step of a motion, that minimizes the errors between the experimental IMU orientations and the model's IMU Frames is calculated using an inverse kinematics method. Following that, the angles can be used as inputs for various OpenSim tools and studies, or they can be visualized in the OpenSim GUI. The calibration and inverse kinematics stages are accessible via the OpenSim GUI as of version 4.2. [35]

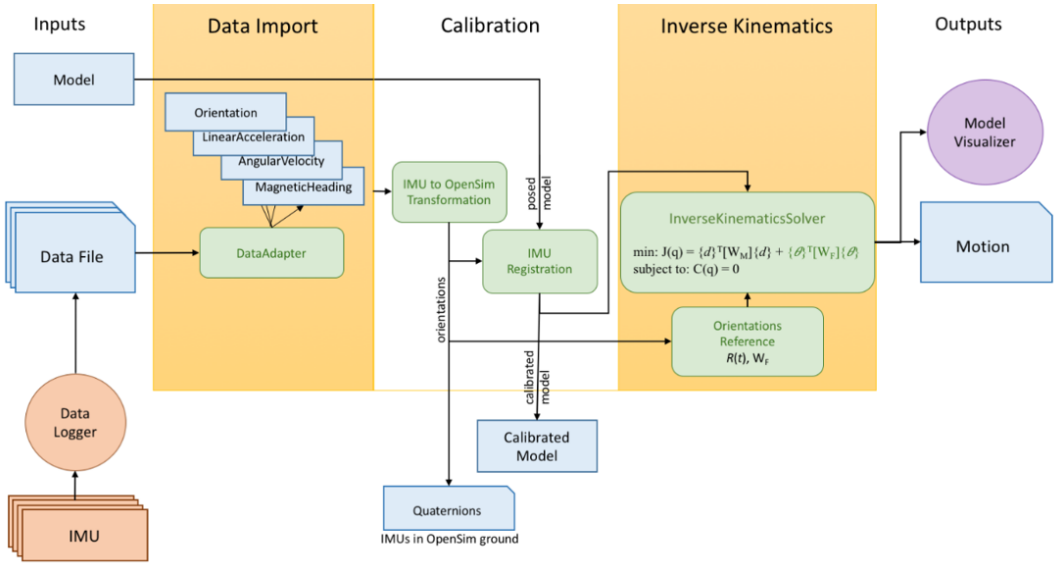

Fig. 2.7 Opensense Overview [35]

2.3.3 Running OpenSense to Compute Gait Kinematics

The following are the fundamental procedures for carrying out an IMU-based OpenSense kinematics analysis:

1) **Collect and prepare IMU data:** Collecting your data and converting it into a format that OpenSim can read and analyze using the OpenSense workflow is the first step:
    - The sensors must be placed on the subject, usually one sensor for each segment being tracked.
    - Then calibration must be performed, with the subject in a known pose (i.e., specify or record each joint angle), because OpenSense will register the IMUs to the OpenSim model using these calibration data.
    - During the calibration phase, the OpenSense workflow also enables to execute a heading correction to help orient the model in 3D space. A base IMU (such as the pelvis) and its heading (i.e., which axis is pointing forward) must be specified to do this correction.

- Use the same IMU placement to record the desired movement, such as gait.
- Pre-process your data. Sensor fusion, time synchronizing, and data interpolation for missing entries are frequently offered by IMU sensor systems like Xsens and APDM. The current version of OpenSense assumes that you are providing processed rotation matrices and that this pre-processing has already been completed.

2) **Read data into OpenSense:** a conversion to OpenSim's file format must be done and associate it with an OpenSim model. IMU data can be stored in a variety of forms, including numerous files with sensor-specific numbering or a single file with numbered sensor names (APDM, for example) (e.g., Xsens). During import, OpenSim will transform the rotation matrices into quaternions and create a single, time-synchronized Storage (.sto) file type for orientations.

   In this project data from the Xsens system will be used, that has been pre-processed (e.g., time-syncing and sensor fusion). During import, the rotation matrices are transformed into quaternions and a storage file (.sto) type is created with the orientation data for each sensor, where each column is named according to the Frame in the corresponding OpenSim model. In fact, each IMU sensor is represented as a Frame, where a Frame is an orthogonal XYZ coordinate system, and it is named as <bodyname>_imu (*e.g., femur_r_imu*) [35].

3) **Calibrate an OpenSim model:** The IMUs must then be calibrated to an OpenSim model. The OpenSense Calibration step determines the initial orientations of the IMU Frames (i.e., offsets) with respect to the OpenSim body segments using an OpenSim Model and the IMU calibration data (an orientation file containing collected sensor orientation at the default model pose). This step can be executed directly from the Opensim GUI with the *IMU placer tool* (Fig.2.8). This specific tool finds the initial orientations of the IMU frame (i.e., coordinate systems) relative to the OpenSim model's body segments.

   The required inputs and outputs are as follows [36]:

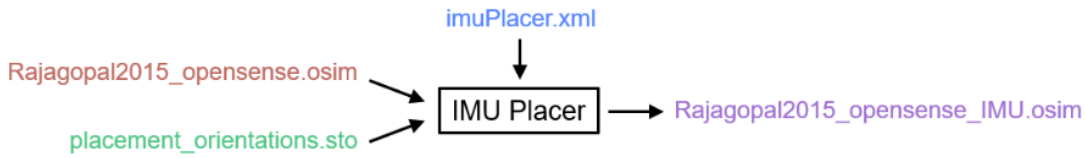

Input:

Rajagopal2015_opensense.osim: an OpenSim model that will be used to place the IMUs and *placement_orientations.sto* quaternions representing the experimental orientations, used to position the IMUs on the model. Only the file's first frame is used.

Settings:

imuPlacer.xml: A file containing all the settings information for the IMU Placer tool.

Output:

*walking_orientations.mot***:** a new Model (.osim) updated with IMUs with the correct orientation on each body segments.

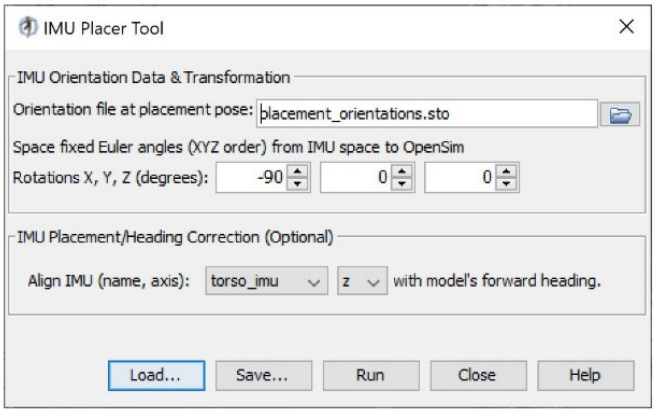

Fig. 2.8 IMU placer tool to calibrate an OpenSim model [36]

It is also possible to correct the discrepancy between the forward direction of the IMU data and the of the model, by specifying the name of the sensor and the axis that should line up with the forward direction of the motion. (Fig. 2.9).

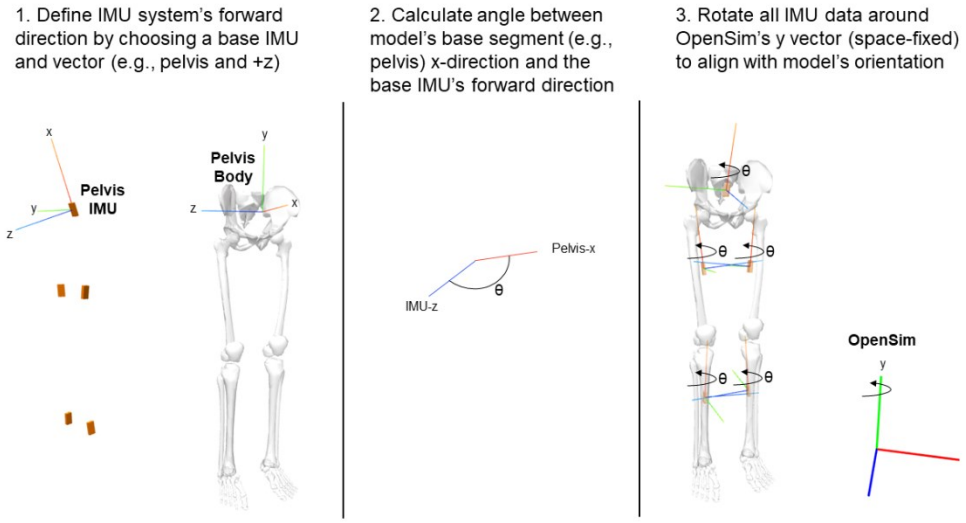

Fig. 2.9 Heading correction performed by the IMU placer tool [36]

4) **Perform IMU sensor tracking**: OpenSense's Kinematics can be used to track orientation data from IMU sensor. It determines the pose of the model at each time-step that minimizes the difference between the orientation data from the IMU sensors and the IMU frames on the calibrated model, in terms of least-squares [37].

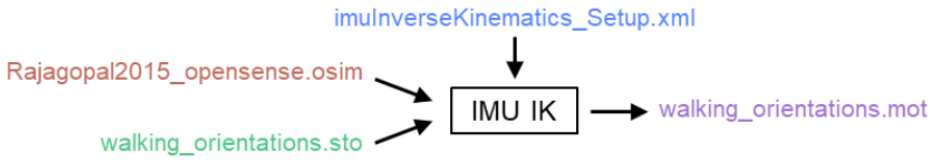

The input files needed are the model file (*Rajagopal2015_opensense.osim)* with the set of IMUs placed on the model, a sensor orientation file (*walking*_orientations.sto) in quaternions and a settings file (*imuInverseKinematics_Setup.xml*) containing all the information for the IMU IK tool. The output is a motion file (*walking_orientations.mot*) containing the joint angles and/or translations calculated by the IMU IK [37].

5) **Visualize the IMU tracking results:** using the OpenSim application (GUI) visualizer the results of the simulations and IK can be plot.

The example of the entire workflow is depicted in the flowchart below (Fig. 2.10)

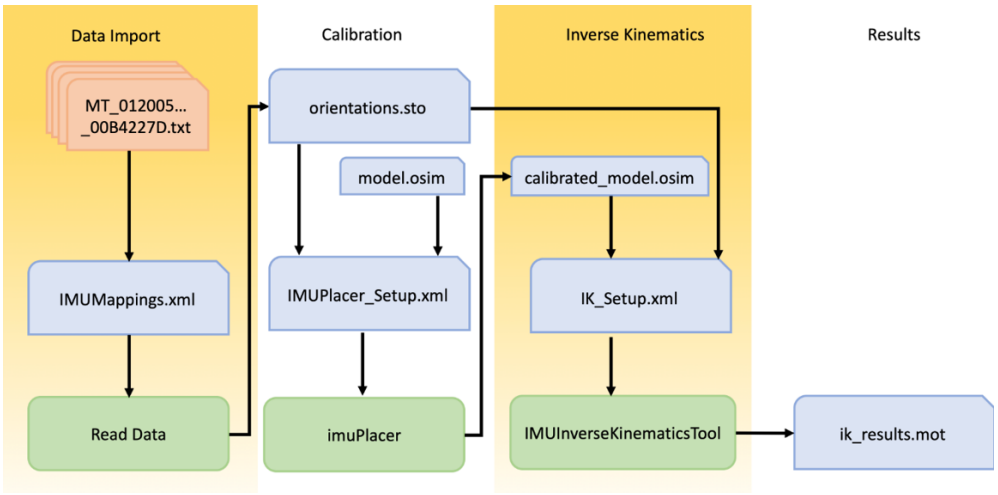

Fig. 2.10 Example workflow of OpenSense [35]

Chapter 3

3. Knee joint

3.1 General description of the knee joint

The knee joint is the largest in the human body and undoubtedly one of the most complex, both anatomically and functionally. Despite its high mobility, it is extremely stable due to the presence of a complex ligament structure. The joint is composed of a bone structure and a capsule-ligament complex. The femoral distal epiphysis, tibial proximal epiphysis, and patella form the bone structure, while the capsule ligament apparatus consists of the joint capsule, two menisci, two collateral ligaments, and two cruciate ligaments (Fig. 3.1). The knee joint, while commonly perceived as a simplified hinge joint, has 12 degrees of freedom (DOF). It can rotate and translate in all three dimensions for both the tibiofemoral (TF) and patellofemoral (PF) joints. However, 11 DOF are severely limited due to the presence of ligaments, menisci, and muscle activity, which constrain most motions with the exception of tibiofemoral flexion/extension, which has a much larger range of motion and is driven by muscle activity.

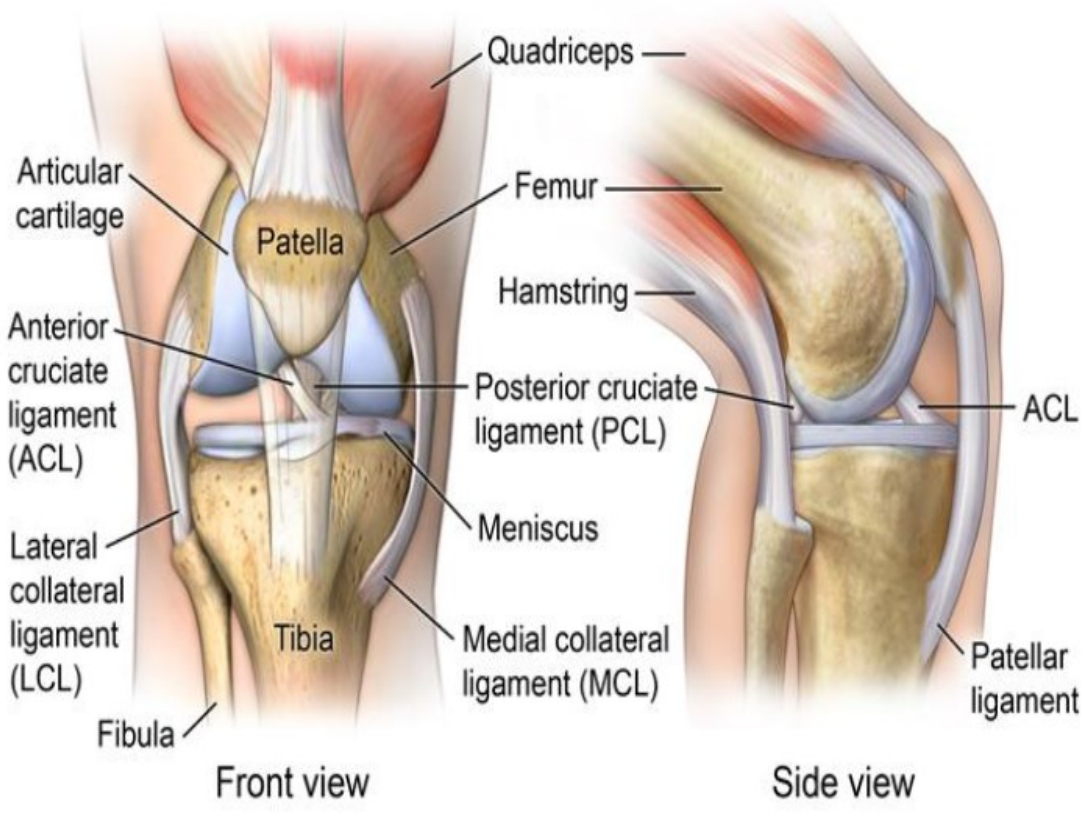

Fig. 3.1 Anatomy of the entire knee, including the bones and soft tissues [15]

The femoral condyles and tibial glenoids are the articular surfaces of the knee, two surfaces with a very complex curvature that allow for simultaneous rolling and sliding movement due to the presence of the patella. The coupling surface of the condyles on the tibia is called the tibial plateau. The surfaces of the tibial condyles are very different from each other: the medial condyle has a wider surface than the lateral one and, while the first is concave with respect to both a transverse and anterior-posterior section, the second is transversely concave but convex anteriorly posteriorly. These differences indicate inconsistencies in the shape of the femur-tibia coupling, and in order to make the two articular surfaces as congruent as possible, the tibial plates have two shock absorbers: the menisci (Fig.3.2). They are semilunar pads that connect the femoral condyles to the tibial plateaus. Their shape enables them to maximize articulation conformity, particularly during flexion, by distributing contact forces and reducing stresses on the structures. The patella, present in the knee joint, is important during the flexion-extension movement of the knee, which is controlled by the quadriceps muscle via the patellar ligament [15].

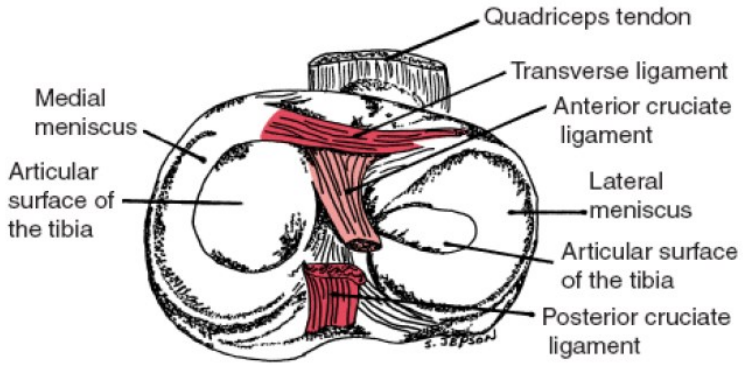

Fig. 3.2 Inside of the right knee joint seen from above with the two menisci in evidence [15]

All of the articular surfaces of the knee are covered with cartilage, and the means of union that keep them together are represented by four strong ligaments: two internal ones called anterior cruciate and posterior cruciate ligaments, and two lateral ones called medial collateral and lateral collateral ligaments (Fig.3.3). They essentially contribute to joint stability by limiting translations and rotations within certain ranges and acting passively until those limits are reached. When the knee is fully extended, the ACL is the primary restraint on anterior tibial translation and a secondary restraint on rotations. The PCL functions similarly, but in the posterior translation and deep flexion. The collaterals are important because they prevent the tibia's lateral inclination movements on the knee; in fact, the ends of the two ligaments reach their maximum tension with the knee extended, while they loosen during flexion. Overall, they

stabilize the knee along the unresisted DoF and are the most frequently used during daily activities [15].

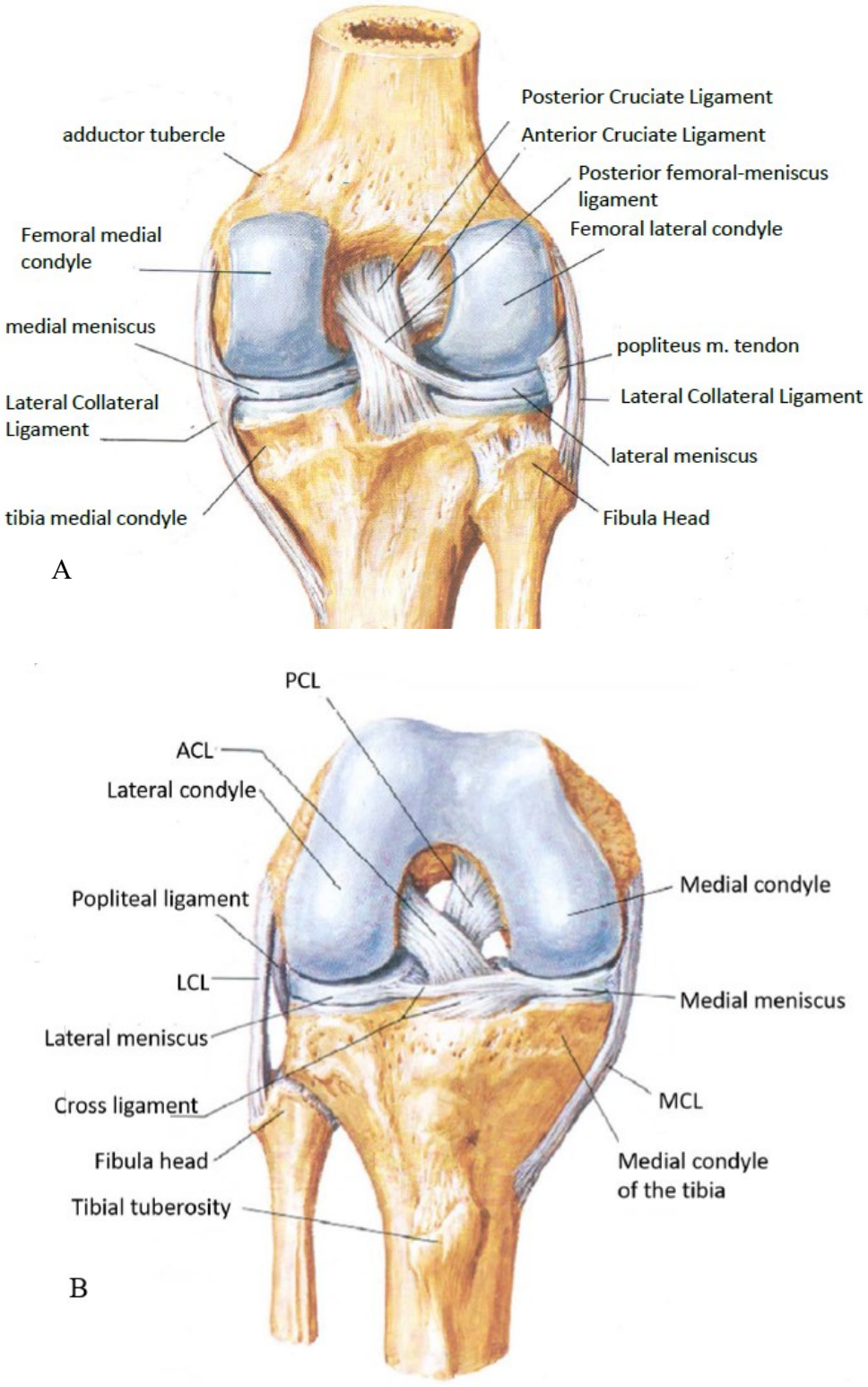

Fig. 3.3 Anterior (A) and posterior (B) view of the knee joint [15]

Articular cartilage injury is recognized as a significant cause of musculoskeletal morbidity. OA degeneration changes the internal structure of the cartilage, causing changes in its mechanical properties and affecting the stability of the knee joint and overall locomotion. As a result, accurate knowledge of structural and mechanical changes could lead to a better understanding of the onset and progression of OA, resulting in improved treatment therapies. Muscles that act on the knee joint can be efficiently divided based on their function:

- **Flexors:** gastrocnemii (medial and lateral), semimembranosus, semitendinosus, biceps femoris short head, biceps femoris long head, gracilis, and sartorius.
- **Extensors**: include the vasti (medial, internal, and lateral) and the rectus femoris
- **Abductors:** include the iliotibial band (tendon) and tensor fascia latae

3.1.1 Knee model

Many different types of knee models have been used to analyze human mobility. From the most basic 1-DOF hinge joint [38] to intricate 12-DOF contact models [2] and finite element models [39], these cover a wide spectrum of applications. In order to reduce error sources and improve computing efficiency, a simpler hinge joint is typically used, unless high detail knee mechanics are necessary [40].

However, 12-DOF knee models are used, either as simplified contact models or finite element models, where high detail information is necessary. Digitized MRIs are used to ensure precise geometries, insertion sites, and cartilage thickness in order to adequately represent the joint for either sort of 12-DOF model (Figure 3.4). The created model can then be incorporated to an existing full body model that already has a 1-DOF knee joint, or it can be simulated separately using the observed ligament volumes and attachment locations [2].

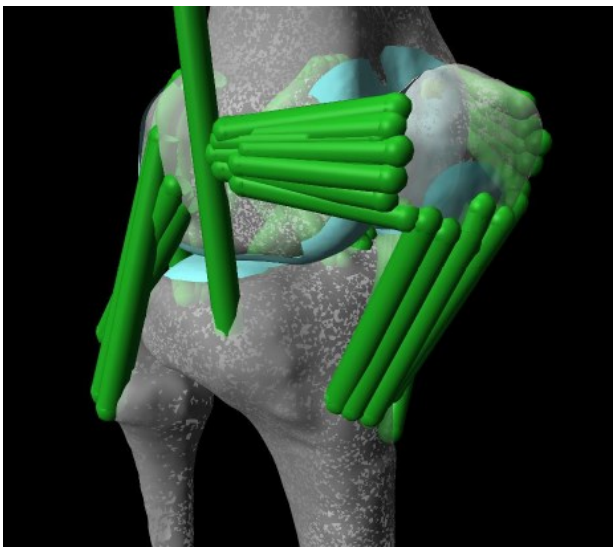

Fig. 3.4 Digitally reconstructed 12-Degree of Freedom knee joint model [2]. Green lines represent the lines of action of ligaments, femoral and tibial cartilage is shown in cyan. View is from the lateral side of the right knee.

Depending on the research's topic, different levels of information are needed, but in general, detail is only needed for the study in order to avoid using more resources to solve auxiliary parameters. When performing in-depth evaluations, such as determining how various reconstructive procedures may impact knee biomechanics, finite element models work well. In order to create a solid model, each knee component—including the bones, ligaments, menisci, and articular cartilage—is first reconstructed from images. A mesh of thousands of discrete elements is produced for this model, and material properties are assigned to each body. The cost of calculation is extraordinarily high because each element is solved for separately, therefore solving FE models within the framework of a multibody gait simulation remains computationally difficult. Even though FE modelling for knee joint can be used to determine cartilage pressure in the tibiofemoral and patellofemoral joints under the influence of muscle and joint contact forces acquired by a multiscale model.

The knee model used in this study is the one developed by Lenhart, Smith et al. [2]. They developed and validated a subject-specific, multi-body knee model that allows for six DOF motion at both the tibiofemoral and patellofemoral joints. This novel method makes it possible to get beyond some of the drawbacks of traditional multi-body models, such as the representation of the knee as 1 DOF joint, in which all the PF kinematics and TF secondary kinematics are estimated as a function of the knee flexion. This approach cannot calculate the loading patterns of soft tissues, such as ligaments and cartilage, and it ignores the significant variation in kinematics brought on by these patterns during the gait cycle.

For this reason, this model instead of depending on pre-assumed behavior based on cadaveric research, it is able to simultaneously predict the TF and PF mechanics that result from the interaction of muscle, ligament, and contact forces. As a result, articular cartilage may be incorporated into the model, and the effect that secondary kinematics have on the motion pattern can be used to precisely explain the variance in magnitude and location of contact pressures. They used high resolution magnetic resonance (MR) images of the right knee of a healthy young adult female (age = 23 years, height = 1.65 m, mass=61 kg) to create a knee model that included ligamentous constraints and articular cartilage contact. The tibia, femur, and patella's bone and cartilage surface geometries were manually segmented from the MR images and transformed into triangulated surface meshes (MIMICS, Materialise Group, Leuven, Belgium). The origins, insertions and paths of 14 ligaments were also segmented and represented as bundles of nonlinear springs. A generic lower extremity musculoskeletal model [41] that contained 44 muscles functioning around the hip, knee, and ankle joints included the knee as part of it (Figure 3.5) [42].

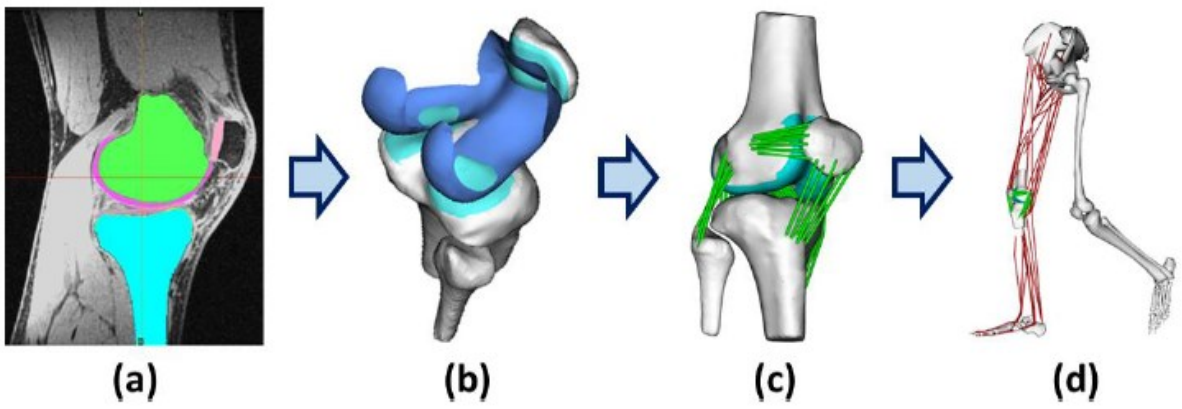

Fig. 3.5 : Model development: a) Cartilage, bone and ligament geometries were manually segmented from MR images b) Bone and cartilage geometries were converted to triangulated surface meshes c) Ligaments were represented as bundles of nonlinear springs spanning from origin to insertion d) The knee model was integrated into a generic lower extremity model (Arnold et al. [41]).

The 14 ligaments are: superficial and deep medial collateral ligament (sMCL, dMCL), lateral collateral ligament (LCL), anteriomedial and posteriolateral anterior cruciate ligament (aACL, pACL), anteriolateral and posteriomedial posterior cruciate ligament (aPCL, pPCL), patellar tendon (PT), medial and lateral patellofemoral ligaments (MPFL, LPFL), popliteofibular ligament (PFL), posteriomedial capsule (pmCAP), the posterior capsule (CAP), and the iliotibial band (ITB). Each one was represented by a bundle of non-linear springs spanning from the ligament origin footprint to its insertion footprint. Wrap objects were defined for the medial collateral ligament, posterior capsule, and patellar tendon so that they wrapped appropriately

around the tibia, femur, and patella respectively. Each ligament bundle was represented by a discrete number of strands. Tensile forces were computed assuming each strand behaved as a non-linear stiffening spring at low strains (e<0.06) and having a linear stiffness at higher strains. The linear stiffness of each ligament was estimated as the product of the average ligament cross-sectional area and an assumed ligament elastic modulus of 125 MPa.

Tibiofemoral and patellofemoral cartilage contact pressures were computed using an elastic foundation model in which pressure is assumed to be a function of the depth of penetration between contacting cartilage surfaces. According to the elastic basis theory, cartilage is an elastic tissue attached to a strong bone substrate. Since pressure on each element in contact is calculated independently of neighboring elements, cartilage surface meshes are free to interpenetrate. The following law is used to compute the contact pressure (p) [42]:

$$p = -\frac{(1-\nu)E}{(1+\nu)(1-2\nu)}\ln(1-\frac{d}{h})$$

Where:

- p: contact pressure on each mesh triangle
- E: cartilage elastic modulus
- ν: Poisson ratio of the cartilage
- d: local overlap depth
- h: local cartilage thickness

For the cartilage thickness 4mm (tibial) and 7mm (patellar) were assumed, while an elastic modulus of 10MPa and a Poisson's ration of 0.45 for cartilage.

Overall, the musculoskeletal model (Figure 3.6) included three hip rotations, six DOF tibiofemoral, patellofemoral, and tibiomeniscal joints, and a one DOF ankle joint.

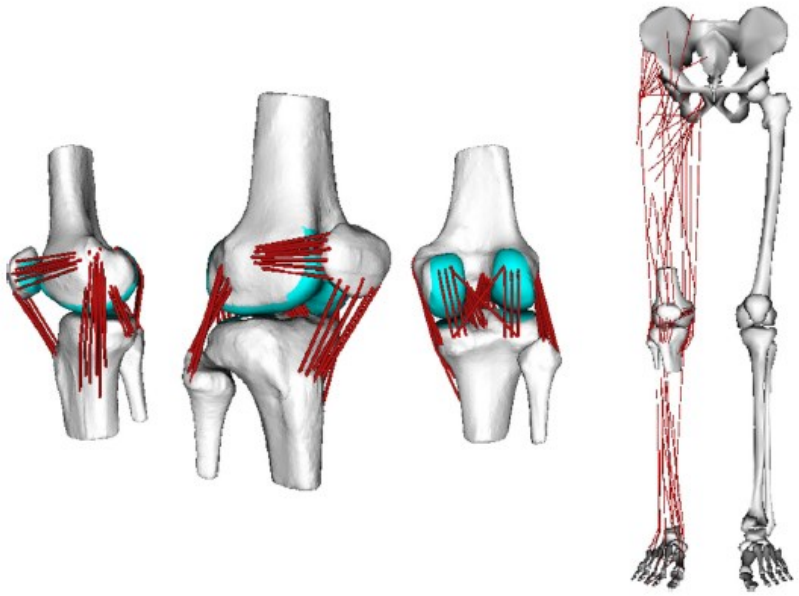

Fig. 3.6 (Left) Ligament, skeletal and cartilage geometries were reconstructed from segmented MR images. The 12 degree of freedom knee model included 14 ligament bundles (76 elements) acting across the tibiofemoral and patellofemoral joints. **(Right)**The knee model was included into a generic lower extremity musculoskeletal model for simulating functional movement. [2]

Chapter 4

4. Materials and Methods

The current chapter will go over the methods, techniques, and operations utilized for the experimental portions of the thesis. In specific, the data needed to begin the work, the programs and algorithms used, the protocols used, and the necessary alterations made will all be covered.

4.1 Data acquisition

The goal of this thesis is to develop a method for biomechanics and rehabilitation researchers to measure human movement and musculoskeletal function outside of the traditional laboratory-based 3D motion capture. Consequently, use the data collected with wearable sensors as input for musculoskeletal modelling to allow for the estimation of various movement parameters (such as muscle activations and joint contact forces).
The first step will be to obtain the results using the gold standard for capturing human motion as input for the MSK workflows, i.e., MoCap combined with in-ground embedded force plate systems, to get as results the knee contact forces. These results will be used to compare and evaluate the outcomes obtained with an approach that aims to use as little marker-based information as possible.

3D motion capture (MoCap) data was collected at the Movement & Posture Analysis Laboratory Leuven (MALL), at the Department of Movement Science, KU Leuven, Leuven, Belgium. Ten healthy adults with no musculoskeletal or neurological disorders volunteered for the study (4 males and 6 females; age: 59.7 ±7 yr; height: 1.55 ± 0.52 m; weight: 66.5 ± 24.0 kg) and performed multiple walking trials. A full-body Plug-in-Gait (known as Davis protocol) marker set was used to place the retro-reflective markers which were supplemented with 3-marker clusters on the upper and lower arms and legs, as well as anatomical markers on the sacrum, medial femur epicondyles, and medial malleoli, for a total of 65 markers. Ground-reaction forces and marker trajectories were then recorded using 3 ground-embedded force plates (AMTI, Watertown, USA,1000Hz) and a 10-camera motion capture system (100 Hz, Vicon, Oxford, UK).

3D Inertial capture (InCap) was used to synchronously measure using an Xsens IMC system (Xsens Awinda, Xsens Technologies BV, Enschede, Netherlands) sampled at 60 Hz and processed by the matching software Xsens MVN Analyze 2018 (Xsens Awinda, Xsens Technologies BV, Enschede, Netherlands). 17 IMU modules were mounted on the head, sternum, pelvis, upper legs, lower legs, feet, shoulders, upper arms, forearms and hands.

The individuals were told to move barefoot at their own, personal walking pace. Table 4.1 displays an overview of the subjects' attributes and gait information. Each participant stood upright while their segment dimensions were recorded and later entered into the XsensMVN program before starting trials. The measures included the length of the foot as well as the lengths between the ankle, knee, hip, and top of the head from the ground, the width of the pelvis, and the shoulders. The individual was in a neutral stance throughout the calibration of the IMC system, which was then followed by a walk calibration. Then, using a sensor-to-segment calibration technique, XsensMVN 2018 determines the kinematics of 23 body segments by relating the 17 sensor orientations [24].

In order to scale and register the generic musculoskeletal model [2], participants were next required to complete a static calibration trial that was captured by the MoCap system. The opto-reflective markers employed in this trial identified key anatomical landmarks. The subjects conducted 3D motion analysis following the calibration of both motion capture devices. While performing a number of walking trials, the two motion capture systems simultaneously and synchronously captured ground reaction forces and moments as well as 3D body movements. The synchronization was based on the manufacturer's guidelines with a specific trigger at the start/stop recording time.

The total number of gait trials is not the same across participants because it reflects the variation in the number of valid trials per participant.

	Body weight (kg)	Height (m)	BMI (kg/m^2)	N° of walking trials	Average gait speed (m/s)
TBM_H01	87.6	1.81	26.25	3	1.65
TBM_H02	77.5	1.69	26.96	5	1.22
TBM_H03	76.5	1.70	26.30	4	1.33
TBM_H04	55.6	1.62	20.96	6	1.34
TBM_H06	68.0	1.58	26.84	4	1.08
TBM_H07	78.5	1.85	23.08	5	1.46
TBM_H08	71.2	1.63	26.72	4	1.44
TBM_H11	66.5	1.76	21.63	3	1.19
TBM_H12	87.5	1.78	27.77	6	1.29
TBM_H14	63.4	1.60	25.39	4	1.12

Tab. 4.1: Summary of 10 healthy subject characteristics and gait data.

4.2 COMAK

In the previous chapter, it has been discussed how the estimation of inverse dynamics, muscle activations, metabolic cost, and joint contact forces, among other things, can be done using modelling. However, solving musculoskeletal models is more difficult than imagined, it is quite challenging due to the problem of muscle redundancy. It is hard to estimate the forces of individual muscles since each degree of freedom is not controlled by a single muscle.

Static optimization (see *Paragraph 2.1.6*) is one of the most popular approaches to address the muscle redundancy issue; but other approaches are frequently used as alternatives to address musculoskeletal models, such as the Concurrent Optimization of Muscle Activation and Kinematics (**COMAK**) tool, which will be used in this study [1].

The COMAK tool is a modified static optimization technique that minimizes muscle activation while solving for secondary kinematics and muscle activations to achieve measured primary DOF accelerations [1]. Several musculoskeletal modelling studies have effectively used each of these strategies.

More in detail, the Concurrent Optimization of Muscle Activations and Kinematics (COMAK) algorithm predicts muscle forces, secondary (unmeasurable) joint kinematics, ligament forces, and articular contact pressures from motion capture and ground reaction data. COMAK optimizes the muscle activations and secondary kinematics to generate the measured accelerations in the primary degrees-of-freedom while minimizing an objective function. Concurrent simulations frequently demand a set of primary DOFs (on the sagittal plane, e.g.

flexion/extension), which are easily measured with motion capture, and a set of secondary DOFs (abduction/adduction and internal/external rotation), which are more difficult to measure accurately. The simulation's multibody model dynamics predict a set of secondary kinematics, muscle forces, ligament forces, and articular contact pressures that are dynamically consistent with the measured ground reactions and primary kinematics.

For COMAK, inverse kinematics is used to compute the coordinates, speeds, and accelerations $(q, \dot{q}, \ddot{q})$ of the *primary* model degrees of freedom. The secondary kinematics, muscle, ligament, and articular contact forces that cause the measured primary joint accelerations are then solved numerically while minimizing a cost function that resolves inherent muscle redundancy. As described in section 1.5.1 skin-motion artifacts cause errors in the computation of joint kinematics, and the difference between measurable DOFs of high (primary) and low (secondary) confidence is a very important aspect in COMAK. The algorithm predicts tibiofemoral flexion and ankle flexion as the main degrees of freedom while concurrently solving for the muscle and soft tissue loads required to produce the measured fundamental kinematics (Fig. 4.1). Since motion capture cannot be used to accurately measure tibiofemoral translations, nonsagittal rotations, and all patellofemoral and meniscal DOFs, they are referred to as *secondary* DOFs. Pelvic rotations and translations are quantifiable as well, but they are classified as prescribed DOFs because the multibody model must account for their accelerations via constraint forces to be consistent with observable multi-body dynamics [43].

Prescribed	DOF
pelvis	6
Primary	
hip	3
tibiofemoral flexion	1
ankle	1
Secondary	
tibiofemoral	5
Patellofemoral	6
Meniscal	12

Fig. 4.1: Classification of model degrees-of-freedom for COMAK [43]

Following inverse kinematics, a COMAK optimization problem is solved to estimate the secondary kinematics and muscle and soft tissue loads required to generate the measured primary accelerations. The optimization seeks secondary coordinates and muscle activations that satisfy the overall dynamic constraints while minimizing an objective function. Overall, the simulation framework of the Concurrent Optimization of Muscle Activations and Kinematics is shown in figure 4.2, describing each step:

- **Knee Model Construction**: from medical photos, subject-specific bone, cartilage, and ligament geometries are segmented. Experimental data can be used to calibrate constitutive properties, or they can be assumed from cadaver experiments
- **Personalized Model:** based on segment lengths determined with motion capture in a static stance, a generalized musculoskeletal model is scaled. To create a customized model, the knee model is added to the scaled musculoskeletal model
- **Prescribed Flexion Forward Simulation:** a forward dynamic simulation is performed with the personalized model where tibiofemoral flexion is prescribed from 0° to 120°, and the secondary knee kinematics are predicted based on the contact, ligament, and passive muscle forces. These results are used to develop constraint equations that couple the secondary knee kinematics to tibiofemoral flexion during inverse kinematics
- **Experimental Data:** while the subject makes functional motions like walking, motion capture data and ground reactions are gathered
- **Inverse Kinematics:** a global optimization routine is used to calculate primary kinematics that minimize the differences between measured and modeled marker locations. In this phase, the secondary DOFs are constrained to be functions of tibiofemoral flexion
- **Initialization Forward Simulation:** the primary model DOFs are fixed at their initial (t_0) values from inverse kinematics and the secondary DOFs are allowed to settle into an equilibrium configuration. The resulting posture provides the initial seed to COMAK
- **COMAK** simulation routine then leverages a high throughput computing grid to perform a Monte Carlo analysis in which neuromuscular coordination strategy is varied to generate probabilistic predictions of secondary knee kinematics, muscle forces, ligament forces, and articular contact pressures

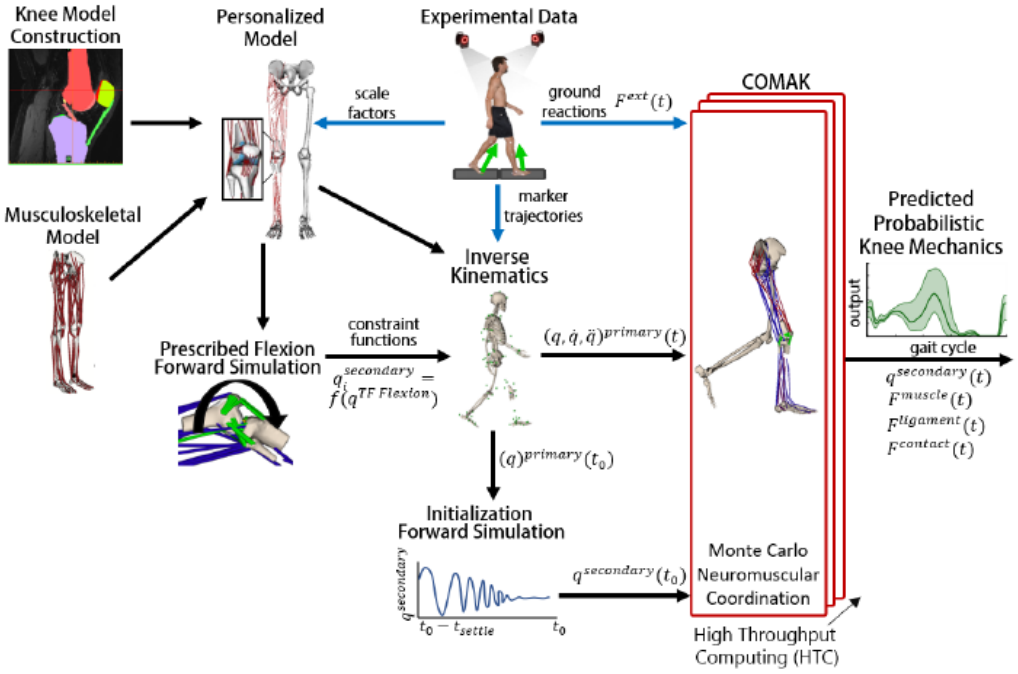

Fig. 4.2: Simulation framework of COMAK [43]

4.3 Experimental setup

The workflow that was followed is shown in figure 4.3, a two-way scheme to highlight the different procedures used for the two strategies, but ultimately to arrive at the same results of interest, namely the knee loadings. All the steps and procedures for the two approaches are detailed in two separate sections.

It should be noted that the subjects in this thesis are healthy control subjects, and only the right leg motion is examined, as the results for the left leg are supposed not significantly different. As a consequence, only right leg models were created, since the Lenhart et al. [2] knee model is created for only one lower limb and two symmetric models are required to analyze the knee mechanics of both legs.

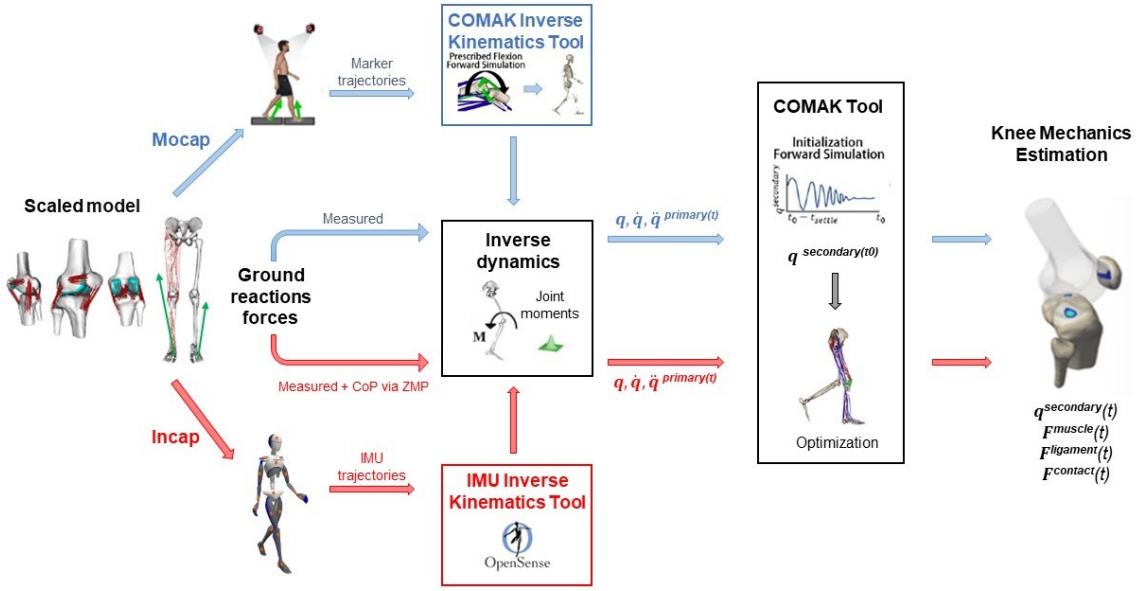

Fig. 4.3 General workflow followed for this research project. In blue is characterized the MoCap approach (standard approach), while in red the InCap procedures.

4.3.1 Motion capture workflow

The data used as a starting point consisted of the .c3d files for each walking trial, a standard format that contains all the information needed to read, display, and analyze 3D motion data with additional analog data from force plates, electromyography, accelerometers, and other sensors. Instead of using custom-built MATLAB 2021a scripts, Nexus 2.12 was used to export .trc (Track row Column) and .mot (motion) formats containing respectively the marker trajectories coming from the 10 camera system and ground reaction forces from the force plates. In addition, a .csv file was exported containing the time instants of the main gait events (i.e., Heel-strike, Toe-off…). Each subject's walking trial file (.c3d) was analyzed prior to the export process to verify that the acquisition was valid. It had to be ensured that each marker was properly labeled, that there were no gaps in any marker trajectories, and, most importantly, that each foot was perfectly inside the force platform, with the ground reaction forces correctly detected.

The model of the lower limb [2] integrating the 12 DOFs knee model, was scaled to each participant's anthropometry and mass, using the markers defining significant anatomical landmarks obtained from static calibration trials. This was done, as described in *section 2.1.3,* by reducing as much as possible the least-square difference between the modeled and measured marker trajectories, while also optimizing the segment lengths and local marker coordinates of markers not placed on bone landmarks.

After the models had been scaled, the joint angles for the scaled musculoskeletal models were calculated using the specific *COMAK Inverse Kinematics tool* utilizing the marker trajectories obtained from the dynamic trials. Next, the inverse dynamics problem was solved to get the reaction forces and moments in each of the joints. Furthermore, the concurrent optimization of muscle activations and kinematics algorithm, which simultaneously solves for the secondary knee kinematics (12 DoF), was used to calculate the muscle forces necessary to produce the measured accelerations in the primary DOFs (i.e., hip flexion, hip adduction, hip rotation, knee flexion, and ankle flexion). This algorithm minimizes the weighted sum of squared muscle activations and contact energy. Finally, the resultant contact forces on the medial and lateral tibiofemoral compartments were calculated, as they are the final goal of this thesis.
The main muscles analyzed in this study are the ones most involved during a normal walking and are reported in the table below 4.2.

Thigh muscles
Biceps femoris long head
Semimenbranosus
Semitendinosus
Rectus femoris
Vastus lateralis
Vastus medialis
Leg muscles
Gastrocnemius lateral
Gastrocnemius medial
Soleus
Tibialis anterior
Tibialis posterior

Tab. 4.2 Main muscles analyzed that are involved in a walking motion

4.3.2 IMU workflow

The data of each walking trials acquired by the InCap measurement system was available in the .mnvx format. Therefore, conversion to OpenSim's file format was needed, and it was performed by means of custom-built MATLAB scripts. More specifically a Matlab function (see *Appendix B*) was used to load the Xsens data from .mvnx files and save them in the .mat format, where a *structure array* was created to store values of acceleration, orientation, and magnetic field data for each sensor, and all the information about the static calibration,

segments' and joints' names. Another Matlab function (see *Appendix B*) was then used to create an OpenSense file for kinematic analysis in OpenSim. It transforms the rotation matrices into quaternions to create a single, time-synchronized storage (.sto) file type for orientations. The output file *walk_00x_orientations.sto* contains orientations for each sensor, where each column corresponds to an IMU sensor represented as a Frame (X, Y, Z coordinates), named as <*bodyname*>*_imu.* Each sensor was associated with the respective body segment, in this study, only the lower limb and trunk were taken into consideration, while upper body segments were avoided to lower computation costs. All the sensors used in this project are listed in the following table.

Body name	**Sensor attached**
T8	torso_imu
Pelvis	pelvis_imu
RightUpperLeg	femur_r_imu
RightLowerLeg	tibia_r_imu
Rightfoot	calcn_r_imu
LeftUpperLeg	femur_l_imu
LeftLowerLeg	tibia_l_imu
Leftfoot	calcn_l_imu

Tab. 4.3 List of sensors used and their respective body segments

Once all the input data have been stored and saved in the correct way, OpenSense toolbox can be used to analyze kinematics data measured by IMUs. The next steps followed the Opensense workflow as described in *section 2.3.2.*

A static calibration was performed to connect and register each IMU sensor with a body segment of an OpenSim model, for each subject it was used the model created previously for the motion capture approach [36]. This step was executed using directly the OpenSim GUI with the *IMU placer tool* (Fig. 4.4) giving as input the model and the *walk_00x_orientations.sto* orientations file, to find the initial orientation of the IMU frame relative to the OpenSim model's body segments. To align the forward direction of the IMU data and the model's one, it was defined that the IMU forward direction followed the -z-axis of the pelvis_imu sensor. Additionally, since the reference systems of the Xsens system is different from the OpenSim one, as shown in picture 4.5, a rotation of -90° along the x-axis was carried out to align the y-axis of the IMU Xsens and the OpenSim frame.

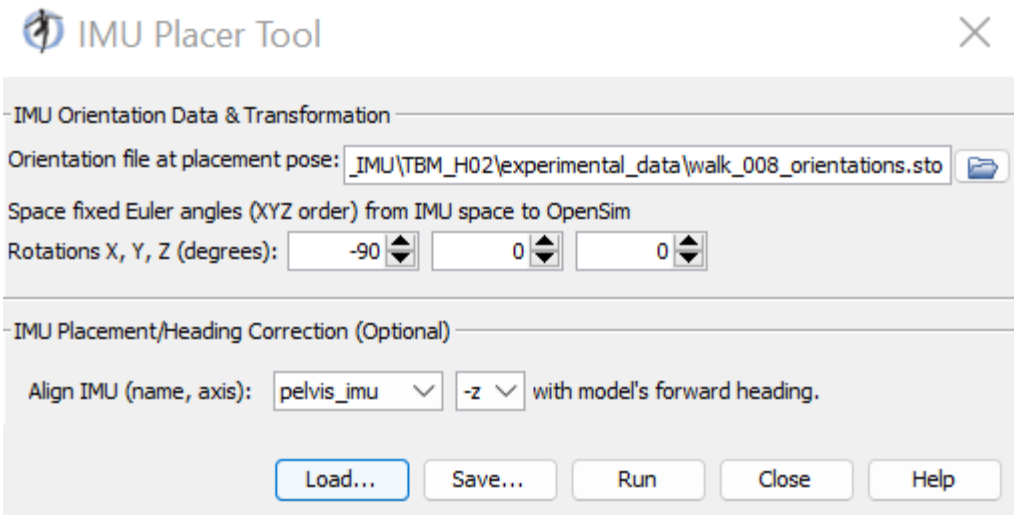

Fig. 4.4 Example of the IMU placer tool input data used

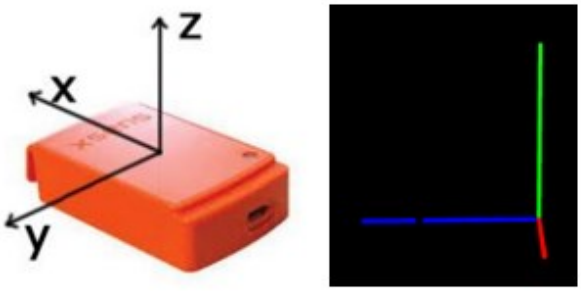

Fig. 4.5 On the left is the coordinate system of an IMU sensor (XSens [24]) and on the right is the OpenSim ground frame (in red the x-axis, in green the y-axis, and in blue the z-axis)

As output, a new model updated with IMU sensors correctly oriented with respect to each body segment (Fig. 4.6), was created.

Fig. 4.6 Output of the *IMU placer tool*, model updated with IMUs with the correct orientation on each body segment. To avoid confusion all muscles have been hidden.

For the next step, the *IMU Inverse Kinematics tool* (Fig. 4.7) was used to find the set of joint angles for each time step of the walking motion, which minimizes the discrepancies between the experimental IMU orientations and the calibrated model's IMU frame. As input the calibrated model and the sensor orientations file were needed, specifying the Euler angles rotations to adopt to correctly transform from the IMU space to OpenSim. At first, the same rotations as the one used in the previous step for the IMU placer tool were adopted, i.e., a rotation of -90° along the x-axis.

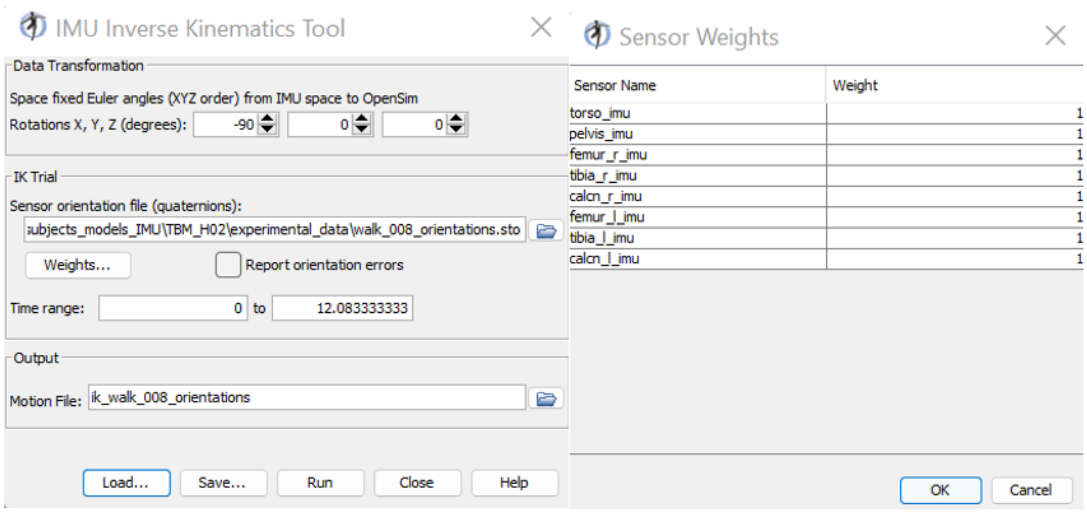

Fig. 4.7 IMU inverse kinematics tool, using the same rotations as for the IMU placer tool. It is shown that each sensor has a weight of 1 to resolve the IK problem.

However, the output motion file containing the joint angles and/or translations calculated by the IMU IK, revealed that the forward direction of the inertial capture system was not the same as the motion capture one. In fact, there was an angle between the IMU forward direction (along the -z-axis of the pelvis sensor) and the MoCap forward direction, as illustrated in figure 4.8.

Fig. 4.8 IMU IK shows that the forward direction is not the same as the one of the MoCap system (along x positive axis). The model is rotated of an angle about the y-axis of the Opensim frame.

Therefore, a correction to align the forward direction of the two systems was applied, along the x-axis (positive or negative depending on the specific walking trial). The quaternions of the pelvis were acquired in the first frame of acquisition (static pose), using the output (.mat) from the Matlab function described previously; they were converted to rotation angles by means of the Matlab function *quat2angle,* obtaining a set of rotation angles useful for perfectly aligning the two coordinate systems. Finally, the rotation angles were specified in the section "Data Transformation" of the *IMU Inverse kinematics tool*, precisely:

- A rotation of -90° around the x-axis for each subject
- A rotation of a specific angle around the y-axis, as result in the conversion of the quaternions previously described. This angle is different for every walking trial of each subject

When comparing the results of the inverse kinematics problem of the two approaches it was discovered that the two systems were not automatically synchronized, the IMU IK file had more time instants of the walking motion than the MoCap system, so a synchronization and resampling of these files had to be performed. For every walking trial, at the beginning of the movement, the Xsens system started recording earlier than the MoCap. Then after some time interval, a trigger pulse was sent to the 3D MoCap system, and the VICON cameras started recording the subject's motion too. Therefore, the time instants of the trigger pulse needed to be found, in order to understand when the cameras started the acquisition, while the InCap was already recording.
Then, using this information, the IMU IK file was cut and taken into consideration in the same time interval of the MoCap. In addition, since the sampling frequency of the two systems are different, all movements files were resampled at the same frequency (fs=60 Hz) of the inertial capture measurement, and the same process was done for the ground reaction files (.mot) since the force plates frequency was 1000 Hz.

The final IMU IK output file showed a walking motion with the pelvis fixed at the origin of the Opensim ground frame (Fig. 4.9), in fact in the section *Coordinates* of Opensim the values of *pelvis_tx, pelvis_tz*, indicating the translation of the pelvis along the x, z axis respectively were fixed zero for the entire gait cycle. This is because the pelvis is fixed in space and all kinematic quantities are expressed relative to the pelvis, for the XSens system [24].

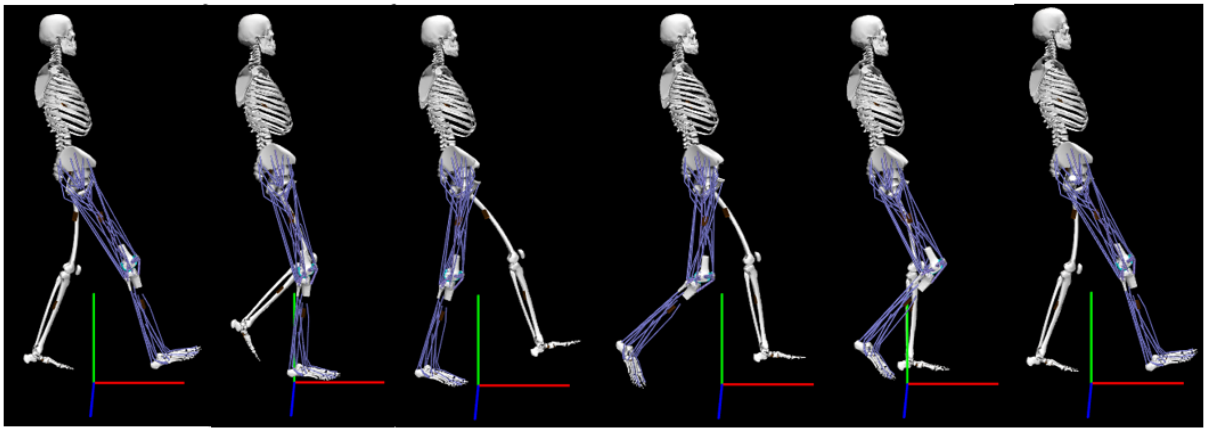

Fig. 4.9 IMU IK walking motion obtained as output from IMU IK tool. The pelvis is fixed at the origin, and the subject is not moving forward.

As a first approach to compare the IK of the two systems, the MoCap's pelvic coordinates (tx, ty,tz) were replaced the ones of the IMUs IK. As a result, the model finally had a real walking motion in the forward direction, similar to the MoCap, and they were compared to provide a preliminary assessment of the IMU IK results.

However, the goal of this thesis is to develop an approach that is not dependent on markers or to avoid using marker-based information. However, the measured ground reaction forces by the force plates cannot be used without the pelvis coordinates because their point of application is moving in space, along the forward direction. In the InCap case, on the other hand, the pelvis is fixed, and the feet move in a "sinusoidal" manner along the positive and negative x-axis. As a result, it was necessary to find a method for adjusting the ground reaction forces for the IMU approach, and for estimating the point of application of the ground reaction forces-centre of pressure (COP).

Some literature research was conducted in order to gather as much information as possible about techniques and methods developed by other researchers. A study [44] used statistical modelling to estimate the COP solely from raw gyroscope, accelerometer, and magnetometer data from IMUs. They used a linear model and a non-linear Long-Short-Term Memory (LSTM) neural network model. Karatsidis et al. [45] used a dynamic model with only IMUs to predict the COP; Jung et al. [46] developed dynamically adjustable foot-ground contact models for GRF estimation, which also provided COP estimation. Funk et al. [47] presented an ANN-based method for estimating COP during Tai Chi movements from video frames. Another study [48] evidenced the promising information predicted by acceleration and angular velocity data from various placement sensors using machine learning techniques, with the goal of

predicting COP by conducting various combinations of IMU(s) set at different locations with the LSTM models. Overall, all these techniques involve the use of machine learning methods and ANN (Artificial Neural Network), and they are not applicable to this project.

An interesting technique was found in the article of Dijkstra et al. [49], to obtain the GRFs for normal human gait called Zero Moment Point (ZMP). The ZMP is defined as the point on the ground where the horizontal moment components of the collected external loads are zero. It is commonly used in bipedal robot balance control by limiting the ZMP to remain within the base of support (BoS), resulting in a stable bipedal robotic gait. For the entire system to be dynamically stable, the point of application of the GRF in single stance should be within the base of the foot, according to the ZMP definition. This indicates that when the human body is dynamically stable, the ZMP coincides with the center of pressure (CoP).
In this study [49] they investigated the possibility of computing the GRFs and consequently joint moments during walking, using the ZMP as a tool. Essentially, they intended to validate the ZMP approach, which does not require force plates, for computing GRFs. Xiang et al [50] ZMP's approach was used to determine the GRFs at each foot. First, resultant forces and moments at the pelvis segment were computed using an inverse dynamics computation in OpenSim without GRFs. Then the computed ZMP, which is located on the ground where the horizontal components of the moment are zero, was found by translating the resulting forces and moments (Fig. 4.10).

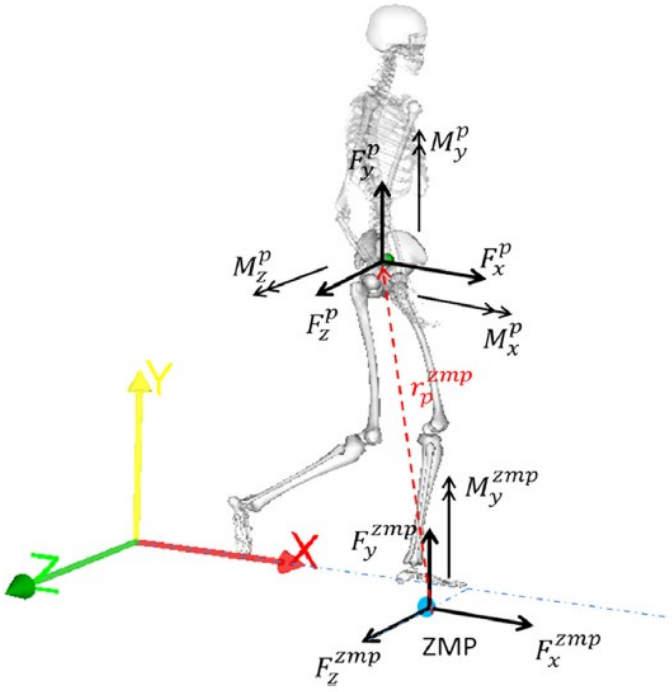

Fig. 4.10 The location of the ZMP is determined by translating the residual forces and moments at the pelvis to a point on the ground where the horizontal components of the moment are zero [49]

For this reason, the ZMP method can be exploited in this thesis for the estimation of the point of application of the GRFs, because the ZMP is the point on the ground where the resultant tangential moments of the active forces are zero. The position of ZMP can be calculated using the conditions: $M_z = 0$ and $M_x = 0$ (x is the walking direction, z is the lateral direction, and y is the vertical direction).

Basically, ZMP computations use a force and moment balance to transform a set of forces and moments applied at any point on the system to a dynamically equivalent set applied at the ZMP, which is a globally defined point on the ground [51].

Given a set of forces and moments ($\overline{F_p}$, $\overline{M_p}$) applied at the pelvis ($\overline{r_p}$), the equivalent forces and moments ($\overline{F_{ZMP}}$, $\overline{M_{ZMP}}$) applied at the ZMP ($\overline{r_{ZMP}}$):

$$\overline{F_{ZMP}} = \overline{F_p} \tag{1}$$

$$\overline{M_{ZMP}} + \overline{r_{ZMP}} \times \overline{F_{ZMP}} = \overline{M_p} + \overline{r_p} \times \overline{F_p} \tag{2}$$

Since the $\overline{F_{ZMP}}$ and $\overline{M_{ZMP}}$ are applied at the ground, $\overline{M_{ZMP}}$ consists of only the free moment, or the vertical component, such that $\overline{M_{ZMP}} = (0,\ M_{ZMP}, 0)$ and $\overline{r_{ZMP}}$ does not have a vertical component, such that $\overline{r_{ZMP}} = (X_{ZMP}, 0,\ Z_{ZMP})$, as represented by Fig. 4.10. Thus:

$$X_{ZMP} = f\left(MZ_p, FX_p, FY_p\right) = X_p + \frac{(MZ_p - Y_p FX_p)}{FY_p} \quad (3)$$

$$Z_{ZMP} = g\left(MX_p, FZ_p, FY_p\right) = Z_p - \frac{(MX_p + Y_p FZ_p)}{FY_p} \quad (4)$$

Using Equations 1-4, the resultant active moment at ZMP along the y-axis (also known as "free moment") is obtained as follows:

$$MY_{ZMP} = g\left(FX_p, FY_p, FZ_p, MX_p, MY_p, MZ_p\right) = MY_p + \frac{FX_p MX_p}{FY_p} + \frac{FZ_p MZ_p}{FY_p} \quad (5)$$

An assumption was made that $F_p(FX_p, FY_p, FZ_p)$ and $M_p(MX_p, MY_p, MZ_p)$ represent the set of forces and moments equivalent to only the experimental GRF forces (F_{GRF}) and moments (F_{GRF}) applied at the pelvis. The $\overline{r_{ZMP}}$, $\overline{F_{ZMP}}$, $\overline{M_{ZMP}}$ would be identical to the experimental COP, $\overline{F_{GRF}}$, $\overline{M_{GRF}}$ respectively when transformed using ZMP computations. In this way, it is possible to get the new centers of application of the measured GRFs, that are correctly positioned in space relative to the IMU frame. It is necessary to calculate only the x and z position of the ZMP (X_{ZMP}, Z_{ZMP}) and only the free moment MY_{ZMP} (vertical component). Hence, these equations were used and implemented in Matlab, to get the center of pressure of the measured GRFs for the inertial-based approach, where the pelvis is fixed at the origin. Therefore, the coordinates of the pelvis were imposed to zero ($X_p = 0, Z_p = 0$), except for the vertical coordinate Y_p which was equal to the height of the pelvis, derived from the IK file of the relative walking trial. The code with the implementation of the ZMP method can be found in the *Appendix B* section.

Dijkstra et al. [49] took a step further and used the resultant active forces at ZMP to calculate the GRF, showing how there are two major advantages of using the preceding ZMP formulation: the first is that calculating resultant active forces from equations of motion is very convenient and straightforward; and the second is that the resultant active forces (F_{ZMP}, MY_{ZMP}) and ZMP position r_{ZMP} are obtained simultaneously.

Only measured ground reaction forces and moments were used for this project, and a new GRF (.mot) file (Tab.4.4) was created for each walking trial, with the updated CoP calculated with ZMP for both the right and left foot.

Time	***ground force1 vx***	***ground force1 vy***	***ground force1 vz***	***ground force1 px***	***ground force1 py***	***ground force1 pz***	***ground torque1 x***	***ground torque1 y***	***ground torque1 z***
t_HS	.	.	.	Eq. (3)	0	Eq. (4)	0	Eq. (5)	0
.	.	.	.	.	.	.	.	.	.
.	.	.	.	.	.	.	.	.	.
.	.	.	.	.	.	.	.	.	.
.	.	.	.	.	.	.	.	.	.
t_TO	.	.	.	Eq. (3)	0	Eq. (4)	0	Eq. (5)	0

Tab. 4.4: Example of a .mot file during stance phase (from Heel-Strike (t_HS) to Toe-Off (t_TO)) with the measured GRF and the center of pressure updated with the ZMP method. Where:

- *ground_force1_vx, ground_force1_vy, ground_force1_vz* = equal to the measured ground reaction forces
- *ground_force1_px, ground_force1_py, ground_force1_pz* = X_{ZMP} (Eq. 3), $Y_{ZMP} = 0$, Z_{ZMP} (Eq. 4)
- *ground_torque1_x, ground_torque1_y, ground_torque1_z* = $MX_{ZMP} = 0$, MY_{ZMP} (Eq. 5), $MZ_{ZMP} = 0$

This new external load file was used as input for Inverse Dynamics and the Concurrent Optimization of Muscle Activation and Kinematics (COMAK) tool, which produced all the joint moments, muscle activations, and knee contact forces.

However, some issues with both the ID results, particularly the Hip and Knee flexion/extension moments, as shown in figure 4.11, and the COMAK results, particularly the knee contact forces for the vertical component, were discovered, highlighting a significant distinction between the two approaches (Fig. 4.12).

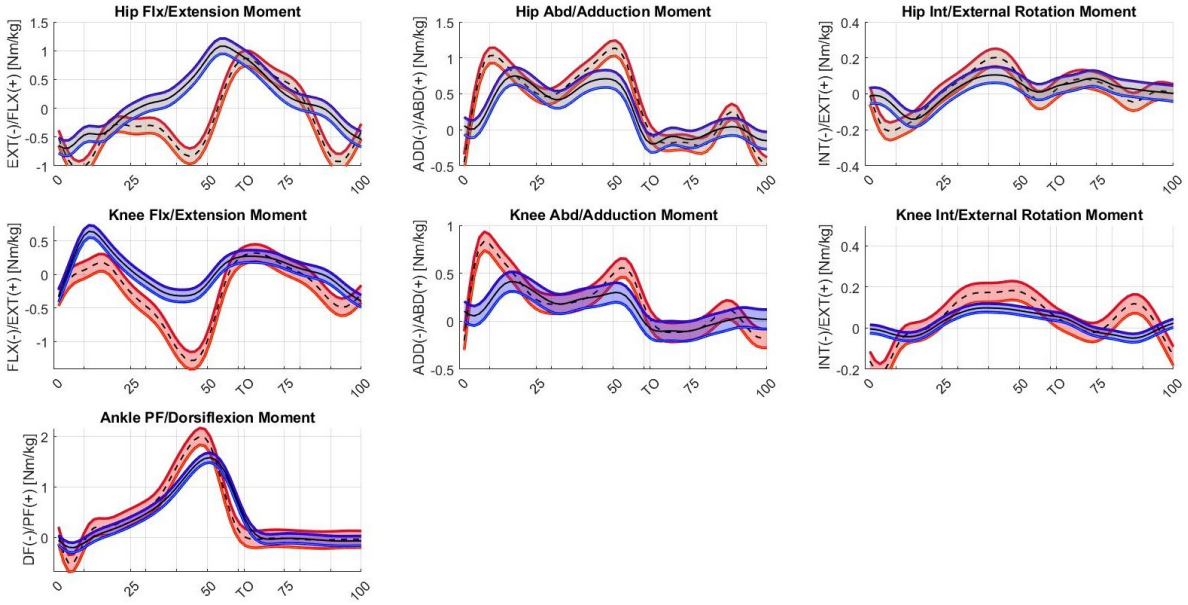

Fig. 4.11 ID results of one subject, in blue is the average over the walking trial (±std) for the MoCap system, in red is the average over the walking trial (±std) for the InCap system.

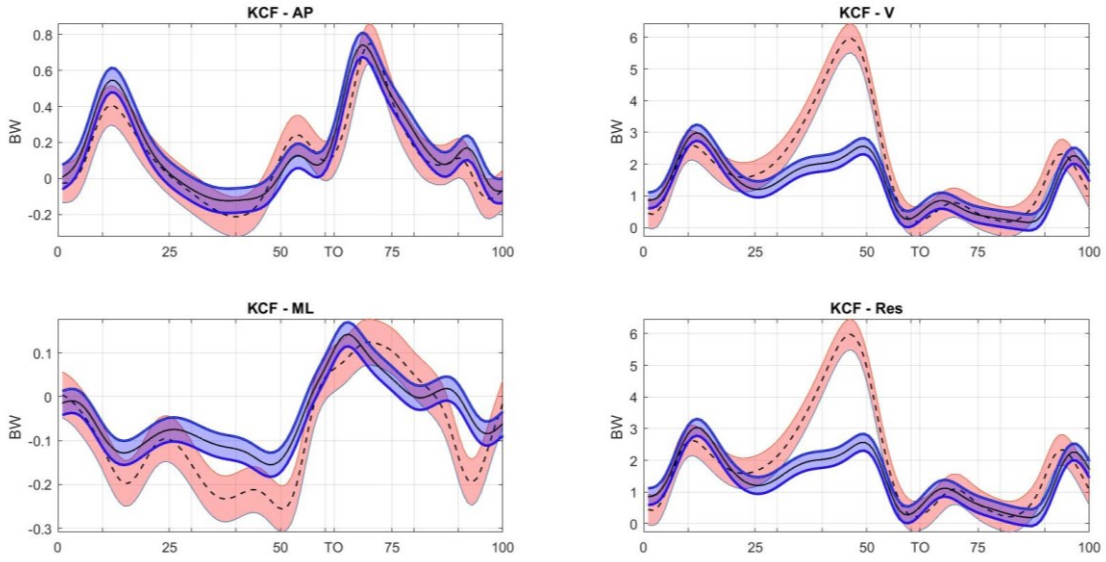

Fig. 4.12 Knee contact forces (KCF), for the anterior-posterior direction (AP), mediolateral (ML), and vertical (V). In blue is the average (±std) over the walking trial of one subject for the MoCap system and in red is the average over the walking trial (±std) for the InCap system

A solution was needed to correct and improve the estimation of the CoP, particularly at the beginning and end of the stance phase, where the point of application of the GRF was not very correct and was not inside the foot, as shown in figure 4.13.

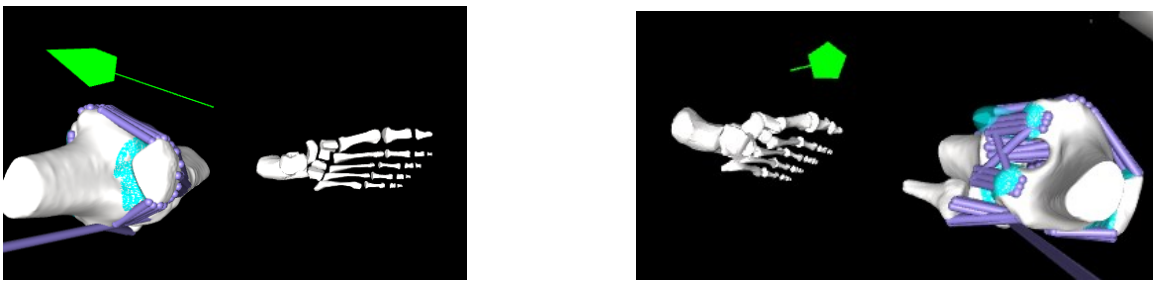

Fig. 4.13 On the left the position of the GRF is calculated via ZMP at Heel-Strike, while on the right at the instant of Toe-Off, viewed from the top

The first attempt made was to saturate the signal of the center of pressure along x and z (*x* is the walking direction, *z* is the lateral direction) to zero at the start and at the end of the stance phase. More specifically, from the moment of Heel-Strike (same for Toe-Off) to 10% of the stance phase, the variables *ground_force1_px*, *ground1_force_pz* (CoP along x and z-axis), *ground_force1_vx, ground_force1_vy, ground_force1_vz* were imposed to zero. Despite this, there was no evidence of improvements.

A more "direct" method was also tried, without interfering with the CoP, by using them as input to ID and COMAK Tool. The only change made was not to use the entire walking interval, but only the stance phase interval where the estimation of the CoP was reasonably correct. The idea was, that by removing the 3-4 frames in which the GRF's point of application was impossibly outside the foot, i.e., by eliminating any unhelpful/incorrect information, the results would improve. Despite this, no differences in the results were observed, as illustrated in Fig. 4.14 the minimal difference in the estimation of knee total contact force along the vertical direction, between using the entire stance phase interval (in blue) and the cut interval (in red).

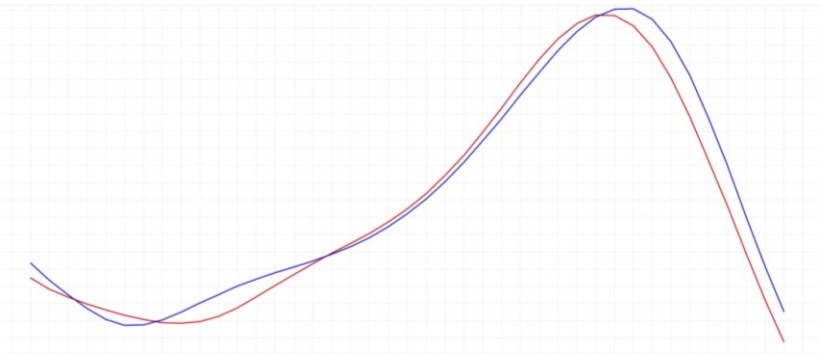

Fig. 4.14 Difference between the knee total contact force (y-axis in Netwon) estimation along vertical direction via COMAK, using the entire stance phase interval (in blue) and a specific interval of the stance phase (in red).

The main issue with the estimated CoP with ZMP was that the force was outside the foot during the Heel-Strike and Toe-Off. It was necessary to find a way to impose that, at the beginning of the stance phase, the point of application started approximately where the calcaneus was, while at the end it could not exceed the toes. In other words, the information on the position of the heel and toes was required to impose this "limit" on the CoP, at the start, and at the end.

First, the model of the specific subject was loaded into Matlab using the OpenSim API [32], and the position of the calcaneus' center of mass with respect to the calcaneus frame was determined `Xcom`, while `Zcom=0`:

```
Xcom = calcn_r.get_mass_center
```

The *Analyze Tool* of OpenSim was then used for each walking trial of every subject, specifically, the *BodyKinematics* analysis, which records the configuration (center of mass position and orientation) of each body, as well as their velocities (linear and angular) and accelerations (linear and angular) in the global coordinate systems. It also records the model's overall center of mass, as well as the velocity and acceleration of that center of mass. In this way, `calcn_r_X, and calcn_r_Z` described the position, along the x and z axis respectively, of the calcaneus' center of mass in time. Then, the calcaneus frame's position (`calcn_frame`) in time was calculated, using the information retrieved before on the distance from its CoM (`Xcom`) (Fig. 4.15), using the following line of pseudo-code:

```
calcn_frame_X = calcn_r_X - Xcom

calcn_frame_Z = calcn_r_Z
```

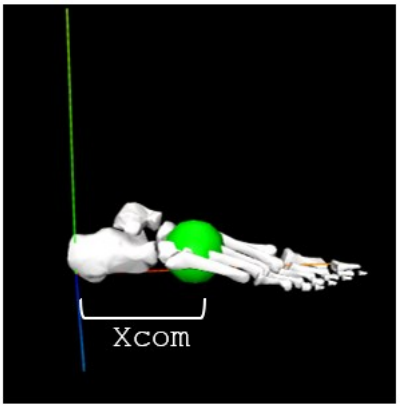

Fig. 4.15 It is shown the right leg calcaneus frame and its center of mass (in green). The distance along the x-axis (Xcom) was calculated to get the position of the calcaneus frame in time

This information was exploited to impose the *ground_force_px* and *ground_force_pz* equal to the `calcn_frame,` in a specific interval at the beginning of the stance phase:

```
ground_force_px = calcn_frame_X

ground_force_pz= calcn_frame_Z
```

Because the force coming out of the floor appears to be under the heel during loading in a normal walking, while under the toes during push off, as shown in figure 4.16. For this reason, for the end of the stance phase, the toes' center of mass was used to limit the GRF to exceed "outside" of the foot.

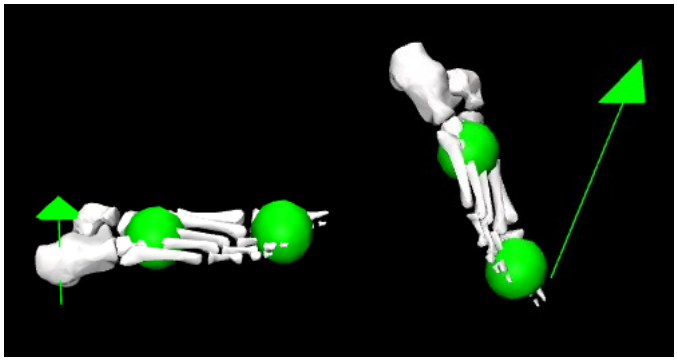

Fig. 4.16 Example of a MoCap walking motion, with measured GRF at the instant of Heel-Strike on the left, the calcaneus frame and center of mass (in green) are shown. On the right at the instant of Toe-Off with the toes' center of mass in green.

In this way, it was imposed that, for the first 3-4 frames, the point of application of the external force was inside the foot and it continues to be equal from the HS to 10% of the stance phase for the x direction, while for the z direction up to 15%. This is because it has been noted that the estimate of the *ground_force_pz* with ZMP is worse than the one along the x. The same thing was done for the final interval, except that the position of the toes along the x and z direction was exploited.

Finally, a Matlab function called *smoothdata* was used to smooth the obtained signal, particularly at the point of intersection between the calcaneus/toes trend and the estimation via ZMP. It computes a moving average of the elements of a vector using a heuristically determined fixed window length. The window moves down the vector's length, computing an average of the elements within each window. Specifically, the *"sgolay"* Savitzky-Golay filter is used as a smoothing method, which smooths according to a quadratic polynomial that is fitted over each window of data. When the data varies rapidly, this method may be more effective than others.

Consequently, the measured GRF with their CoP estimated via ZMP and improved with the previous method were used to generate the inverse dynamics and COMAK Tool results.

In the following chapter, it will be possible to look at the graphical comparison between the angles obtained with the COMAK IK Tool for the marker data and the angles obtained from the IMU IK Tool of OpenSense. The angles compared are the average values of the 10 healthy subjects, each of whom is represented by the average of their individual walking trials.The same comparison is shown for the joint moments resulting from ID, between the marker-based data using the measured ground reaction forces, and the measured GRF but with their point of application estimated via ZMP and saturation method described above. Moreover, all the activations of the main muscles (Tab. 4.2) will be illustrated and compared, and finally the results of the knee loadings. In particular, there will be displayed the tibiofemoral contact forces in the lateral and medial compartments, but also a total representation will be analyzed.

To provide a statistical evaluation of the COP estimation method for the InCap approach, a method for comparing the point of application measured of external forces and the one with ZMP was also required. The problem was always related to the fact that the pelvis is fixed for the IMU walking motion, therefore the trend of the CoPx, and CoPz is different from the ones of the MoCap. In fact, reference trends of the center of pressure over time, for the anterior-posterior and medial-lateral directions are illustrated in Fig. 4.17, while the ZMP ones are in Fig. 4.18.

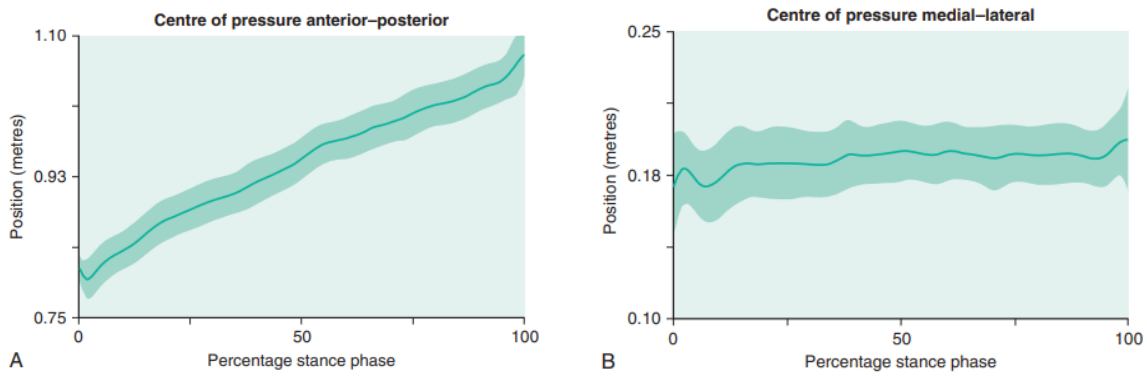

Fig. 4.17 Reference trend over time of the CoP, along anterior-posterior and medial-lateral direction [22]

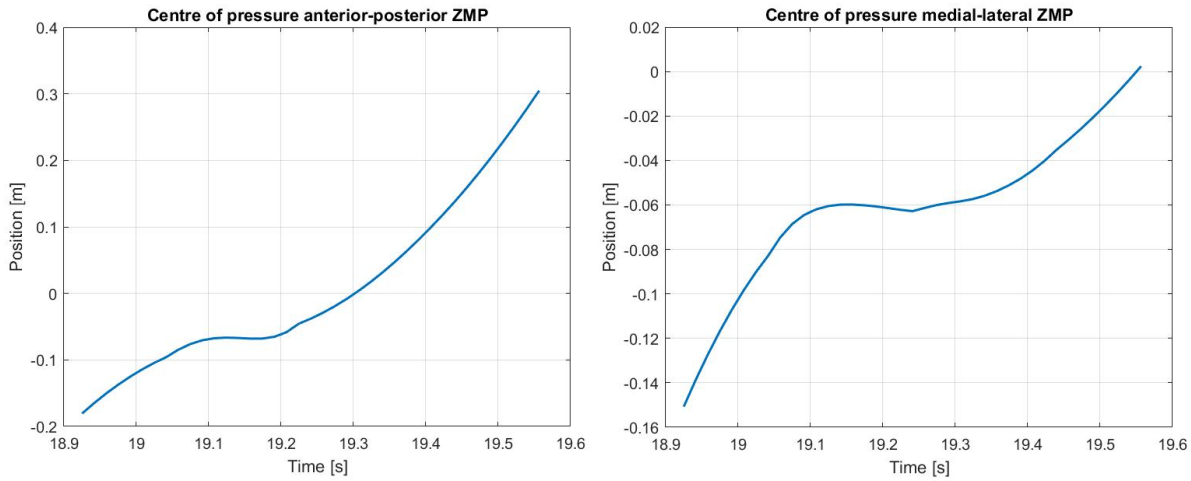

Fig. 4.18 Position over time of the saturated ZMP CoP, along anterior-posterior and medial-lateral direction

The position of the centers of pressure along the x-axis is different because the foot goes forward (anterior direction) and backward (posterior direction) since the pelvis is fixed. It is a matter of reference systems because all coordinates are expressed with respect to OpenSim's global coordinate system, and the CoP must be transformed into local coordinates to be comparable. For this reason, a transformation from the global coordinate system to the calcaneus coordinate system was performed in both the AP and ML directions, producing the CoP's position over time with respect to the calcaneus' frame.

To carry out this transformation, the *BodyKinematics* analysis for both IMU IK and marker IK had to be calculated to get the global position of the calcaneus. Then it was subtracted to it the respective *ground_force_px/pz* global, to determine the *ground_force_px/pz* "local"(`CoPx_local`,`CoPz_local`):

```
CoPx_local = calcn_frame_X - ground_force_px

CoPz_local = calcn_frame_Z - ground_force_pz
```

Finally, the local coordinates of the different approaches can be compared using the RMSE, median difference value, and Pearson correlation coefficient.

RMSE is commonly used in statistics to verify the experimental results, it shows the difference between the predicted and observed values in a model/estimator. In this project, it is used to calculate the error between the average results obtained from the marker-based and IMU-based approaches. Hence, to understand how the IMUs results are close to the "gold-standard" ones of the MoCap system. It is the square root of the mean of the difference between model prediction and target value. RMSE is never negative, and a value of 0 (which is almost never

reached) indicates a perfect fit to the data. A lower RMSE is generally preferable to a higher one. Different types of data cannot be compared since the value depends on the unit of measure. In addition to the RMSE value, the maximum difference between the average results of the two strategies will be displayed. Data were averaged over the specific number of trials of each participant's right leg. To account for participant-specific mass, contact forces were normalized to body weight (BW).

The Pearson correlation coefficient (r) is used to assess the strength of a linear relationship between two random variables, with $r = 1$ indicating a perfect positive correlation and $r = -1$ indicating a perfect negative correlation, while 0 indicates that the two variables are independent. In the work mentioned, it is used to look for a correlation between two curves (the average of each subject's walking trials) of the two strategies in comparison:

- Joint angles for IK
- Joint moments for ID
- Muscle activations
- Knee contact forces
- Local CoP

If a positive correlation is considered (same for the negative situation) the correlation is considered weak for values between 0 and 0.3, while moderate if $0.3 < r < 0.7$, and strong if it is greater than 0.07.

With all of these values, a general discussion of how the two systems estimate the various variables under consideration can be conducted, with particular emphasis on the accuracy of the inertial-based approach's estimates of knee loadings based on measured kinematics.

Chapter 5

5. Results

All of the results obtained using the appropriate workflow for each approach (as described in detail in *Sections 4.3.1* and *4.3.2*) will be displayed in the following chapter for a first visual comparison. The stereophotogrammetric system combined with in-ground embedded force plate systems, measured all the information used as input for the MoCap one, whereas the other approach followed a procedure whose data was not laboratory-related, but fully mobile, except for the use of the measured ground reaction forces' magnitude.
To allow for a more accurate comparison of the results, the average and the respective standard deviation data across all subjects were calculated, with each subject distinguished by the average over the specific number of trials of each participant's right leg. By overlapping the mean trend of both approaches, a clearer graphical comparison of the outcomes was possible. The calculation was computed in Matlab 2021a, but some adjustments were needed before computing the average. The Gait Cycle (GC) of each trial has a different duration and to obtain the average it was necessary to have the same number of samples. Therefore, resample was performed (*resample* function), so that each GC was of the same size. In particular, given that the time duration was expressed as a percentage of the GC, all movements were time-normalized as 101 data points at 1% intervals of a gait cycle. Once the resampled tests had been obtained, it was possible to calculate the mean and the standard deviation. This was done both for the MoCap and InCap results. The average trends and the standard deviation of the two approaches are therefore represented on the same graph, making the representation clearer.

As a legend for the graphs, blue always indicates the marker-based approach, and red always the IMU-based one. The average value of each result is represented with the dashed line for the MoCap, while a continuous line for the other approach, each band is constructed as on the mean values ± 1 standard deviation.
The x-coordinate corresponds to the gait cycle (GC) as a percentage, and the ordinate axis represents the value of the variables under analysis:

- Degrees for joint angles (IK)
- Nm/kg for joint moments (ID)
- Excitations [0-1] for muscle activations

- Body weight for knee contact forces

For the first two points, the graphs are presented in such a way that the rows correspond to a joint and the columns to a type of movement. The first row is dedicated to the hip, the second to the knee, and the third to the ankle. As for the columns, the first is dedicated to flexion-extension, the second to abduction-adduction, and the third to intra-extra rotation.

The Root Mean Square Error (RMSE) value, as well as the maximum and median differences, will be available for each result. Pearson's correlation was used to assess the agreement and consistency of the two estimation systems.

It is important to understand that because the dataset is made up of ten subjects, each with a different number of walking trials, variability can be seen at many levels. The difference found in the same subject in multiple repetitions of the same task is referred to as intra-subject. Inter-subject variability refers to the variation of motor patterns that occurs when multiple subjects perform the same motion.

The data analysis focused on comparing the performance of the InCap-driven musculoskeletal model to the MoCap-driven musculoskeletal model in estimating knee contact forces. Furthermore, the kinematics obtained from the COMAK IK Tool and the *OpenSense* tool were compared to better understand the accuracy of the *IMU Inverse Kinematics* tool in comparison to the optimized COMAK one.

5.1 Inverse kinematics MoCap vs InCap

The comparison of the joint angles computed with IMU orientations, and the joint angles computed from optical motion capture was done using root mean square (RMS) difference. The Pearson correlation between each subject and joint angle was calculated and it was also reported the mean and standard deviation for the correlation coefficients, RMSE, and maximum difference.

Figure 5.1 shows a representative estimate of joint angles for the two approaches. The following lower limb joints are examined: hip, knee, and ankle. Except for the ankle (which only has dorsi/plantar flexion), flexion/extension, abduction/adduction, and internal/external rotation are all taken into account.

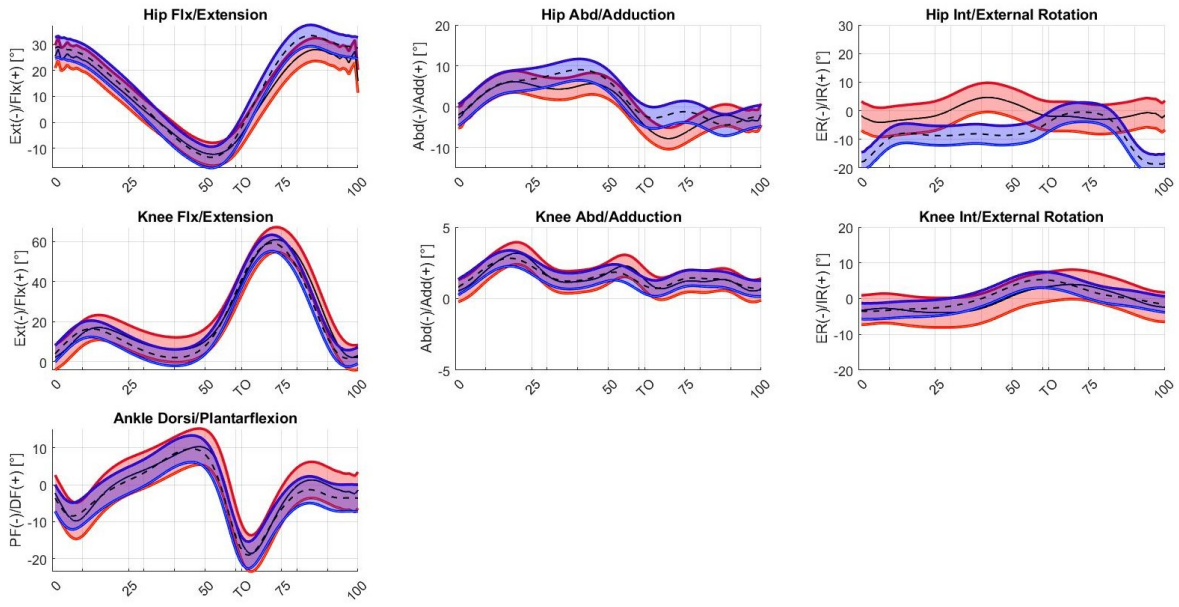

Fig. 5.1 Joint angles obtained from Inverse Kinematics using the two different approaches. In blue is the MoCap system, while in red is the inertial-based one. In black (-- dashed line) the mean (± std) across the 10 subjects of the MoCap. In black (- continue line) the average (± std) of the 10 subjects for the IMU approach.

From a graphical perspective, it can be seen that the primary kinematics (the sagittal plane) are very good for both approaches, whereas the results for other anatomical levels worsen, especially on the transversal plane. The literature [52] confirms this distinction between the sagittal plane and the other planes, stating that the frontal plane and the transverse plane are more prone to errors.

It must be remembered that for both approaches the secondary kinematics are obtained through

COMAK, therefore they are optimized to generate the measured accelerations in the primary degrees of freedom while minimizing an objective function (see *Section 4.2*).

Average joint angles comparison between MoCap and InCap (inter-subject)

	mean ± std		
	Correlation coefficient	**RMSE (°)**	**Maximum difference (°)**
Hip Flx/Ext	0.98 ± 0.01	4.74 ± 2.29	12.06 ± 4.72
Hip Abd/Add	0.78 ± 0.15	3.68 ± 1.60	7.02 ± 2.70
Hip Int/Ext Rot	-0.03 ± 0.46	10.06 ± 4.42	12.49 ± 5.51
Knee Flx/Ext	0.98 ± 0.02	5.52 ± 3.02	11.22 ± 5.92
Knee Abd/Add	0.43 ± 0.21	1.05 ± 0.44	2.38 ± 1.07
Knee Int/Ext Rot	0.64 ± 0.28	3.73 ± 1.85	11.27 ± 5.86
Ankle Dors/Plt Flex	0.95 ± 0.03	4.43 ± 1.91	8.27 ± 3.27

Tab. 5.1 Average value (± standard deviation) of the correlation coefficient (Pearson value), root mean square error, and maximum value of the difference between each joint angle of the two approaches. It is the average between subjects **(inter-subjects)**, each one characterized by the average of their walking trials (intra-subjects)

Average RMS differences between IMU and optical-based kinematics were 1-6° for all joint angles except hip rotation (10°); these values are within the reported variability and uncertainty of optical motion capture [53].

IMU-based hip rotation showed the least agreement with optical-based kinematics with a negative Pearson coefficient r=-0.03. While for the other movement it was found moderate and strong correlations between the IMU-based kinematics and the optical-based kinematics ranging from r = 0.63–0.98 (table 5.1)

The mean value, calculated for each subject over the respective walking trials can be found in the *Appendix*, for the correlation coefficient, RMSE, and maximum difference.

5.2 Inverse Dynamics MoCap vs InCap

Figure 5.2 shows joint moments for the hip, knee, and ankle joints during overground walking. In blue are the outcomes from the optical-based approach that used the kinematics and ground reactions measured by the stereophotogrammetric system as input. In red the inertial derived kinematics and measured GRF, but with the point of application obtained via ZMP calculations.

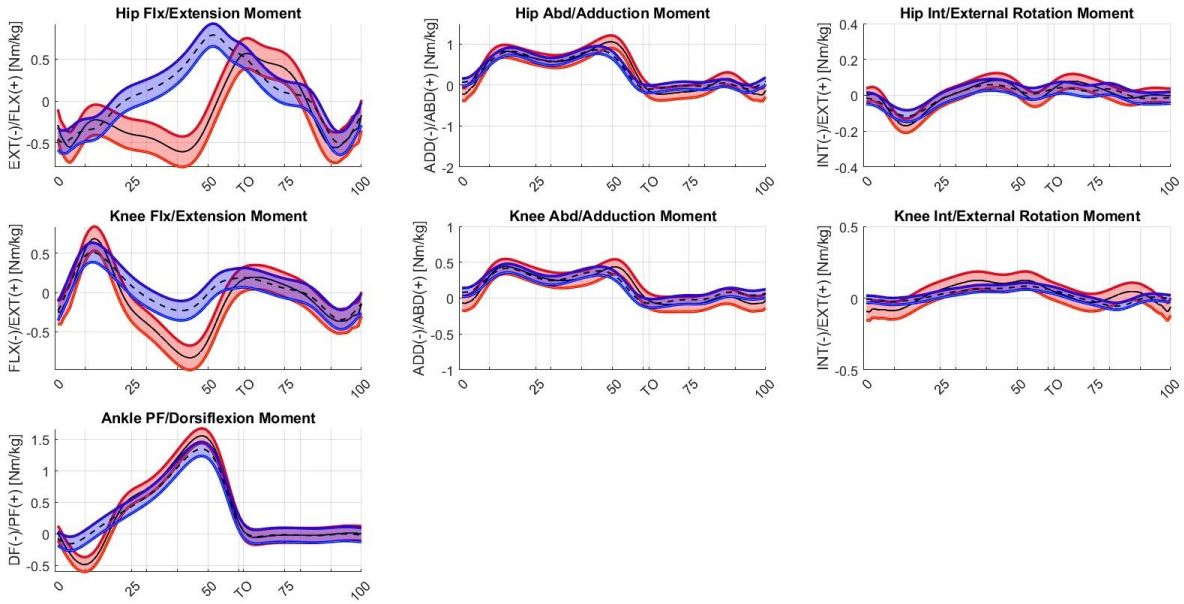

Fig. 5.2 Joint moments obtained from Inverse Dynamics using the two different approaches. In blue is the MoCap system, while in is red the inertial-based one. In black (-- dashed line) the mean (± std) across the 10 subjects of the MoCap. In black (- continue line) the mean (± std) across the 10 subjects of the InCap system.

The marker approach results are consistent with the literature [54].

For the hip the GRF passes quite far anterior to the joint during heel strike, resulting in a peak flexion moment. The GRF still passes anterior to the hip after a heel strike, but the distance from the force to the hip is much shorter. After midstance, the force is directed posteriorly to the hip, creating an extension moment. The first thing that is noticed between the two methodologies is the large difference in the moment of the hip joint in the sagittal plane. The non-wearable approach has a trend consistent with the literature [54], whereas the InCap average trend deviates significantly from the reference. Above all, there is a greater moment of extension in the middle of the gait cycle, when the moment of maximum flexion should occur after a few instants. This is because the GRF position estimated with ZMP is posterior to the hip center, creating an extension moment.

The GRF initially passes anterior to the knee joint during heel strike, resulting in an extension moment. The GRF then rapidly passes behind the knee joint, causing flexion. After midstance,

the force returns to the front of the knee until toe off. This is noticeable in the blue trends, but there is still a big difference in the sagittal plane for the IMU-based approach in red, where there is a bigger flexion moment of the knee at 50% of the GC, due probably to the CoP estimation position, that seems to be too behind the joint center, increasing the flexion moment. While for the ankle the ground reaction force (GRF) passes very close to the joint center during the heel strike, producing a very small moment, for the MoCap case, the GRF passes behind the ankle joint, resulting in a dorsiflexion moment. Similarly, to what occurred in the InCap case in which the calcaneus origin was used as the first point of application of the free body diagram, behind the ankle joint. In fact, in red it is represented a joint moment reaching 0.5 times the body weight (BW).
Then, the GRF moves in front of the ankle joint after the heel strike, resulting in a plantarflexion moment. This increases as the force moves under the metatarsal heads and during push off.

Average joint moments comparison between MoCap and InCap (inter-subject)

	mean ± std		
	Correlation coefficient	**RMSE (Nm/kg)**	**Maximum difference (Nm/kg)**
Hip Flx/Ext Mom	0.37 ± 0.137	0.48 ± 0.17	1.10 ± 0.39
Hip Abd/Add Mom	0.86 ± 0.051	0.24 ± 0.09	0.61 ± 0.26
Hip Int/Ext Rot Mom	0.73 ± 0.161	0.05 ± 0.02	0.93 ± 0.34
Knee Flx/Ext Mom	0.75 ± 0.104	0.3 ± 0.13	0.72 ± 0.29
Knee Abd/Add Mom	0.76 ± 0.104	0.15 ± 0.06	0.35 ± 0.17
Knee Int/Ext Rot Mom	0.52 ± 0.150	0.07 ± 0.03	0.46 ± 0.19
Ankle Dors/Plt Flex Mom	0.94 ± 0.028	0.22 ± 0.09	0.58 ± 0.23

Tab. 5.2 Average value (± standard deviation) of the correlation coefficient (Pearson value), root mean square error and maximum value of the difference between each joint moment of the two approaches. It is the average between subjects **(inter-subjects)**, each one characterized by the average of their walking trials (intra-subjects)

Table 5.2 confirms the description previously made just from the visual comparison, highlighting the big differences between the hip flexion/extension moment, with a maximum difference of 1.10 Nm/kg, a RMSE=0.48 Nm/kg, and a moderate correlation (r=0.37). The same for the knee moment in the sagittal plane with a maximum difference of 0.93, a RMSE=0.3 Nm/kg, but a strong correlation (r=0.75). Overall, the other results have RMSE ranging from 0.05-0.24 Nm/kg and moderate/strong correlation coefficient (r=0.52-0.94).

5.3 Muscle activations MoCap vs InCap

In this section the muscle activations outcomes are displayed, only the main muscles involved in a normal walking motion were considered. A distinction was made between the thigh and leg muscles. For the thigh, there are the hamstrings (biceps femoris, semimembranosus, semitendinosus) and quadriceps (rectus femoris, vastus lateralis, vastus medialis).

The primary function of the hamstrings is to flex the knee joint and extend the hip, while the function of the quadriceps femoris muscle is to extend the leg at the knee joint and flex the thigh at the hip joint.

The lower limb movement pattern observed during walking is the result of an interaction between external forces (joint reaction and ground reaction) and internal forces (produced by muscles and other soft tissue). Therapists who need to understand how muscle activity and timing contribute to stability and propulsion will benefit from understanding the ground reaction force.

Thigh muscles

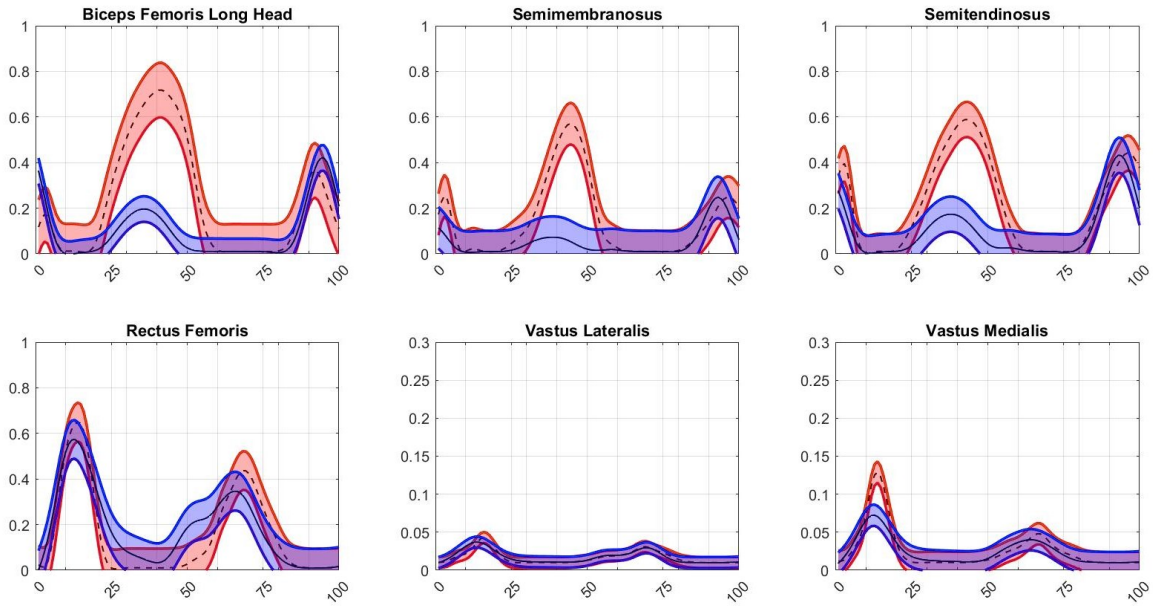

Fig. 5.3 Thigh muscle activations, in blue is the MoCap system, while in red is the inertial-based one. In black (-- dashed line) the mean (± std) across the 10 subjects of the MoCap. In black (- continue line) the mean (± std) across the 10 subjects of the InCap system

Leg muscles

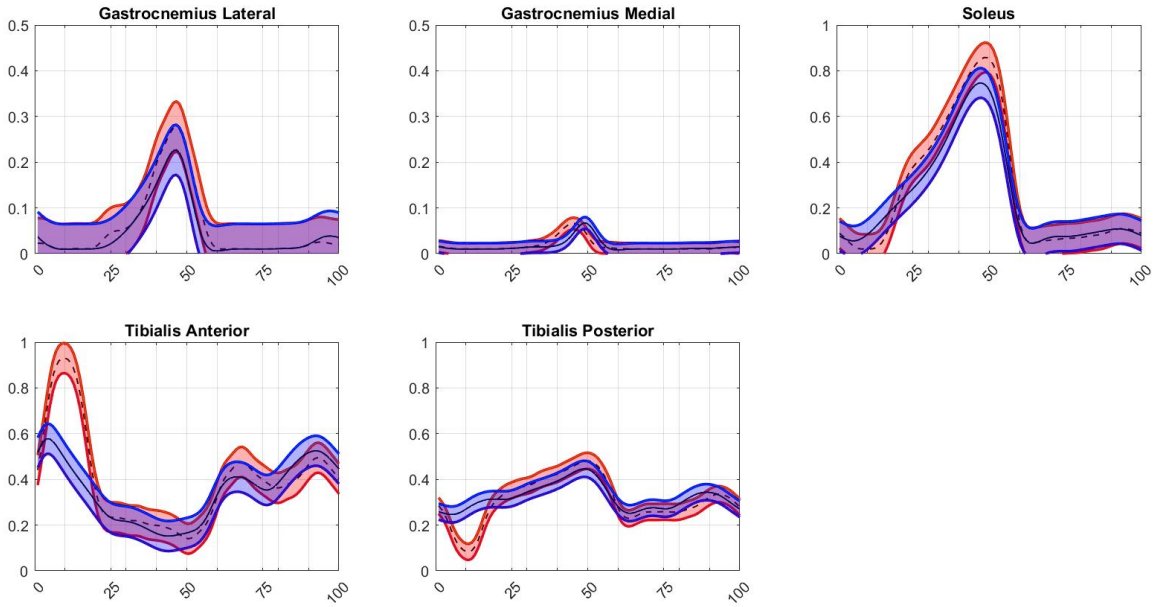

Fig. 5.4 Leg muscle activations, in blue is the MoCap system, while in red is the inertial-based one. In black (-- dashed line) the mean (± std) across the 10 subjects of the MoCap. In black (- continue line) the mean (± std) across the 10 subjects of the InCap system

The results shown in figures 5.3 and 5.4 can be explained by dividing the gait cycle into sub-phases.

During the **loading response** (0-12% of GC), as the foot swings through to make contact with the ground at heel strike, the ankle dorsiflexors (tibialis anterior) act eccentrically to prevent the foot from slapping on the ground. In fig.5.4, there is a greater activation for the IMU case, most likely due to the GRF position passing anterior to the ankle center, resulting in a greater dorsi-flexion moment at the ankle. The quadriceps control knee flexion eccentrically, while the hamstrings control hip flexion isometrically (primarily biceps femoris, semimembranosus, and semitendinosus).

During **midstance** (12-31% GC), as the body moves over the stance limb, the foot rolls forward into the foot flat position, controlled by eccentric contraction of the ankle dorsiflexor muscles (tibialis anterior). The quadriceps act concentrically to initiate knee extension, with the vastus medialis being especially active for the InCap.

The ankle plantar flexors (gastrocnemius, soleus, and tibialis posterior) continue to function in the **terminal stance** (31 to 50% of GC), becoming isometric at around 35 to 40% of the gait cycle, when the upper part of the body causes the heel to move up from the floor. During this phase, the quadriceps are inactive because ground reaction forces, hamstrings, and plantar flexor activity keep the knee extended. There is a significant difference in activation of the knee flexors in the inertial case versus the other approach.

Forceful plantarflexion occurs during **preswing** (50-62% of GC) due to the action of the gastrocnemius and soleus muscles, as well as the tibialis posterior, creating propulsion during the heel-off and toe-off stages. Rectus femoris also works with the vastus lateralis and medialis to limit knee flexion and increase hip flexion.

During the very brief phase of the **initial swing** the hip flexors and knee extensors (primarily rectus femoris) continue their preswing activity. Dorsiflexors work together to allow the forefoot to leave the ground.

Except for the dorsiflexors, muscle activity virtually stops during the **midswing** as the extremity's inertia carries it through the swing like a pendulum.

Finally, in the **terminal swing**, the hamstrings act to slow the swinging limb, while the dorsiflexors maintain ankle position for initial contact. The quadriceps initiate activity just before the foot touches the ground, revealing the existence of a feedforward mechanism by which the body prepares for the large ground reaction its joints will encounter at initial contact.

Overall, the *JointMechanics* tool results agree with the kinematics and kinetics outcomes for both procedures. The main differences are most likely due to the different position of the GRF, which causes a different joint moment and thus different muscle activations

5.4 Knee contact forces MoCap vs InCap

The tibial-femoral contacts were obtained as output of the *JointMechanics* tool of COMAK. A distinction between the lateral and medial compartments was made, as shown in figure 5.5 the division of the knee joint.

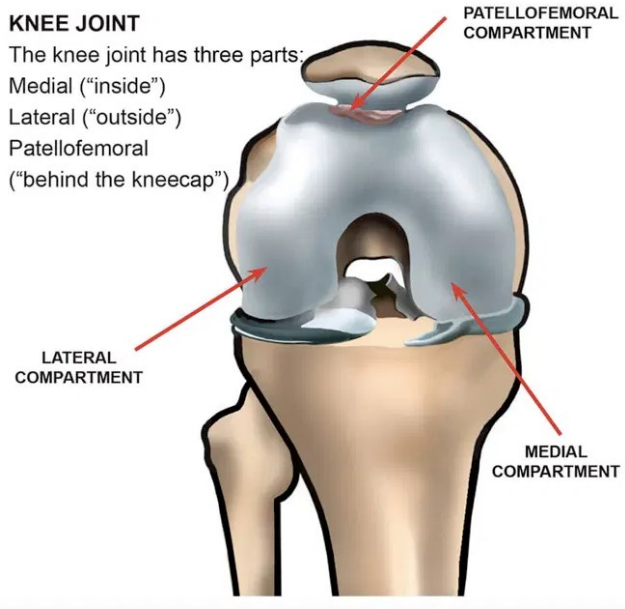

Fig. 5.5 The three major compartments of the knee joint: medial, lateral, and patellofemoral

Knee contact forces-Medial compartment

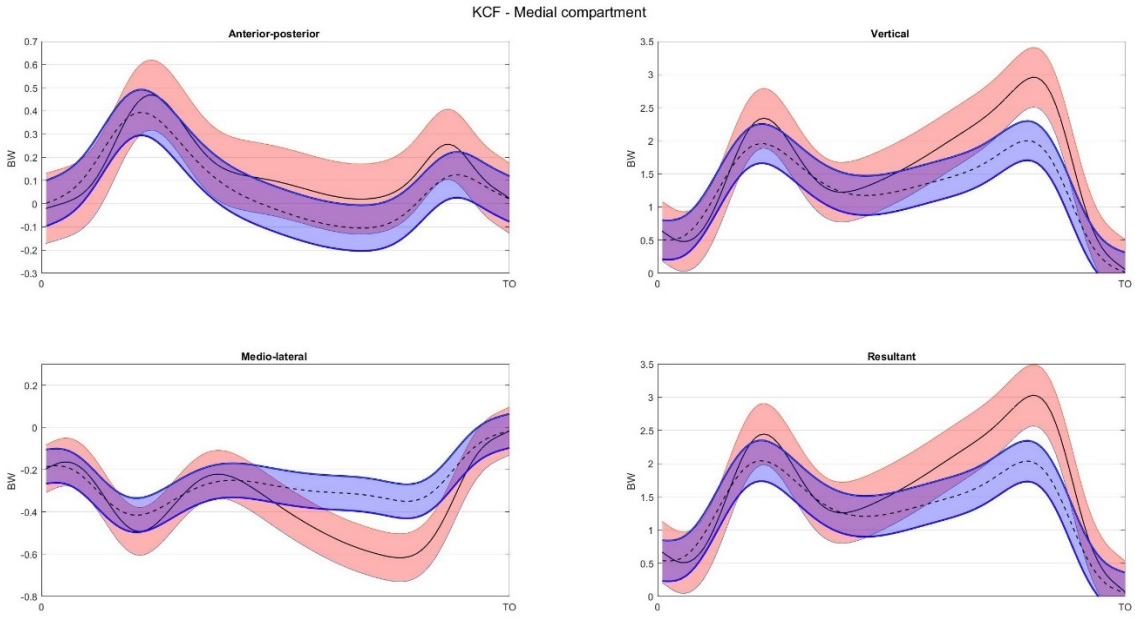

Fig. 5.6 Knee contact forces in the **medial** compartment (KCF), anterior-posterior (AP), vertical (V), medial-lateral (ML), resultant (Res) obtained via COMAK using the two different approaches as input. In blue is the MoCap system, while in red is the inertial-based one. In black (-- dashed line) the mean (± std) across the 10 subjects of the MoCap. In black (- continue line) the mean (± std) across the 10 subjects of the InCap system.

Knee contact forces-Lateral compartment

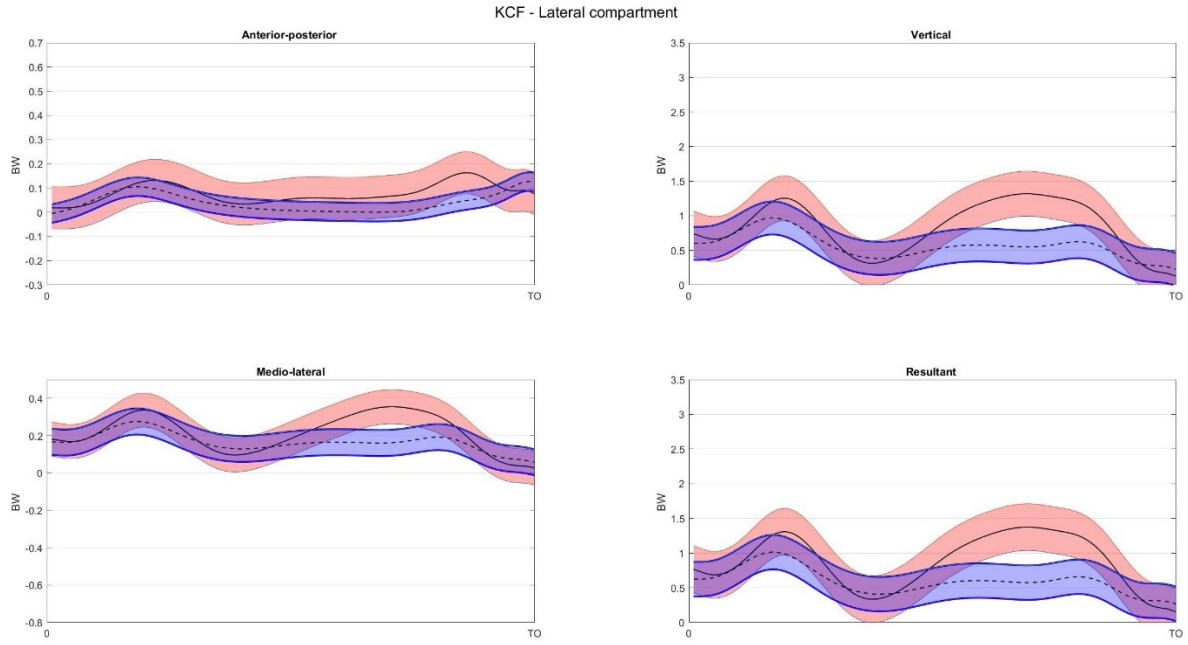

Fig. 5.7 Knee contact forces in the **lateral** compartment (KCF), anterior-posterior (AP), vertical (V), medial-lateral (ML), resultant (Res) obtained via COMAK using the two different approaches as input. In blue is the MoCap system, while in red is the inertial-based one. In black (-- dashed line) the mean (± std) across the 10 subjects of the MoCap. In black (- continue line) the mean (± std) across the 10 subjects of the InCap system

The majority of the contact forces during gait pass through the medial condyle [55], as shown in fig 5.6 with higher CF values. The total knee contact forces exhibited double peaks during the stance phase, and the majority of the loading was distributed vertically, as expected.

The IMU case has larger peaks between the two approaches, which is likely because the joint moments are different, as previously discussed, resulting in greater compression forces and higher contact pressures at the knee. The maximum vertical peak reached by the medial compartment is 3.5 times the body weight, while the lateral compartment reaches 1.5 BW. Because the total knee contact force is the sum of the medial and lateral compartments for each direction, the values of the peaks are increased to nearly 5 times the BW for the InCap. The resultant KCF (Res) shown in the figures before, represents the resultant of the forces acting in the respective compartments of the knee, and it is the root square of the sum of the three squared directions components:

$$KCF(Res) = \sqrt{KCF\_AP^2 + KCF\_V^2 + KCF\_ML^2}$$

Knee total contact forces

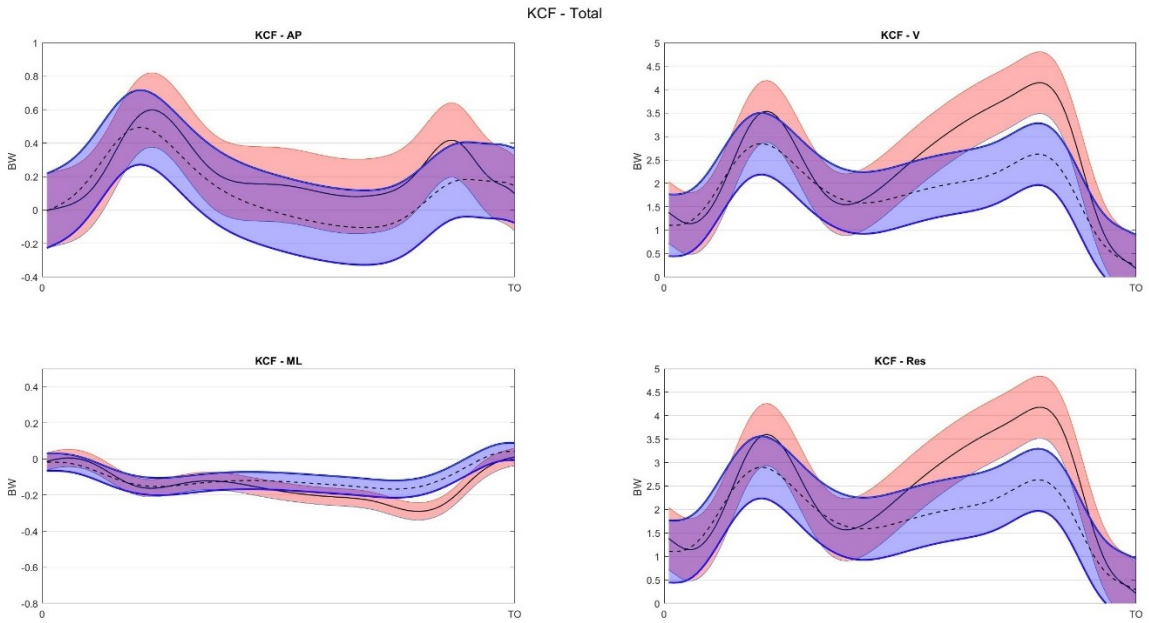

Fig. 5.8 Knee total contact forces (KCF), anterior-posterior (AP), vertical (V), medial-lateral (ML), resultant (Res) obtained via COMAK using the two different approaches as input. In blue is the MoCap system, while in red is the inertial-based one. In black (-- dashed line) the mean (± std) across the 10 subjects of the MoCap. In black (- continue line) the mean (± std) across the 10 subjects of the InCap system.

Average Knee contact forces comparison between MoCap and InCap (inter-subject)

	mean ± std		
	Correlation coefficient	**RMSE (BW)**	**Maximum difference (BW)**
Knee contact force Anterior-Posterior (AP)	0.70 ± 0.24	0.24 ± 0.13	0.49 ± 0.18
Knee contact force Vertical (V)	0.75 ± 0.09	1.10 ± 0.34	2.48 ± 0.87
Knee contact force Medio-Lateral (ML)	0.70 ± 0.13	0.10 ± 0.05	0.21 ± 0.05
Knee contact force Resultant (Res)	0.75 ± 0.10	1.11 ± 0.33	2.51 ± 0.85

Tab. 5.3 Average value (± standard deviation) of the correlation coefficient (Pearson value), root mean square error and maximum value of the difference between each total CFs of the two approaches. It is the average between subjects **(inter-subjects)**, each one characterized by the average of their walking trials (intra-subjects)

Table 5.3 demonstrates a strong correlation for all directions of total knee contact forces. The average root mean square error in the vertical direction is 1.10 times the BW, with a maximum difference of 2.48. The anterior-posterior direction had an RMSE of 0.24 and a maximum difference of 0.49, while the medio-lateral direction had an RMSE of 0.10 and a maximum difference of 0.21. This agrees with the magnitude of the peaks depicted in figure 5.8 because the ML direction has the least contact forces in comparison to the others.

To compare the outcomes obtained with other research studies found in the literature, it is important to remember that the gold standard for assessing the magnitude of a joint loading is *in vivo* measurement. The ability to measure in vivo muscle and joint contact forces during normal and pathological walking would help clinicians diagnose musculoskeletal disorders and develop new or improved treatments. Because direct measurement of these internal forces is not clinically feasible, musculoskeletal modelling has emerged as the primary method for generating estimates.

In the past studies of musculoskeletal modelling that estimated in vivo tibial contact forces during gait, have used a sequential computational approach. The conventional "Sequential Solution" resolves muscle forces first with a simplified multibody model, then applies these forces to a detailed joint model. While this method allows complex, high-fidelity joint-level models to be used to assess ligament and cartilage loading, it decouples muscle forces from joint-level mechanics [43].

The "Concurrent Solution" called COMAK approach has recently been proposed, in which the muscle forces and joint mechanics are solved concurrently, so that the joint kinematics, ligament forces, and cartilage pressures are directly coupled with the muscle forces [1]. As discussed previously the gait results predicted the characteristic bimodal loading of the tibiofemoral joint during the stance phase of walking. The medial contact pressure was higher than on the lateral side. In vivo tibiofemoral contact loadings during gait have not been measured, thus direct validation is not feasible. However, the outcomes of the MoCap agree favorably with image-based measures of tibiofemoral contact patterns during normal gait [56]. Gait simulations of Smith's (Fig. 5.9) study [1] show similar trends, with a second peak bigger than the first reaching almost 3.5 times the body weight for the total force. Also, the timings of the two peaks are similar to the one found in this project, at approximately 18% and 48% of the gait cycle.

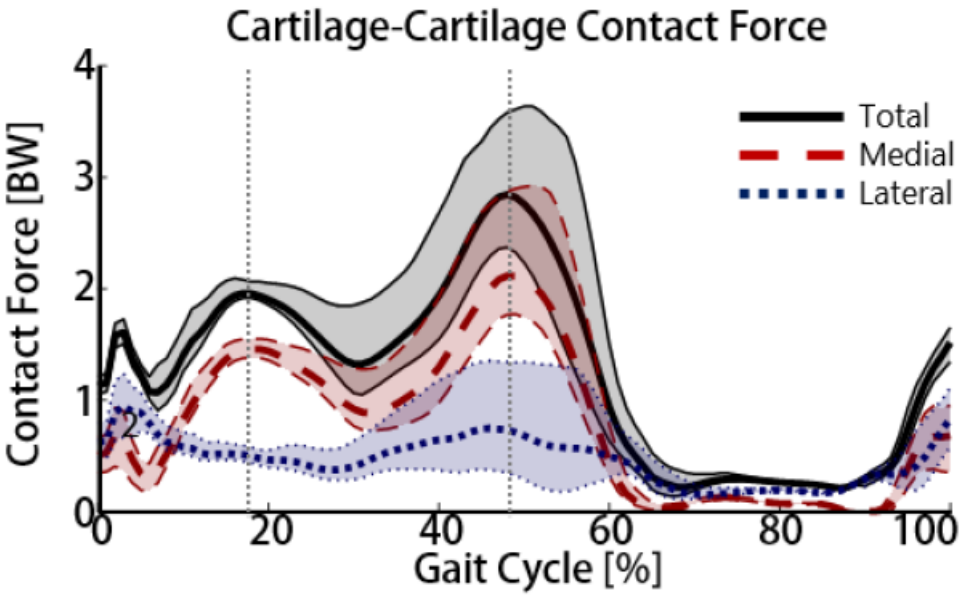

Fig. 5.9 Predicted tibiofemoral contact forces during a simulated gait cycle. The bold centerlines are the mean and shaded regions show the 5th to 95th percentiles of the Monte Carlo analysis of neuromuscular coordination. The vertical dotted lines indicate the instances of 1st and 2nd peak total tibiofemoral contact force [43]

Deepak et al. [57] calculated the loading by balancing the external moments with internal muscle and contact forces, of both healthy and pathological (OA) patients. The average peak total loading for the control subjects was in the range of 2 – 4.5 BWs which agrees with another report (3 – 4.4 BWs) using similar techniques [58]. While values reported from the instrumented knee studies range from 2.1 – 3.5 BWs [59].

Peak medial loading reported using mathematical models range from 2.3 – 2.4 BWs [60], [61]. Deepak et al. data for average peak medial loading range from 0.8 – 3 for the control subjects which is close to previous predictions.

Overall, the marker-based knee contact forces estimate agrees with the literature findings, while for the IMU there is a difference of a maximum of 1 BW that may be due to many different aspects. First of all, muscles' contribution has an important role in determining the joint loading, as well is related to the joints' moment behavior.

5.5 Center of pressure MoCap vs InCap

In the chapter of Materials and Method it had been discussed about the problem of estimating the center of pressure of the measured ground reaction forces for the inertial-based approach. A comparison of the two approaches was required to validate the method and understand the errors made using the ZMP and then the saturation procedure.

The figure below (Fig.5.10) provides an example of how the method, used to compare the two CoPs, is correct. The two trends diverge more at the beginning and end of the stance phase, because GRF acquisition is rarely perfect, even when using force platforms, and there may always be minor errors or settlements at the beginning and end. Another reason to mention is that the file containing the measured external forces (.mot) has been resampled at the same acquisition frequency as the InCap (60 Hz), so the number of final samples is much lower, and it is normal for errors and differences to exist.

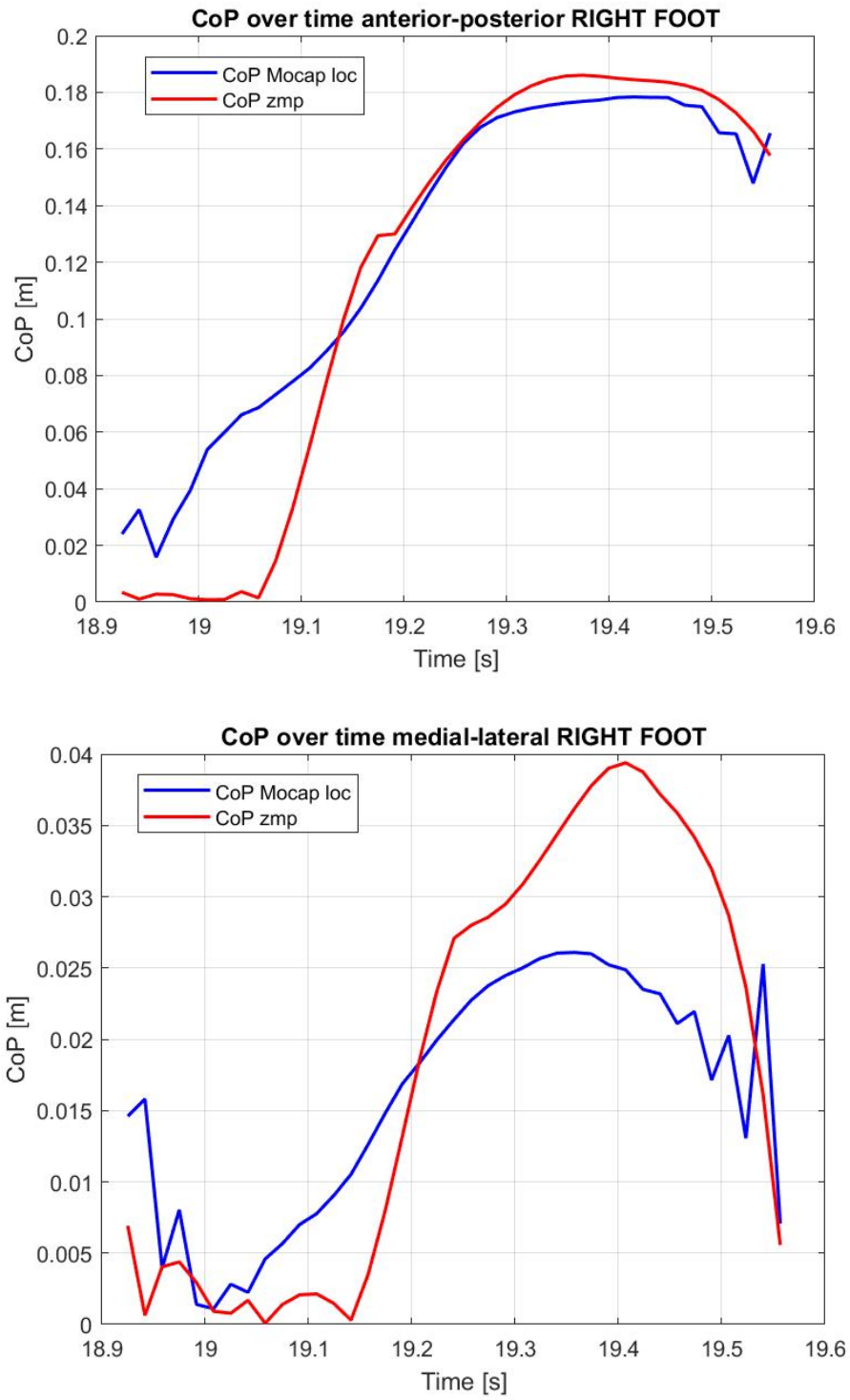

Fig. 5.10 Example of a CoP comparison between the CoP MoCap (in blue) and the CoP ZMP (in red) expressed in local coordinates (calcaneus' frame). Over the anterior-posterior direction (x-axis) and medio-lateral direction (z-axis). The time interval considered is the stance phase of the right foot.

Average CoP comparison between MoCap and InCap (inter-subject)

	mean ± std		
	Correlation coefficient	**RMSE (cm)**	**Median error (cm)**
CoP Anterior-Posterior	0.94 ± 0.29	3.1 ± 1.0	2.6 ± 0.7
CoP Medio-Lateral	0.22 ± 0.42	1.5 ± 0.6	1.3 ± 0.6

Tab. 5.4 Average value (± standard deviation) of the correlation coefficient (Pearson value), root mean square error and median value of the difference between the local MoCap and ZMP over all the subjects. It is the average between subjects **(inter-subjects)**, each one characterized by the average of their walking trials (intra-subjects)

Table 5.4 revealed a strong correlation (r = 0.94) between the CoP trends in the anterior-posterior direction, but a low correlation (r = 0.22) in the mediolateral direction. This is also demonstrated in figure 5.10, which shows how the GRF's point of application along the z-axis is more variable. The RMSE is in the range of 3 cm for AP and 1.5 cm for ML. This was also compared to the literature, studies that attempted to estimate the position of CoPs using data obtained from inertial sensors were taken into consideration.

Chen et al. [48] used machine learning techniques to predict the COP during a gait cycle using acceleration and angular velocity data from different placement sensors. Such as the long short-term memory (LSTM), which is frequently used in time series data and aims to reduce the user's burden while utilizing novel wearable technology. They reported a normalized RMSE of 5.88 ± 0.96% in the AP direction and 25.33±2.35% in the ML direction.

LSTM was used in a linear and non-linear neural network model in another study [44]. Models were trained on COP ground truth data collected using an instrumented treadmill and achieved an average intra-subject root mean square (RMS) error of 12.3mm and an average inter-subject RMS error of 23.7mm.

Karatsidis et al. [45] predicted the COP using only IMUs; Jung et al. [46] developed dynamically adjustable foot-ground contact models for GRF estimation that also provided COP estimation. It was also taken into account the research of Audu et al. [62] who developed a three-dimensional biomechanical model of human standing that enabled COP estimation using an optical motion tracking system.

Table 5.5 summarizes both the literature and the results of this project. In general, both the obtained results and the results from the literature show that the RMS error is greater in the anterior direction than in the lateral direction.

Study	**AP**	**ML**
Results	31	15
[44] Linear model LSTM	19.6	13.0
[44] Non linear LSTM	14.9	9.0
[45]	45	29
[46]	23.1	8.4
[62]	45	10

Tab. 5.5 RMSE (mm) comparison between the results of this thesis and results from references [44], [45], [46], [62]. They are reported for the anterior and lateral directions.

5.6 Discussion, conclusions, and further development

The findings above make it possible to draw some conclusions about the use of IMUs in the analysis of human movements, particularly in understanding the knee loading mechanism. The goal of this thesis was to develop an approach that follows similar steps of the marker-based approach, calculating contact forces at the knee joint as final results, but attempting to replace some of it without using any marker-derived information to make it more mobile and laboratory independent.

In general, optical motion capture systems with skin-mounted reflective markers are used to capture human motion kinematics. However, gathering in-vivo secondary knee kinematic data is difficult. Secondary (non-flexion) tibiofemoral (TF) bone motions are minor and using skin-mounted markers introduces significant error due to the deformable soft tissue layer between the bone and the marker. As a result, skin-mounted optical motion capture is not a reliable method for measuring dynamic three-dimensional TF kinematics.
Although not ideal for collecting secondary kinematics, medical imaging is a useful tool for digitally reconstructing the geometries of the articulating surfaces within the knee. These data are required to predict contact in the knee joint and estimate pressure distribution on the contact area. MRI or CT scans are frequently used to collect images, which are then digitized and converted to 3D femur and tibia mesh files used to estimate contact. The geometry of these surfaces is critical in determining the contact area, which is used to estimate pressure, which is the final component required to study knee mechanics. Tibiofemoral contact is calculated using an elastic foundation model that determines pressure as a function of articulating cartilage surface interpenetration.
Hence, in-vivo data collection is not always feasible because it is costly, difficult to monitor, and often invasive if instrumented implants must be inserted into the body. Musculoskeletal modelling, which allows analyses to be performed on a musculoskeletal model scaled to represent a subject, is a useful alternative to in-vivo measurements.
For this reason, the starting point for both approaches was the 12 DOFs knee model of Thelen et. al [2], kinematics and kinetics values were evaluated as well, as they are loading pre-cursors. In addition, to have a complete view of the knee mechanics, the activations of the main muscle involved in a walking motion were assessed.

Regarding the results of the inverse kinematics, it can be stated that the joint angles obtained using *OpenSense* toolbox for the IMUs data were consistent with those of the motion capture data, obtained using the specific COMAK IK tool. The secondary knee kinematics (5-

TF, 6-patellofemoral) for both approaches were obtained via COMAK algorithm and evolved naturally as a function of muscle, ligament, and cartilage contact forces under zero instantaneous acceleration constraints.

The RMS differences were all between 1-6 °, apart from hip rotation (10 °). Previous research compared the sagittal, frontal, and transverse plane movement kinematic estimation accuracy of the InCap and MoCap systems, with sagittal and non-sagittal plane angle errors ranging from 5° to 18° [63], [64]. An error of less than 2° is acceptable in most clinical applications, while errors of 2° to 5° are also acceptable but require specific interpretation. The differences observed could be caused by sensor-to-segment calibration, which is performed using the *IMU Placer tool* and is an important process for estimating body segment orientations. As a result, some errors may be generated during this process, resulting in differences in the kinematics outcomes. Another method that could be used to improve the calibration procedure is dynamic calibration [65], which is based on functional movements such as hip abduction/adduction, sit-to-stand, and walking and can improve sensor-to-segment accuracy, particularly for non-sagittal plane kinematics.

To make the approach more mobile, the next step was to use the measured GRF magnitude but estimate the COP using ZMP. In the previous chapter, it was demonstrated that this method can produce comparable results in terms of COP estimation to the references, with an error of 1.5cm for the mediolateral displacement and a larger error of 3 cm for the anterior-posterior displacement. Because estimating the center of pressure (COP) is an important part of gait analysis, such as when assessing the functional capacity of individuals with motor impairment. Inertial measurement units (IMUs) are commonly used to measure gait characteristics of healthy and impaired subjects, and in the future, they can be used to estimate the COP solely from sensor data, using machine learning and artificial neural network techniques, as their application has increased exponentially in recent years. All of the advantages of inertial measurement units, such as their minimal price, portability, and thus suitability for use in non-laboratory settings, can therefore be realized. It is also possible to track successive steps while walking over multiple steps, which was previously impossible to do in gait laboratories equipped with one, two, or three force plates.

The main differences in the Inverse Dynamics results were in the knee and hip flexion/extension moments. The source of these errors is most likely related to the GRF point of application; because it is an estimate for the InCap case, its position may not be completely correct. As a result, the GRF can generate a different moment because the lever arm changes depending on the CoP position, and a larger lever arm generates a larger joint moment.

Naturally, all discrepancies are due to the method used: ZMP and saturation. The timing used for the imposition at the beginning and end of the saturation process to be equal to the calcaneus origin and toes respectively, may be the source of the main errors.

Because muscle forces generate 60-80% of total intrinsic knee load and are distributed through the medial compartment of the tibio-femoral joint. The pattern and magnitude of knee compressive forces are directly influenced by how people activate their muscles. As a result, assessments of muscle forces and joint moments are required to fully comprehend the altered loading mechanisms. The majority of gait studies have concentrated on knee kinematics and kinetics, muscle activations, and muscle forces. As a result, it is critical to investigate all of these variables concurrently and relate them to the involvement of knee loading.
It was discussed in detail in section 5.4 how and why each muscle is activated, from the comparison of the two approaches the results were reasonable, except for the over activation of the hamstrings during the terminal stance, probably related to the inverse dynamics, thus to the center of application of the GRF.
Overall, muscle forces have been suggested as the principal factors of joint contact forces [66], with correct predictions of muscle forces resulting in reasonable joint contact load estimates. However, accurate measurement and prediction of individual muscle forces remains a major challenge to date.

Because musculoskeletal loading is influenced by a variety of inter-individual factors, including weight and gender, as well as the activity performed. The combination of complex structural anatomy, complicated movements, and dynamic, often indeterminate muscle function makes determining the in vivo loading environment in the human knee difficult. While direct measurement techniques such as instrumented prostheses have been used to determine loading in the hip and spine, the outcomes of instrumented implants in the knee have yet to be determined. As a result, mathematical models for estimating muscle and joint contact forces have been developed [67].
Recent advancements in musculoskeletal simulation offer improved methods for estimating in vivo soft tissue loads. New multibody musculoskeletal simulation algorithms allow for the simultaneous resolution of limb dynamics and joint mechanics. This ensures dynamic consistency between scales and more accurately simulates physical reality.
However, the main algorithms suffer from long computation times, numerical instability, and simplifying assumptions. COMAK present a novel simulation framework that uses software and hardware advancements to investigate the interaction of limb, muscle, and joint mechanics across the entire parameter space of a musculoskeletal model during simulation.

Tibiofemoral contact pressure was measured as output of COMAK, and all of the subjects had double-peaked tibiofemoral loading curves. For repetitions of the same activity, small intra-individual variations were observed, with comparatively greater inter-individual variation for different subjects repeating the same task. The intra-subject variability is shown in the *Appendix* for all of the results, not just the KCFs. The IMU approach had a higher peak in the x- and y-direction, precisely peak tibio-femoral contact forces during walking were 2.7 (MoCap) and 4.1 (InCap) BW on average. The second peak was the highest because the knee was in extension and the gastrocnemii (the strongest muscle in the knee joint's stance phase) was mostly active there.

Thus, the estimates from the marker-based approach are more reasonable and comparable to the results from the literature than those from the inertial-based approach. However, this was to be expected given the number of factors that influenced the wearable approach negatively. First of all it must be remembered that the ZMP was never use in this specific way to estimate the center of application of the ground reaction forces, and also the saturation process was an attempt made for this project. More research is needed to improve the method and better understand how to improve the signal obtained from the ZMP Matlab code. Aside from errors in the GRF point of applications, kinematic errors influence the final results of the KCFs, and muscle activations.

The musculoskeletal model properties and error introduced by the optimization process in COMAK are two of the limitations of contact location computation. In additions the main limitations of COMAK simulation framework are caused by the uncertainty in model parameters and fidelity of the experimental motion analysis measurements. Therefore, musculoskeletal models are useful because they enable detailed analyses of factors that are difficult to study in vivo; however, these analyses can be sensitive to model properties such as muscle strength, mass distribution, or soft tissue artifact, which are difficult to accurately measure and apply to the model.

To summarize, the primary goal of the thesis was to determine whether it is possible to perform a complete analysis of human movement, focusing on understanding the knee loading, outside of the traditional laboratory of 3D motion capture. Although InCap systems have become an appealing alternative to 3D MoCap systems, many factors must be considered. Given the current limiting accuracy, particularly for non-sagittal plane kinematics, improving the accuracy of InCap 3D joint kinematic estimations to achieve the same level of accuracy as seen in 3D MoCap is critical. Such developments would have obvious applications in a variety of MSK dysfunction (for example, osteoarthritis (OA)), where the joints' range of motion

(ROM) or movement extremes are required in clinical practice to properly analyze and monitor joint loading. The ability of current InCap systems to detect such clinically relevant differences is limited, making advancements in InCap kinematic estimation even more critical for clinical application.

The ultimate goal of developing a marker-free approach would be to avoid using the measured GRFs by force plates and instead estimate them using only the information retrieved by the sensors. Many researchers are investigating methods to estimate GRF and moments using sensor accelerations using machine learning techniques and neural networks, and this will be the direction for future developments.

Appendix A

For each subjects the Pearson coefficient, RMSE and maximum difference was calculated averaging over their number of walking trials.

Average joint angles (IK) comparison between MoCap and InCap (intra-subject)

	Correlation coefficient						
	Hip Flx/Ext	**Hip Abd/Add**	**Hip Int/Ext Rot**	**Knee Flx/Ext**	**Knee Abd/Add**	**Knee Int/Ext Rot**	**Ankle Dors/Plt Flex**
TBM_H01	0.99	0.88	-0.09	0.99	0.45	0.82	0.95
TBM_H02	0.97	0.88	-0.50	0.95	0.53	0.94	0.92
TBM_H03	0.98	0.53	-0.39	0.99	0.73	0.81	0.96
TBM_H04	1.00	0.81	-0.46	0.99	0.24	0.37	0.96
TBM_H06	0.96	0.86	-0.28	0.98	0.55	0.74	0.90
TBM_H07	0.99	0.93	0.18	0.97	0.51	0.96	0.97
TBM_H08	0.98	0.87	0.21	0.97	0.48	0.79	0.94
TBM_H11	0.99	0.67	-0.36	0.99	0.20	0.15	0.97
TBM_H12	0.99	0.85	0.67	0.98	0.58	0.52	0.99
TBM_H14	0.98	0.51	0.74	0.94	0.03	0.33	0.90
AVERAGE	0.98	0.78	-0.03	0.98	0.43	0.64	0.95

	Root mean square error (°)						
	Hip Flx/Ext	**Hip Abd/Add**	**Hip Int/Ext Rot**	**Knee Flx/Ext**	**Knee Abd/Add**	**Knee Int/Ext Rot**	**Ankle Dors/Plt Flex**
TBM_H01	7.84	4.07	12.61	3.59	1.65	4.74	2.79
TBM_H02	5.22	4.01	7.40	7.15	1.01	6.20	4.77
TBM_H03	4.17	6.73	7.49	7.34	0.65	2.89	3.78
TBM_H04	5.15	4.58	12.64	5.51	1.01	2.85	4.60
TBM_H06	5.88	4.12	10.52	4.04	1.14	3.61	3.99
TBM_H07	3.40	2.92	10.38	6.42	1.54	2.31	5.54
TBM_H08	7.28	3.28	11.61	5.64	1.23	3.35	7.50
TBM_H11	2.61	4.17	14.56	2.87	0.99	3.48	4.64
TBM_H12	6.87	3.55	16.14	6.32	1.18	5.24	5.66
TBM_H14	3.73	3.07	7.33	11.89	1.11	6.41	5.45
AVERAGE	5.22	4.05	11.07	6.08	1.15	4.11	4.87

	Maximum difference (°)						
	Hip Flx/Ext	**Hip Abd/Add**	**Hip Int/Ext Rot**	**Knee Flx/Ext**	**Knee Abd/Add**	**Knee Int/Ext Rot**	**Ankle Dors/Plt Flex**
TBM_H01	18.76	7.79	15.18	7.83	3.65	15.69	5.96
TBM_H02	12.22	8.24	15.94	19.40	2.09	16.12	9.68
TBM_H03	9.92	10.49	22.88	12.89	1.49	7.77	7.73
TBM_H04	12.62	7.63	10.85	9.58	2.26	9.96	7.64
TBM_H06	10.35	8.10	10.68	8.32	2.39	11.92	8.03
TBM_H07	12.66	5.28	14.19	14.02	4.11	8.91	9.97
TBM_H08	14.01	6.88	9.94	11.85	2.76	11.83	11.15
TBM_H11	12.39	9.17	11.07	6.03	2.17	22.87	8.44
TBM_H12	16.42	7.00	12.43	12.57	2.72	11.86	10.00
TBM_H14	13.27	6.68	14.28	20.97	2.54	7.07	12.32
AVERAGE	13.26	7.72	13.74	12.35	2.62	12.40	9.09

Average joint moments (ID) comparison between MoCap and InCap (intra-subject)

	Correlation coefficient						
	Hip Flx/Ext Mom	Hip Abd/Add Mom	Hip Int/Ext Rot Mom	Knee Flx/Ext Mom	Knee Abd/Add Mom	Knee Int/Ext Rot Mom	Ankle Dors/Plt Flex Mom
TBM_H01	0.64	0.86	0.81	0.81	0.75	0.64	0.88
TBM_H02	0.36	0.80	0.75	0.88	0.65	0.59	0.94
TBM_H03	0.36	0.86	0.52	0.86	0.86	0.57	0.98
TBM_H04	0.39	0.92	0.77	0.69	0.82	0.42	0.96
TBM_H06	0.08	0.84	0.72	0.77	0.79	0.38	0.92
TBM_H07	0.30	0.89	0.93	0.89	0.63	0.47	0.95
TBM_H08	0.39	0.88	0.87	0.73	0.86	0.43	0.95
TBM_H11	0.44	0.79	0.52	0.65	0.61	0.60	0.92
TBM_H12	0.35	0.94	0.90	0.59	0.90	0.83	0.96
TBM_H14	0.35	0.81	0.50	0.68	0.69	0.32	0.95
AVERAGE	0.37	0.96	0.73	0.75	0.76	0.52	0.94

	Root mean square error (Nm/kg)						
	Hip Flx/Ext Mom	Hip Abd/Add Mom	Hip Int/Ext Rot Mom	Knee Flx/Ext Mom	Knee Abd/Add Mom	Knee Int/Ext Rot Mom	Ankle Dors/Plt Flex Mom
TBM_H01	0.57	0.30	0.06	0.40	0.19	0.09	0.29
TBM_H02	0.49	0.29	0.06	0.29	0.17	0.08	0.25
TBM_H03	0.57	0.23	0.05	0.20	0.12	0.06	0.12
TBM_H04	0.51	0.21	0.05	0.35	0.17	0.11	0.26
TBM_H06	0.55	0.29	0.04	0.28	0.19	0.11	0.24
TBM_H07	0.55	0.32	0.05	0.27	0.24	0.10	0.21
TBM_H08	0.58	0.26	0.05	0.42	0.13	0.07	0.25
TBM_H11	0.52	0.28	0.04	0.37	0.15	0.07	0.27
TBM_H12	0.54	0.18	0.04	0.48	0.11	0.05	0.25
TBM_H14	0.43	0.26	0.06	0.27	0.17	0.09	0.31
AVERAGE	0.53	0.26	0.05	0.33	0.16	0.08	0.24

	Maximum difference (Nm/kg)						
	Hip Flx/Ext Mom	**Hip Abd/Add Mom**	**Hip Int/Ext Rot Mom**	**Knee Flx/Ext Mom**	**Knee Abd/Add Mom**	**Knee Int/Ext Rot Mom**	**Ankle Dors/Plt Flex Mom**
TBM_H01	1.33	0.86	0.95	0.85	0.51	0.52	0.87
TBM_H02	1.05	0.73	1.19	0.76	0.41	0.56	0.71
TBM_H03	1.30	0.54	0.96	0.53	0.21	0.44	0.34
TBM_H04	1.09	0.43	1.21	0.75	0.36	0.67	0.53
TBM_H06	1.43	0.86	0.88	0.77	0.49	0.46	0.59
TBM_H07	1.27	0.90	1.01	0.62	0.57	0.37	0.69
TBM_H08	1.29	0.59	1.21	1.02	0.26	0.65	0.65
TBM_H11	1.25	0.77	0.77	0.96	0.31	0.33	0.68
TBM_H12	1.17	0.45	1.03	1.00	0.24	0.54	0.62
TBM_H14	0.88	0.64	0.98	0.62	0.51	0.56	0.67
AVERAGE	1.21	0.68	1.02	0.79	0.39	0.51	0.63

Average Knee contact forces comparison between MoCap and InCap (intra-subject)

	Correlation coefficient			
	Knee contact force Anterior-Posterior (AP)	**Knee contact force Vertical (V)**	**Knee contact force Medio-Lateral (ML)**	**Knee contact force Resultant (Res)**
TBM_H01	0.88	0.78	0.80	0.77
TBM_H02	0.84	0.80	0.42	0.80
TBM_H03	0.26	0.82	0.74	0.81
TBM_H04	0.72	0.71	0.61	0.71
TBM_H06	0.78	0.75	0.66	0.74
TBM_H07	0.86	0.91	0.88	0.92
TBM_H08	0.84	0.62	0.76	0.62
TBM_H11	0.82	0.78	0.65	0.77
TBM_H12	0.79	0.59	0.77	0.58
TBM_H14	0.26	0.78	0.75	0.77
AVERAGE	0.70	0.75	0.70	0.75

	Root mean square error (BW)			
	Knee contact force Anterior-Posterior (AP)	**Knee contact force Vertical (V)**	**Knee contact force Medio-Lateral (ML)**	**Knee contact force Resultant (Res)**
TBM_H01	0.11	1.27	0.08	1.28
TBM_H02	0.30	1.02	0.09	1.04
TBM_H03	0.30	0.59	0.07	0.61
TBM_H04	0.19	0.93	0.08	0.93
TBM_H06	0.14	1.18	0.09	1.19
TBM_H07	0.44	0.86	0.23	0.89
TBM_H08	0.19	1.49	0.10	1.49
TBM_H11	0.12	1.24	0.11	1.25
TBM_H12	0.16	1.68	0.08	1.68
TBM_H14	0.46	0.73	0.09	0.78
AVERAGE	0.24	1.10	0.10	1.11

	Maximum difference (BW)			
	Knee contact force Anterior-Posterior (AP)	**Knee contact force Vertical (V)**	**Knee contact force Medio-Lateral (ML)**	**Knee contact force Resultant (Res)**
TBM_H01	0.26	2.80	0.20	2.80
TBM_H02	0.60	2.39	0.19	2.45
TBM_H03	0.72	1.33	0.17	1.37
TBM_H04	0.40	1.99	0.16	1.97
TBM_H06	0.37	2.77	0.22	2.78
TBM_H07	0.68	1.55	0.31	1.61
TBM_H08	0.49	3.89	0.21	3.90
TBM_H11	0.37	3.18	0.28	3.20
TBM_H12	0.31	3.39	0.16	3.39
TBM_H14	0.73	1.53	0.16	1.63
AVERAGE	0.49	2.48	0.21	2.51

Average CoP comparison between MoCap and InCap (intra-subject)

	Correlation coefficient	
	CoP Anterior-Posterior	CoP Medio-Lateral
TBM_H01	0.95	0.29
TBM_H02	0.97	0.91
TBM_H03	0.96	0.44
TBM_H04	0.89	-0.37
TBM_H06	0.98	0.41
TBM_H07	0.96	0.80
TBM_H08	0.94	-0.33
TBM_H11	0.96	0.06
TBM_H12	0.88	-0.06
TBM_H14	0.87	0.07
AVERAGE	0.94	0.22

	Root mean square error (cm)	
	CoP Anterior-Posterior	CoP Medio-Lateral
TBM_H01	2.91	1.95
TBM_H02	3.04	0.71
TBM_H03	2.03	0.99
TBM_H04	4.74	1.53
TBM_H06	2.73	1.16
TBM_H07	2.90	2.32
TBM_H08	3.00	2.07
TBM_H11	3.35	2.28
TBM_H12	4.84	1.80
TBM_H14	4.74	1.20
AVERAGE	3.22	1.60

	Median error (cm)	
	CoP Anterior-Posterior	CoP Medio-Lateral
TBM_H01	2.70	1.66
TBM_H02	2.20	0.59
TBM_H03	1.55	0.63
TBM_H04	3.91	1.13
TBM_H06	2.38	0.96
TBM_H07	2.53	2.25
TBM_H08	2.14	1.82
TBM_H11	2.39	1.93
TBM_H12	3.08	1.29
TBM_H14	3.34	0.63
AVERAGE	2.62	1.29

Appendix B – Codes used

Function Batch_Transform.m converts from .mvnx files to .mat

```
%% Read and Save data structs Xsens
%%%%% This script loads the Xsens data from mvnx files. These files are
%%%%% loaded from a patient directory, and the resulting struct is saved in
%%%%% that same directory.
%%

% point to the datafoldern
datafolder = pwd;
InitialPath = pwd;
cd(datafolder);
directory = datafolder;                 % dir = current directory
div = strfind(directory, '\');          % div = divider of directory (\)
ppId = directory(div(1)+1:end);         % participant name / number / id

%% Creating the data struct

for id= 1:numel(files)
    [~,name, ~] = fileparts(files(id).name);
    [fileName] = regexprep(name, '-', '_');
    fileList{id,1} = fileName;

    % Displaying which file is beeing analyzed
    disp(['Analyzing file: ' fileName '....']);
    [tree] = load_mvnx(files(id).name);
    rawData.(fileName).suitLabel = tree.subject.label;
    rawData.(fileName).framerate = tree.subject.frameRate;
    rawData.(fileName).segmentcount = tree.subject.segmentCount;
    rawData.(fileName).originalFilename = tree.subject.originalFilename;

    % define the sensor locations
    for i=1:numel(tree.subject.sensors.sensor)
        sensorLocation{1,i} = tree.subject.sensors.sensor(i).label;
    end

    % define the segmentNames
    for i=1:numel(tree.subject.segments.segment)
        segmentNames{1,i} = tree.subject.segments.segment(i).label;
    end

    % define the jointNames
    for i=1:numel(tree.subject.joints.joint)
        jointNames{1,i} = tree.subject.joints.joint(i).label;
    end


    %% separating the identity, t-pose and n-pose orientation and position data
    % identity
    rawData.(fileName).staticData.identity.orientation = tree.subject.frames.frame(1). ↙
orientation;
    rawData.(fileName).staticData.identity.position = tree.subject.frames.frame(1).position;
    % t-pose
    rawData.(fileName).staticData.tpose.orientation = tree.subject.frames.frame(2). ↙
orientation;
    rawData.(fileName).staticData.tpose.position = tree.subject.frames.frame(2).position;
    % t-pose-isb
    rawData.(fileName).staticData.tpose_isb.orientation = tree.subject.frames.frame(3). ↙
orientation;
    rawData.(fileName).staticData.tpose_isb.position = tree.subject.frames.frame(3).position;

    tree.subject.frames.frame(1:3) = [];

    % restructuring the segment data
    for i = 1:numel(tree.subject.frames.frame)
        for sn = 1:numel(segmentNames)
            s2=sn * 3;
```

```
            s1=(sn * 3)-2;
            rawData.(fileName).segments.(segmentNames{sn}).segmentPosition(i,:) = tree. ↙
subject.frames.frame(i).position(s1:s2);
            rawData.(fileName).segments.(segmentNames{sn}).segmentVelocity(i,:) = tree. ↙
subject.frames.frame(i).velocity(s1:s2);
            rawData.(fileName).segments.(segmentNames{sn}).segmentAcceleration(i,:) = tree. ↙
subject.frames.frame(i).acceleration(s1:s2);
            rawData.(fileName).segments.(segmentNames{sn}).segmentOrientation(i,:) = tree. ↙
subject.frames.frame(i).orientation(sn*4-3:sn*4);
            rawData.(fileName).segments.(segmentNames{sn}).segmentAngVelocity(i,:) = tree. ↙
subject.frames.frame(i).angularVelocity(s1:s2);
            rawData.(fileName).segments.(segmentNames{sn}).segmentAngAcceleration(i,:) = ↙
tree.subject.frames.frame(i).angularAcceleration(s1:s2);
        end
    end

    % restructuring the joint data
    for i = 1:numel(tree.subject.frames.frame)
        for jn = 1:numel(jointNames)
            s2 = jn*3;
            s1 = (jn*3)-2;
            rawData.(fileName).joints.(jointNames{jn}).jointAngle(i,:) = tree.subject.frames. ↙
frame(i).jointAngle(s1:s2);
            rawData.(fileName).joints.(jointNames{jn}).jointAngleXZY(i,:) = tree.subject. ↙
frames.frame(i).jointAngleXZY(s1:s2);
        end
    end

    %restructuring the sensor data
    for i = 1: numel(tree.subject.frames.frame)
        for sl = 1:numel(sensorLocation)
            s2 = sl * 3;
            s1 = (sl *3) -2;
            rawData.(fileName).sensors.(sensorLocation{sl}).sensorAcceleration(i,:) = tree. ↙
subject.frames.frame(i).sensorAcceleration(s1:s2);
            rawData.(fileName).sensors.(sensorLocation{sl}).sensorOrientation(i,:) = tree. ↙
subject.frames.frame(i).sensorOrientation(sl*4-3:sl*4);
            rawData.(fileName).sensors.(sensorLocation{sl}).sensorMagneticField(i,:) = tree. ↙
subject.frames.frame(i).sensorMagneticField(s1:s2);

        end
    end
    save('walk-014');
    cd(InitialPath);

end
```

Function OpenSense.m to create an OpenSense file (.sto) from .mat

```
%% Generate Opensense file for kinematic analysis in OpenSim
%-------------------------------------------------------------
%% Settings

Xsens_datafolder = pwd;
OpenSense_folder = pwd;

OutPath = [OpenSense_folder '\OpenSense'];
R = load(fullfile(Xsens_datafolder, 'walk-014' ));
%% Export the storage files

Headers = {'torso_imu', 'pelvis_imu',...
    'femur_r_imu','tibia_r_imu','calcn_r_imu','femur_l_imu',...
    'tibia_l_imu','calcn_l_imu'};

Headers_MatF = { 'T8', 'Pelvis',...
    'RightUpperLeg','RightLowerLeg','RightFoot','LeftUpperLeg',...
    'LeftLowerLeg','LeftFoot'};

Names   = fieldnames(R.rawData);
ntr     = length(Names);
nbodies =  length(Headers);
if ~isfolder(OutPath)
    mkdir(OutPath);
end
%%
for i=1:ntr
    % get the file data
    filename = Names{i};
    dat = R.rawData.(filename);

    % pre-allocate the data matrix
    SensorsNames = fieldnames(dat.sensors);
    nfr = size(dat.sensors.(SensorsNames{1}).sensorOrientation,1);
    DataMatrix = zeros(nfr,nbodies*4);
    DataMatrix_acc = zeros(nfr,nbodies*3);
    DataMatrix_ang = zeros(nfr,nbodies*3);
    DataMatrix_mag = zeros(nfr,nbodies*3);

    % fill the data matrix
    for j = 1:nbodies
        ih = find(strcmp(SensorsNames, Headers_MatF{j}));
        or = dat.sensors.(SensorsNames{ih}).sensorOrientation;
        acc = dat.sensors.(SensorsNames{ih}).sensorAcceleration;
        mag = dat.sensors.(SensorsNames{ih}).sensorMagneticField;
        DataMatrix(:,j*4-3:j*4) = or;
        DataMatrix_acc(:,j*3-2:j*3) = acc;
        DataMatrix_mag(:,j*3-2:j*3) = mag;
    end

    % get the time vector
    fr = dat.framerate;
    time=(0:nfr-1)./fr + 0;

    save('walk-014_DataM','DataMatrix_acc','DataMatrix_mag','DataMatrix');
    pause(2)
    %save the Storage file for OpenSim
    Create_IMU_Storage(fullfile(OutPath,[filename '_orientations.sto']),...
        nfr, nbodies, time', DataMatrix, Headers);
    disp([filename ' Saved']);

end
```

Code Matlab zmp.m with the ZMP implementation

```
% IMPLEMENTATION OF ZERO MOMENT POINT TO GET CoP of the measured GRF
% Force and Moment balance from Pelvis to CoP
% Fp = Fgrf
% Mp = Mgrf
% Fzmp = Fp
% Mzmp + rzmp*Fzmp = Mp + rp*Fp
%-------------------------------------------------------------------
%% read GRF file

path='C:\Users\zanca\OneDrive\Desktop\OpenSimJAM\OpenSimJAM\OpenSimJAM_EMG\'
     'opensim-core-4.3.1-2021-10-11-↙
7dcf3d5c3\Resources\Code\Matlab\JAM\subjects_models_IMU\';

sub_num='TBM_H14';
walk_name='walk_3';
imu_walk_name='walk_004';
file=strcat(walk_name,'_grf_mod.mot');
[data,C,t] =  readMOTSTOTRCfiles_v1([path,sub_num,'\experimental_data\'], file);

%% load ik_InCap.mot cut and correctly oriented with MoCap
%Incap
file=strcat('ik_',imu_walk_name,'_orientations_mod1_cut.mot');

[data1,C1,t1] =  readMOTSTOTRCfiles_v1([path,sub_num,'\OpenSense\'], file);

%% ZMP equation

%Fx,Fy,Fz GRF equal to Pelvis
Fx=data(:,find(C=="ground_force1_vx"));
Fy=data(:,find(C=="ground_force1_vy"));
Fz=data(:,find(C=="ground_force1_vz"));


%Mx,My,Mz GRF equal to Pelvis
Mx=data(:,find(C=="ground_torque1_x"));
My=data(:,find(C=="ground_torque1_y"));
Mz=data(:,find(C=="ground_torque1_z"));


%Position of pelvis FIXED
Yp=zeros(length(data),1);
Xp=zeros(length(data),1);
for i=1:length(data)
    Yp(i)=data1(1,find(C1=="pelvis_ty")); % ty pelvis of IK (height of pelvis)
end
Zp=zeros(length(data),1);



%Position of CoP
Xcop=Xp + (Mz-Yp.*Fx)./Fy;
Ycop=zeros(length(data),1);
Zcop=Zp -(Mx+Yp.*Fz)./Fy;

%Free moment
Mycop= My + (Fx.*Mx)./Fy + (Fz.*Mz)./Fy;

%% Create new grf.mot
%Forces stay the same

%Change torque
data(:,find(C=="ground_torque1_x"))=zeros(length(data),1);
data(:,find(C=="ground_torque1_y"))=Mycop;
data(:,find(C=="ground_torque1_z"))=zeros(length(data),1);
```

```
%Change position px,py,pz
data(:,find(C=="ground_force1_px"))=Xcop;
data(:,find(C=="ground_force1_py"))=zeros(length(data),1);
data(:,find(C=="ground_force1_pz"))=Zcop;


%% other platform
%Fx,Fy,Fz GRF equal to Pelvis
Fx1=data(:,find(C=="ground_force3_vx"));
Fy1=data(:,find(C=="ground_force3_vy"));
Fz1=data(:,find(C=="ground_force3_vz"));


%Mx,My,Mz GRF equal to Pelvis
Mx1=data(:,find(C=="ground_torque3_x"));
My1=data(:,find(C=="ground_torque3_y"));
Mz1=data(:,find(C=="ground_torque3_z"));

%Computation of the position of CoP
Xcop1= Xp + (Mz1-Yp.*Fx1)./Fy1;
Ycop1=zeros(length(data),1);
Zcop1= Zp - (Mx1+Yp.*Fz1)./Fy1;

%Computation of the free moment
Mycop1= My1 + (Fx1.*Mx1)./Fy1 + (Fz1.*Mz1)./Fy1;


%% Recreate new grf.mot
%Forces stay the same

%Change torque
data(:,find(C=="ground_torque3_x"))=zeros(length(data),1);
data(:,find(C=="ground_torque3_y"))=Mycop1;
data(:,find(C=="ground_torque3_z"))=zeros(length(data),1);

%Change position px,py,pz
data(:,find(C=="ground_force3_px"))=Xcop1;
data(:,find(C=="ground_force3_py"))=zeros(length(data),1);
data(:,find(C=="ground_force3_pz"))=Zcop1;

%% generate new grf File
%convert all the NaN to zero
data(isnan(data))=0;
data(isinf(data))=0;

file=strcat(walk_name,'_grf_zmp.mot');
%Incap
generateMotFile(data,C,[path,sub_num,'\experimental_data/',file]);
disp('Data saved')
```

References

[1] S. Brandon, C. Smith and D. Thelen, "Simulation of Soft Tissue Loading from Observed Movement Dynamics," *Handbook of Human Motion, Springer International Publishing,* pp. 1-34, 2017.

[2] R. L. Lenhart, J. Kaiser, S. C. and D. Thelen, "Prediction and Validation of Load-Dependent Behavior of the Tibiofemoral and Patellofemoral Joints During Movement," *Ann. Biomed. Eng.,* vol. 43, no. 11, pp. 2675-2685, Nov. 2015.

[3] A. Tishya and L. Wren, "Efficacy of clinical gait analysis: A systematic review," *Gait and Posture,* vol. 34.2, pp. 149-153, 2011.

[4] T. W. L. Chang and F. Chu, "Biomechanics of human movement and its clinical applications," *Kaohsiung Journal of Medical Sciences,* vol. 28.2, pp. 13-25, 2012.

[5] J. Perry, Gait Analysis: Normal and Pathological Function., 1992.

[6] K. Gaudio and E. Saladin, Anatomia & Fisiologia, Piccin-Nuova Libraria, 2013.

[7] J. Watkins, Fundamental biomechanics of sport and exercise, Routledge, 2014.

[8] "History of the Study of Locomotion," [Online]. Available: http://www.clinicalgaitanalysis.. [Accessed 12 06 2022].

[9] D. H. Sutherland, "The development of mature gait," *The Journal of Bone & Joint Surgery,* vol. 62, pp. 336-353, 1980.

[10] J. Delaram, "A Review on Accelerometry-Based Gait Analysis and Emerging Clinical Applications," *Reviews in Biomedical Engineering,* vol. 11, pp. 177-194, 2018.

[11] Z. Sawacha, "Lectures Notes of Bioengineering of Movement and Rehabilitation course," University of Padua, 2020.

[12] C. O. Bechtol, "Normal human gait," *Atlas of orthotics: American Academy of Orthopaedic Surgeons,* pp. 133-143, 1975.

[13] S. Affatato, "Biomechanics of the knee," in *Surgical Techniques in Total Knee Arthroplasty and Alternative Procedures*, Woodhead Publishing, 2015, pp. 17-35.

[14] J. Wang and S. Wang, "A data process of human knee joint kinematics obtained by motion-capture measurement," *BMC Med Inform Decis Mak,* vol. 21, p. 121, 2021.

[15] N. Petrone, "Lectures Notes of Sport Engineering Course," University of Padova, 2021.

[16] E. S. Grood and W. J. Suntay, "A joint coordinate system for the clinical description of three-dimensional motions: application to the knee," *Journal of biomechanical engineering,* Vols. 105,2, pp. 134-144, 1983.

[17] A. Muro de la Herran, G. Z. Begoña and M. Z. Amaia, "Gait analysis methods: An overview of wearable and non-wearable," *Sensors (Switzerland),* vol. 14.2, pp. 3362-3394, 2014.

[18] A. Cappozzo, "Human movement analysis using stereophotogrammetry. Part 1: Theoretical background," *Gait and Posture,* vol. 21.2, pp. 186-196, 2005.

[19] Davis and Ounpuu, "A gait analysis data collection and reduction technique," *Human Movement Science,* vol. 10, pp. 575-587, 1991.

[20] Cappozzo, Catani, D. Croce and Leardini, "Position and orientation in space of bones during movement: anatomical frame definition and determination," *Clinical Biomechanics,* vol. 10, pp. 171-178, 1995.

[21] L. Alberto and Z. Sawacha, "A new anatomically based protocol for gait analysis in children," *Gait & Posture,* 2007.

[22] J. Richards, Biomechanics in Clinic and Research, Elsevier, 2008.

[23] D.-P. Fong and Y.-Y. Chan, "The use of wearable inertial motion sensors in human lower limb biomechanics studies: a systematic review," *Sensors (Basel),* no. 10, pp. 11556-11565, 2010.

[24] [Online]. Available: https://www.xsens.com/.

[25] J. Söderkvist, "Micromachined gyroscopes," *Sensors and Actuators,* no. 43, pp. 65-71, 1994.

[26] D. Shaeffer, "Mems inertial sensors: A tutorial overview.," *IEEE Communications Magazine,* no. 51, pp. 100-109, 2013.

[27] T. Seel, "IMU-Based Joint Angle Measurement for Gait Analysis," *Sensors,* vol. 14, no. 4, pp. 6891-6909, 2014.

[28] A. Falisse, S. Van Rossom and J. Gijbers, "Opensim Versus Human Body Model: A comparison study for the lower limbs during gait," *Journal of Applied Biomechanics,* vol. 34, pp. 496-502, 2018.

[29] S. Delp, "OpenSim: open-source software to create and analyze dynamic simulations of movement," *IEEE transactions on bio-medical engineering,* vol. 54, no. 11, pp. 1940-50, 2007.

[30] M. Wesseling, E. Ranz and I. Jonkers, "Objectifying Treatment Outcomes Using Musculoskeletal Modelling-Based Simulations of Motion," in *Handbook of Human Motion*, Springer, 2018.

[31] [Online]. Available: https://simtk-confluence.stanford.edu:8443/display/OpenSim/Getting+Started+with+Inverse+Kinematics.

[32] [Online]. Available: https://simtk-confluence.stanford.edu:8443/display/OpenSim/Introduction+to+the+OpenSim+API.

[33] T. Seel, J. Raisch and T. Schauel, "IMU-Based Joint Angle Measurement for Gait Analysis," *Sensors,* vol. 14, no. 4, pp. 6891-6909, 2014.

[34] T. W. Lu and J. J. O'Connor, "Bone position estimation from skin marker co-ordinates using global optimisation with joint constraints," *Journal of biomechanics,* Vols. 32,2, pp. 129-34, 1999.

[35] [Online]. Available: https://simtk-confluence.stanford.edu:8443/display/OpenSim/OpenSense+-+Kinematics+with+IMU+Data.

[36] [Online]. Available: https://simtk-confluence.stanford.edu:8443/display/OpenSim/Getting+Started+with+IMU+Placer.

[37] [Online]. Available: https://simtk-confluence.stanford.edu:8443/display/OpenSim/How+to+Use+the+IMU+IK+Tool.

[38] F. C. Pandy and M. G. Anderson, "Dynamic Optimization of Human Walking," *J. Biomech. Eng.,* vol. 123, pp. 381-390, Oct. 2001.

[39] T. Guess, H. Liu, S. Bhashyam and G. Thiagarajan, "A multibody knee model with discrete cartilage prediction of tibio-femoral contact mechanics," *Comput. Methods Biomech. Biomed. Engin.,* vol. 16, no. 3, pp. 256-270, 2013.

[40] F. C. Pandy and M. G. Anderson, "Dynamic Optimization of Human Walking," *J. Biomech. Eng.,* vol. 123, pp. 381-390, 2001.

[41] E. M. Arnold, S. R. Ward, R. L. Lieber and S. L. Delp, "A Model of the Lower Limb for Analysisof Human Movement," *Ann. Biomed. Eng.,* vol. 38, pp. 269-279, 2010.

[42] C. R. Smith, "Efficient Computation of Cartilage Contact Pressures within Dynamic Simulations of Movement," *Computer Methods in Biomechanics and Biomedical Engineering,* pp. 1-8, 2016.

[43] S. Colin, "Simulating the effects of Anterior Cruciate Ligament Injury and Treatment on Cartilage Loading," University of Wisconsin-Madison, 2017.

[44] J. Podobnik and a. et, "Centre of Pressure Estimation during Walking Using Only Inertial-Measurement Units and End-To-End Statistical Modelling," *Sensors,* vol. 20, 2020.

[45] A. Karatsidis and e. al, "Estimation of Ground Reaction Forces and Moments During Gait Using Only Inertial Motion Capture," *Sensors,* vol. 17, 2017.

[46] Y. Jung, M. Jung, J. Ryu, S. Yoon, S. Park and S. Koo, "Dynamically adjustable foot-ground contact model to estimate ground reaction force during walking and running," *Gait Posture,* vol. 45, pp. 62-68, 2016.

[47] C. Funk, S. Nagendra, J. Scott, B. Ravichandran, J. Challis, R. Collins and Y. Liu, "Learning Dynamics from Kinematics: Estimating 2D Foot Pressure Maps from Video Frames," *arXiv,* 2019.

[48] C.-C. Wu, Y.-J. Chen and C.-S. Hsu, "Multiple Inertial Measurement Unit Combination and Location for Center of Pressure Prediction in Gait," *Frontiers in Bioengineering and Biotechnology,* 2020.

[49] E. J. Dijkstra, E. M. and G. Farewik, "Computation of ground reaction force using Zero Moment Point," *Journal of Biomechanics,* vol. 48, no. 14, 2015.

[50] Y. Xiang, "Optimization-based dynamic human walking prediction," in *Digital Human Modeling for Design and Engineering Conference and Exhibition*, Seattle, WA, 2007.

[51] D. Gupta and e. al, "Physics-Based Guidelines for Accepting Reasonable Dynamic Simulations of Movement," *IEEE transactions on bio-medical engineering,* Vols. 96,3, pp. 1194-1201, 2022.

[52] T. W. Lu and J. J. O. Connor, "Bone position estimation from skin marker coordinates using global optimisation with joint constraints," *Journal of biomechanics,* vol. 32.2, pp. 129-34, 1999.

[53] A. Cappozzo, F. Catani, A. Leardini and M. Benedetti, "Position and orientation in space of bones during movement: Experimental artefacts," *Clin Biomech,* vol. 11(2), pp. 90-100, 1996.

[54] C. Fukuchi and a. et, "A public dataset of overground and treadmill walking kinematics and kinetics in healthy individuals," *PeerJ,* vol. 6, 2018.

[55] S. van Rossom, C. R. Smith, D. G. Thelen, B. Vanwanseele, D. Van Assche and I. & Jonkers, "Knee Joint Loading in Healthy Adults During Functional Exercises: Implications for Rehabilitation Guidelines," *The Journal of orthopaedic and sports physical therapy,* vol. 48(3), pp. 162-173, 2018.

[56] F. Liu, M. Kozanek, A. Hosseini, S. K. Van de Velde and T. J. Gill, "In-vivo Tibiofemoral Cartilage Deformation during the Stance Phase of Gait," *J Biomech,* vol. 43(4), pp. 658-665, 2010.

[57] K. Deepak, P.T. and e. al., "Knee Joint Loading during Gait in Healthy Controls and Individuals with Knee Osteoarthritis," *Osteoarthritis Cartilage,* vol. 21(2), pp. 298-305, 2013.

[58] C. Winby, D. Lloyd, T. Besier and T. Kirk, "Muscle and external load contribution to knee joint contact loads during normal gait," *J Biomech,* vol. 42, pp. 2294-2300, 2009.

[59] I. Kutzner, B. Heinlein, F. Graichen, A. Bender, A. Rohlmann and A. Halder, "Loading of the knee joint during activities of daily living measured in vivo in five subjects.," *J Biomech,* vol. 43, pp. 2164-2173, 2010.

[60] D. Hurwitz, D. Sumner, T. Andriacchi and D. Sugar, " Dynamic knee loads during gait predict proximal tibial bone distribution," *J Biomech,* vol. 31, pp. 423-430, 1998.

[61] K. Shelburne, M. Torry and M. Pandy, "Muscle, ligament, and joint-contact forces at the knee during walking," *Med Sci Sports Exerc.,* vol. 37, pp. 1948-1956, 2005.

[62] M. Audu, R. Kirsch and R. Triolo, "Experimental verification of a computational technique for determining ground reaction in humal bipedal stance," *J. Biomech,* vol. 40, pp. 1115-1124, 2007.

[63] I. Poitras, F. Dupuis, M. Bielmann, A. Campeau-Lecours, C. Mercier, L. Bouyer and J.-S. Roy, "Validity and reliability of wearable sensors for joint angle estimation: A systematic review.," *Sensors,* vol. 19, 2019.

[64] H. Dejnabadi, B. Jolles and K. Aminian, "A new approach to accurate measurement of uniaxial joint angles based on a combination of accelerometers and gyroscopes," *IEEE Trans. Biomed. Eng.,* vol. 52, pp. 1478-1484, 2005.

[65] G. Di Raimondo, B. Vanwanseele, A. van der Have, J. Emmerzaal, M. Willems, B. Killen and I. Jonkers, "Inertial Sensor-to-Segment Calibration for Accurate 3D Joint Angle Calculation for Use in OpenSim.," *Sensors,* vol. 22, 2022.

[66] K. Sasaki and R. Neptune, "Individual muscle contributions to the axial knee joint contact force during normal walking," *Journal of biomechanics,* vol. 43(14), pp. 2780-4, 2010.

[67] W. Taylor, M. Heller, G. Bergmann and G. Duda, "Tibio-femoral loading during human gait and stair climbing," *Journal of Orthopaedic Research,* vol. 22(3), pp. 625-32, 2004.